

OSLO METROPOLITAN UNIVERSITY  
STORBYUNIVERSITETET

Master's Degree in  
**Structural Engineering and Building Technology**  
Department of Civil Engineering and Energy Technology

# MASTER THESIS

THESIS TITLE  The efficiency of NDT methods in existing concrete structures	DATE 09.06.2021
	NUMBER OF PAGES 136/1
AUTHOR(S)  ISMAEL ELHAFEDI SHIVAM SHARMA	SUPERVISOR(S)  BJØRN TÄLJSTEN GRO MARKESET

IN COLLABORATION WITH	CONTACT PERSON

<p><b>SUMMARY</b></p> <p>In this thesis, different NDT methods have been investigated for reinforced and post-tensioned concrete structures. The durability of these structures is mainly affected by concrete composition and deterioration. For that reason, assessment of existing structures is a fundamental approach to ensure long-term performance. This aspect entails that structural condition is monitored by collecting essential data during the service life of the concrete structure, which provides an insight into the structural behavior. Therefore, NDT methods are integrated with SHM to estimate the remaining service life of concrete structures.</p> <p>There are advantages and limitations to applying NDT methods, and the principles of the NDT categories are conclusive for the capability to detect different problems. However, available equipment for NDT methods influences the reliability and interpretation of obtained data. Technical specifications and algorithms for NDT methods can differentiate depending on accuracy, depth, and frequency range. Variations in these parameters can result in the imprecision of promising data, influencing the degree of detection for concrete deteriorations.</p>
---

3 KEYWORDS
NDT
Existing concrete structures
Deterioration

## Preface

The research presented in the following thesis was a concluding work of two students in collaboration with Oslo Metropolitan University (OsloMet) and is a final part of the master's degree program in Structural Engineering and Building Technology.

First and foremost, the authors would like to express their gratitude for our supervisors Björn Täljsten and Gro Markeset, contributing with insightful guidance and help throughout the spring semester of 2021. Your time and patience have been valuable for inspiring the authors throughout different challenges in our research work. In addition, the authors would also like to thank Stellan Kjemperud and the team from Elop AS for allowing us to test the UPE equipment in Hamar. The authors have gained enormous knowledge during the work with the thesis, which they believe can be useful in the future.

## Abstract

The study's main objective was to evaluate the significance of NDT methods for detecting damages and flaws in reinforced and prestressed concrete. Deterioration mechanisms influence the durability and serviceability of concrete structures. Assessment of concrete structures is recommended for reducing high maintenance costs and accomplishing adequate performance levels. Implementing various NDT methods is a suitable approach to achieve the main target of the assessment. Consideration of preliminary assessment is the key to determining applicable NDT methods, which is implemented in the detailed assessment to identify the extent of problems.

Some of the most acknowledged NDT methods emphasizing damages and flaws such as cracks, voids, delaminations, and corrosion have been briefly investigated. The main purpose of these NDT methods is to evaluate the accuracy and efficiency of obtained data. An assessment score strategy will be implemented for the different NDT methods to detect different deterioration types. However, many NDT methods are combined to accomplish an enhanced understanding of concrete structures. The durability of reinforced and prestressed concrete structures can securely be investigated by including multiple NDT methods. Different field tests will be investigated. Besides, the authors will present their mockup test with UPE equipment in Hamar.

Several companies offer quality NDT equipment as a part of the concrete assessment. The main aspects of NDT equipment are related to safety and accuracy performance. Countless NDT products existing in the current market resulting in an advanced interpretation of their reliability and efficiency. The field tests and mockup test evaluation clarify that regular tests with different NDT equipment are preferable regarding their reliability, independent of their time duration and cost. The result of this thesis is that NDT tests and a combination of these methods are efficient approaches for evaluating concrete structures.

## Sammendrag

Studiets hovedmål var å evaluere betydningen av NDT metoder for å oppdage skader og mangler i armert og forspent betong. Forverringsmekanismer påvirker bestandigheten og funksjonaliteten til betongkonstruksjoner. Vurdering av betongkonstruksjoner anbefales for å redusere høye vedlikeholdskostnader og oppnåelse av tilstrekkelig ytelsesnivå. Implementering av ulike NDT metoder er en passende tilnærming for å oppnå hovedmålet med vurderingen. Betraktning av foreløpig vurdering er avgjørende for å bestemme gjeldende NDT metoder som er iverksatt i den detaljerte vurderingen for å identifisere omfanget av problemer.

Noen av de mest anerkjente NDT metodene som er betydelige for forverringer er sprekker, hulrom, delamineringer og korrosjon, og disse er spesifikt undersøkt. Hovedformålet med NDT metodene er å evaluere nøyaktigheten og effektiviteten til de innhentede dataene. Det vil bli gjennomført en poengstrategi for de ulike NDT metodene for å undersøke forskjellige forverringstyper. Imidlertid kombineres mange av NDT metoder for å oppnå en bredere forståelse av betongkonstruksjoner. Bestandighet for slakkarmert og spennarmert betong kan undersøkes ved å inkludere flere NDT metoder. Ulike feltforsøk i litteraturen vil bli undersøkt. Dessuten vil forfatterne presentere sin lab arbeid med UPE-utstyr.

Flere produsenter tilbyr NDT utstyr av høy kvalitet som en del av den betong vurderingen. De viktigste aspektene ved NDT utstyrene er sikkerhet og nøyaktighet. Utallige NDT produkter finnes i det nåværende markedet resulterer i en avansert tolkning av deres pålitelighet og effektivitet. Feltprøver og mockup-testevaluering tydeliggjør at regelmessige tester med forskjellig NDT-utstyr er å foretrekke med hensyn til deres pålitelighet, uavhengig av deres varighet og kostnad. Resultatet av denne oppgaven er at NDT tester og kombinasjon av disse testene er effektive tilnærminger for evaluering av betongkonstruksjoner.

## Table of contents

Preface .....	3
Abstract.....	3
Sammendrag .....	4
List of Figures .....	10
List of Tables .....	7
Abbreviations .....	10
1. Introduction .....	12
1.1 Background.....	12
1.2 Aim and objective.....	13
1.3 Limitations.....	13
1.4 Methodology.....	14
2. Concrete structures and deterioration .....	15
2.1 Reinforced concrete .....	15
2.2 Prestressed concrete.....	16
2.3 Deterioration of reinforced concrete structures .....	18
2.3.1 Cracking .....	19
2.3.2 Mechanical.....	21
2.3.3 Physical .....	24
2.3.4 Structural .....	27
2.3.5 Chemical .....	28
2.3.6 Biological.....	32
2.3.7 Corrosion .....	33
3. Assessment of concrete structures.....	39
3.1 Condition assessment of concrete structures.....	39
3.2 Structural health monitoring (SHM).....	42
3.3 Non-destructive test methods (NDT).....	45
3.3.1 Visual inspection.....	47
3.3.2 Ultrasonic method .....	50
3.3.3 Impact echo (IE).....	62
3.3.4 Impulse response (IR) .....	66
3.3.5 Ground-penetrating radar (GPR).....	71
3.3.6 Concrete Resistivity (CR).....	78

3.3.7 Cover meter (CM) .....	81
3.3.8 Half-Cell Potential (HCP) .....	87
3.4 Combining NDT methods in field tests.....	92
3.4.1 Field test of Farris bridge in Larvik .....	92
3.4.2 Field test of Herøysund bridge .....	93
3.4.3 Field test of Dalselva bridge .....	97
4. Non-destructive tests.....	100
4.1 Test specimen.....	100
4.2 Test procedure .....	104
4.3 Mockup test in Hamar.....	106
4.4 Results .....	111
4.4.1 S-20-1-2 along the tendon duct.....	111
4.4.2 S-20-1-2 across the tendon duct .....	113
4.4.3 S19-1-2 along the tendon duct.....	114
4.4.4 S62 delamination.....	116
5. Discussion.....	118
6. Conclusion and future recommendations .....	126
7. References .....	128
Appendix 1 .....	137

## List of Figure

Figure 1 Flowchart of the methodology in this thesis .....	14
Figure 2 Composite action of reinforced concrete beam [5] .....	16
Figure 3 Stress distribution in prestressed concrete beam [8].....	17
Figure 4 Causes of deterioration [13] .....	18
Figure 5 Cause of structural failure [14] .....	19
Figure 6 Illustration of non-structural cracks [1] .....	19
Figure 7 Causes and types of cracks [15] .....	21
Figure 8 Deterioration due to erosion and abrasion [17].....	22
Figure 9 Schematic representation of abrasion due to friction and abrasion [18] .....	22
Figure 10 Effects of impact load on reinforced beam: (a) Local damage, (b) global flexural failure, (c) global shear failure, (d) global flexural-shear failure [21].....	23
Figure 11 Effects of blast load on reinforced beam: (a) Local damage, (b) global flexural failure, (c) global shear failure, (d) global flexural-shear failure [21].....	24
Figure 12 Damage of different concretes due to freeze-thaw [23].....	25
Figure 13 Surface scaling of normal concrete (NC), high strength concrete (HSC), silica fume concrete (SFC) and fly ash concert (FAC) [27] .....	26
Figure 14 Spalling of concrete beam and column as a result of fire [31] .....	27
Figure 15 Cracking due to settlement [33] .....	28
Figure 16 Electron microscope image of an internal crack due to ASR [37] .....	29
Figure 17 Map cracking due to ASR [23] .....	29
Figure 18 ASR induced crack pattern in reinforced concrete [24] .....	29
Figure 19 Acid attack along the concrete surface from a micrograph [43].....	31
Figure 20 Representation of carbonation adapted from [51] ; a) carbonation of the concrete, b) carbonation reaching and depassivating the reinforcement, c) penetration of carbonation, initiating corrosion cracking and spalling the concrete.....	33
Figure 21 Carbonation rate as a function of relative humidity [13] .....	34
Figure 22 Influence of w/c ratio and carbonation depth [13] .....	35
Figure 23 Chloride induced corrosion of reinforced concrete [1] .....	36
Figure 24 Load-elongation curve and different percentages of corrosion for 6 mm diameter steel bar [57] .....	37
Figure 25 General flowchart for assessment of existing structures (ISO 13822) [64].....	40
Figure 26 Flow chart for detailed assessment of concrete structures considering NDT methods [66].....	41
Figure 27 The relation between SHM, assessment and NDT .....	42
Figure 28 Necessary components to create a digital twin [72] .....	44
Figure 29 Acoustic wave spectrum and frequency for different NDT methods [15] .....	45
Figure 30 Crack width microscope [80] .....	48
Figure 31 Drone inspection of the Daniel Carter Beard Bridge [82].....	49
Figure 32 Pulse travel path from transmitters to receivers in concrete based on UPV [84] ..	50
Figure 33 Type of UPV measurements (a) Direct, (b) Semi-Direct, (c) Indirect [87] .....	51
Figure 34 Principals of crack estimation by a) Bungey and b) BS 1881 .....	53
Figure 35 Principals of crack estimation by a) Method A and b) Method B.....	53

Figure 36 Smooth surface concrete wall vs rough surface concrete wall [96].....	54
Figure 37 Concrete wall with and without reinforcement [96].....	54
Figure 38 Schematic of UPE methods: (a) pulse-echo, (b) pitch-catch and (c) phased array [77].....	57
Figure 39 Illustration of the B-, C- and D-scan [109] .....	59
Figure 40 The coherence between mechanical impact and elastic waves [112] .....	62
Figure 41 Procedure A and procedure B according to ACTM C 1383 [112] .....	63
Figure 42 Principal and set-up of the IR method.....	67
Figure 43 Contour plot from a concrete floor slab showing average mobility values [77].....	68
Figure 44 Rebars in GPR [130] .....	72
Figure 45 Illustration of GPR signals [129].....	72
Figure 46 Detection of potential corrosion in a bridge deck [130] .....	73
Figure 47 Deterioration Index map [131] .....	73
Figure 48 The reflection of voids [130].....	74
Figure 49 Location of post-tensioned ducts [130].....	74
Figure 50 GPR of a concealed crack [134] .....	75
Figure 51 Principal of Wenner four-probe method [77] .....	79
Figure 52 Illustrations of magnetic reluctance meters for: a) small current induced in sensing coil without bar; b) enhancement of current in sensing coil with bar [77].....	82
Figure 53 Illustrations of eddy-current meters for: a) a characteristic current amplitude; b) differences in current amplitude interacting with reinforcing bar [77].....	82
Figure 54 Zone of influence for: a) the search head; b) magnetic reluctance CM; c) eddy-current CM [77].....	83
Figure 55 Schematic setup of HCP in reinforced concrete [156].....	87
Figure 56 Tendon ducts marked with red arrows in segment 1 [76] .....	92
Figure 57 No sign of tendon ducts in segment 2 [76].....	92
Figure 58 Tendon duct 3 at a depth around 150 mm (segment 1) [76].....	93
Figure 59 Tendon duct 3 at a depth between 165-450 mm (segment 2) [76].....	93
Figure 60 Test areas of the bridge [76].....	94
Figure 61 UPE scan from point 5.1 South girder [76] .....	94
Figure 62 GPR from point 5.1 South girder [76] .....	95
Figure 63 UPE scan from point 5.2 South girder [76] .....	95
Figure 64 UPE scan of tendon duct 3SC [76] .....	95
Figure 65 Drilling and visual check of 1SC (left) and 2S (right) [76].....	96
Figure 66 Drilling and visual check of 3SC [76] .....	96
Figure 67 UPE scan from point 5.5 [76] .....	97
Figure 68 (a) Bottom flange of girder 2; (b) Side view of girder 2; (c) Bottom view of girder 2 [11].....	98
Figure 69 The relationship between HCP and ER measurements [11].....	99
Figure 70 Test specimen S-20-1-2.....	101
Figure 71 Drawing of S-20-1-2 .....	102
Figure 72 Test specimen S19-2-2.....	103
Figure 73 Drawing of S19-2-2 .....	103
Figure 74 Delamination of S62 slab .....	104



Figure 75 Scanning S-20-1-2 B with laser pointing on the center chalk marking.....	105
Figure 76 Scanning procedure for S-20-1-2 B along the ducts (dimensions in cm).....	105
Figure 77 Scanning procedure for S-20-1-2 B across the ducts (dimensions in cm) .....	106
Figure 78 Scanning procedure for S19-2-2 across the ducts (dimensions in cm) .....	106
Figure 79 UPE 2 scan vs UPE 1 scan for duct A [76].....	107
Figure 80 UPE 2 scan of empty duct B [76].....	107
Figure 81 Grouted and empty duct in UPE 1 scan [76].....	107
Figure 82 Void in duct and empty duct in UPE 1 scan [76].....	108
Figure 83 Location of testing points on the concrete specimen [76] .....	108
Figure 84 Comparison between test point 1 (TP1) and test point 2 (TP2) [76] .....	109
Figure 85 Peak frequency of void at TP3 [76] .....	109
Figure 86 Peak frequency of void at TP4 [76] .....	109
Figure 87 3D scan of S-20-1-2 along the ducts .....	111
Figure 88 C-scan of S-20-1-2 along the ducts .....	112
Figure 89 D-scans of the grouted duct and empty duct .....	112
Figure 90 3D scan of S-20-1-2 across the ducts .....	113
Figure 91 C-scan a) 13 cm into the concrete, b) 25.9 cm into the concrete .....	113
Figure 92 C-scan of S19-1-2 along the duct .....	114
Figure 93 B-scan 9 cm into S19-1-2 .....	114
Figure 94 B-scan 27.3 cm into S19-1-2 .....	115
Figure 95 Realistic representation of S19-1-2 .....	115
Figure 96 Snapshot of a C-scan of S62 from Elop Insight .....	116
Figure 97 D-scan of S62.....	116
Figure 98 C-scan of S62 backwall.....	117
Figure 99 Realistic Representation of S62 .....	117
Figure 100 Assessment score of cracks in accordance with NDT methods.....	119
Figure 101 Assessment score of voids in accordance with NDT methods .....	120
Figure 102 Assessment score of delamination in accordance with NDT methods .....	120
Figure 103 Assessment score of corrosion of reinforcement in accordance with NDT methods .....	121
Figure 104 Assessment score of corrosion of PT strands in accordance with NDT methods	122
Figure 105 Assessment score of location of reinforcement in accordance with NDT methods .....	123
Figure 107 Assessment score of location of post-tensioning systems in accordance with NDT methods .....	123

## List of Tables

Table 1 Explanation of Figure 6 .....	20
Table 2 NDT methods [15, 76, 77] .....	46
Table 3 Advantages and limitations with visual inspection.....	48
Table 4 Assessment score of a VI.....	49
Table 5 Quality of concrete as a function of UPV from BS [89].....	52
Table 6 Advantages and limitations of using UPV method [15] .....	52
Table 7 Different UPV equipment from Proceq [99-101].....	55
Table 8 Advantages and limitations of using UPE method [15, 77] .....	57
Table 9 Different UPE equipment from Elop, Germann Instruments (MIRA) and Proceq [101, 105, 110] .....	59
Table 10 Assessment score of UPV and UPE .....	61
Table 11 Advantages and limitations of using IE [15, 77].....	63
Table 12 Different Impact Echo equipment for Olson Instruments [99, 100, 117, 118].....	64
Table 13 Assessment score of IE.....	66
Table 14 Advantages and limitations of using IR [77].....	68
Table 15 Different IR equipment from Olson Instruments and FPrimeC [123, 124].....	69
Table 16 Assessment score of IR.....	70
Table 17 Advantages and limitations of ground-penetrating radar[76] [15] .....	74
Table 18 Different GPR equipment from Proceq, Sensors & Software and Hilti [136-138]....	76
Table 19 Assessment score of GPR .....	78
Table 20 Guide for interpretation of CR [15].....	79
Table 21 Advantages and limitations of using CR method [77].....	79
Table 22 Different methods for corrosion by Proceq and other companies [142, 143] .....	80
Table 23 Assessment score of CR .....	81
Table 24 Advantages and limitations of using CM test [77] .....	83
Table 25 Different CM equipment from Proceq and other companies [149] [150].....	84
Table 26 Assessment score of the CR method .....	87
Table 27 Probability of corrosion based on HCP method [156] .....	88
Table 28 Advantages and limitations of using HCP method [15] .....	89
Table 29 Different methods for corrosion by Proceq and other companies [142, 143] .....	89
Table 30 Assessment score of HCP .....	90
Table 31 Test specimen specifications.....	100
Table 32 Testing points along cable ducts .....	108
Table 33.....	124

## Abbreviations

<b>NDT</b>	Non-destructive Testing
<b>LCC</b>	Lifecycle Cost
<b>SHM</b>	Structural Health Monitoring
<b>RC</b>	Reinforced Concrete
<b>AAR</b>	Alkali-Aggregate Reaction
<b>ASR</b>	Alkali-Silica Reaction
<b>ACR</b>	Alkali-Carbonate rock Reaction
<b>GGBS</b>	Ground Granulated Blast-furnace Slag
<b>GPR</b>	Ground-penetrating radar
<b>UPV</b>	Ultrasonic Pulse Velocity
<b>UPE</b>	Ultrasonic Pulse Echo
<b>IE</b>	Impact Echo
<b>HCP</b>	Half-Cell Potential
<b>NPRA</b>	Norwegian Public Roads Administration
<b>CM</b>	Cover meter
<b>EM</b>	Electromagnetic
<b>IR</b>	Impulse Response

# 1. Introduction

## 1.1 Background

A dominant construction material worldwide is concrete, where concrete itself is described as durable over time. Realistically, every structure has an estimated service life depending on the concrete mixture and execution of the construction material. Concrete technology has developed in the last decades, resulting in a major change in the concrete composition, and better mechanical properties have been obtained. These changes have some negative effects, making concrete more sensitive to how the material is mixed and processed due to the detailed chemistry [1].

Thus, the deterioration of concrete structures is a global challenge for structural engineers worldwide, facing challenges in assessing these structures from cost-effective and efficient aspects. Delayed assessments increase the probability of reduced serviceability and higher cost of repairs. Therefore, well-organized strategy tools are recommended for the assessment of concrete structures. Different perceptions of the best possible assessment strategy for concrete structures are still a debate. However, modern tools and approaches such as building information modeling (BIM) and digital twin are considered to improve structural assessments regarding planning, construction, and maintenance. Together with NDT methods, these modern tools are a substantial part of SHM. Furthermore, the mentioned tools minimize repair effort and increase the remaining service life of a structure. These are contributing to significant detection of deterioration and improved structural performance by analyzing, integrating, and interpreting high-quality data [2].

There has also been rigorous discussion about extending the life of the existing concrete structure to minimize resource consumption and minimize the environmental impact. Concrete structures are prone to different deterioration processes, and the need for regular maintenance and repair has increased because of aging concrete constructions [3, 4]. An attractive approach for assessing the condition of existing reinforced and prestressed concrete structures is the use of non-destructive testing (NDT) techniques, which provide information regarding material properties, concrete damages, and ongoing deterioration processes. Considerably, research is ongoing to improve technologies and the processing of data. In general, NDT methods aim to detect the condition of the concrete structure, rank the structure based on a specific property, and quantify these properties related to thresholds. However, there are many limitations regarding the quality of assessment related to uncertainty because of testing methods, such as interference with the environment and material variability and errors caused by human interpretation of data [3, 4]. In this thesis, analyzing different damages and flaws with certain NDT methods will be briefly investigated.

## 1.2 Aim and objective

The aim of this master's thesis is to emphasize NDT (Non-Destructive Testing) methods for evaluation of existing concrete structures, which contributes to determination of durability, structural integrity, and safety. The objective has been to detect and interpret damages in reinforced and prestressed concrete structures with various NDT methods. Here also combination of different methods has been investigated.

The research questions of this thesis are as following:

- *How efficient are NDT methods for the evaluation of damages and flaws in reinforced and post-tensioned concrete?*
- *How does the combination of NDT methods improve the evaluation of reinforced and post-tensioned concrete?*

## 1.3 Limitations

The NDT topic has a wide definition, involving various inspection techniques, and many aspects can therefore be included. However, this is time-consuming, and limitations must be considered to understand the author's approach. Therefore, the authors have chosen to limit the thesis with following considerations:

- Visual Inspection (VI), Ultrasonic Pulse Velocity (UPV), Ultrasonic Pulse Echo (UPE), Impact Echo (IE), Impulse Response (IR), Ground-penetrating radar (GPR), Cover Meter (CM), Half-Cell Potential (HCP), and Concrete Resistivity (CR) are the only methods addressed in this thesis
- Cracks, delaminations, voids, and corrosion are the only investigated damages and flaws
- Post-tensioned concrete is emphasized for the investigation of prestressed concrete

## 1.4 Methodology

The methodology of the thesis primarily includes a literature study and lab testing conducted by the authors. The literature study chapter is divided into deterioration, damages and flaws, assessment of concrete structures, NDT methods, and the combination of NDT methods in field tests. A detailed study of the mentioned categories is interpreted in the form of assessment scores, and a flowchart of the methodology is illustrated in Figure 1.

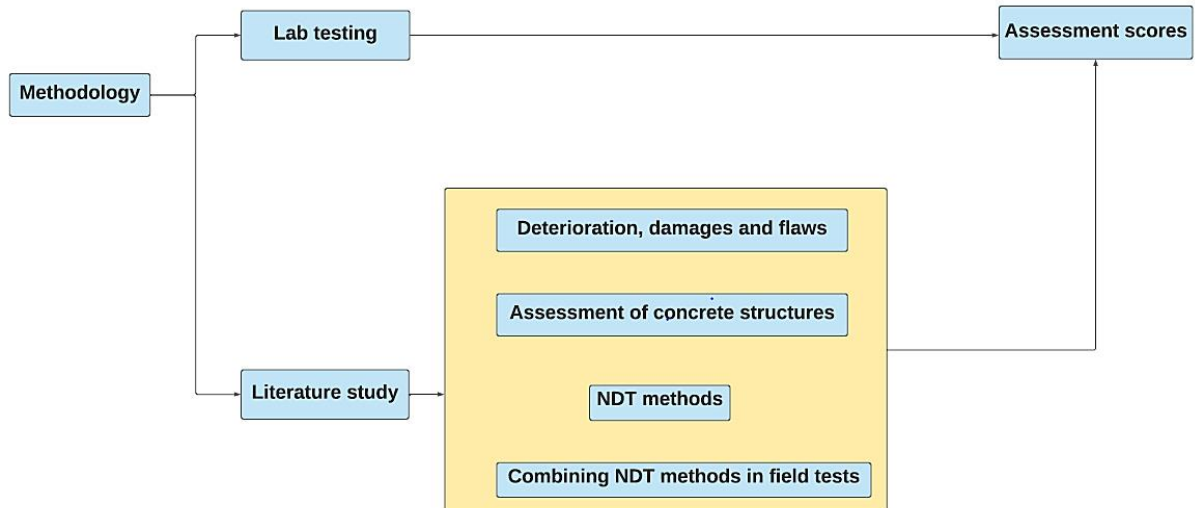


Figure 1 Flowchart of the methodology in this thesis

## 2. Concrete structures and deterioration

### 2.1 Reinforced concrete

Reinforced concrete is defined as a composite material with anisotropic properties, mainly consisted of concrete and steel. By defining the strength of reinforced concrete, the material itself has good compressive strength but cannot withstand tensile forces very well. Steel is strong in both compression and tension. However, a thin steel bar establishes the possibility for buckling in the system. This is the main reason for utilizing steel bars in the tension zone, obtaining decent compressive strength, tensile strength, and shear strength values. According to relevant studies, the tensile strength of the concrete is around 10 percent of its compressive strength. This statement clarifies that concrete has difficulties in resisting tensile forces, meanwhile, steel reinforcement manages to satisfy this condition perfectly. Furthermore, concrete protects the steel bars to maintain durability and fire resistance [5].

Reinforced concrete is valuable in dimensional control of shrinkage and surface cracking. Reinforcement is divided into deformed bars and mesh nets, where mesh nets are either rectangular mesh, square mesh, or trench mesh. The application area for reinforced concrete is habitually for concrete slabs, columns, walls, bridges, pavements, and decks. Concrete is known for brittle failure, occurring instantly without warning, meanwhile, steel reinforcement is familiar for ductile behavior. By combining concrete and steel reinforcement, reinforced concrete undergoes comfortably high deformations during cracking. Stabilized bond between concrete and steel is recommended for adequate force transfer between these materials. Bond depends on friction and mechanical interlocking between steel reinforcement and concrete, where cement paste and steel are influencing the bond. Amount of concrete cover is conclusive in reinforced concrete, decided by the cover thickness withstanding against corrosion, cracking, and fire [5].

In general, minimum essential cover thickness diversifies dependent on environmental and climate conditions. *EC2* specifies environmental classes with minimum concrete cover for both 50 and 100 years of service life [6]. On the other hand, the Norwegian Public Road Administration (NPRA) states that the minimum concrete cover in the marine environment is 100 mm, and clarifies that the durability of concrete structures should be designed for 100 years. [7]. Figure 2 emphasizes the bending behavior of a simply supported beam, showing the position of the steel reinforcement. These reinforcements are resisting the tensile forces, meanwhile the concrete is carrying the compression forces at the top of the beam [5].

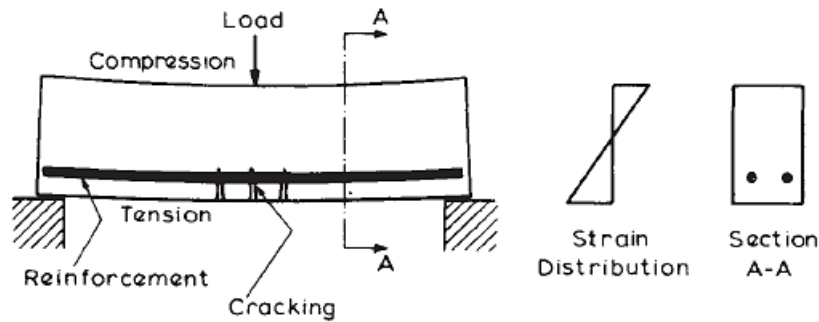


Figure 2 Composite action of reinforced concrete beam [5]

## 2.2 Prestressed concrete

According to EC2, “prestress” defines *all the permanent effects of the pre- and post-stressing process, which comprise internal forces in the sections and deformations of the structure* [6]. Prestressed concrete is divided in pre-tensioned and post-tensioned concrete. In pre-tensioned prestressed concrete, steel tendons are stretched between external buttresses before placing the concrete. After the concrete has obtained the required strength, tendons are released from the buttresses. In other words, the prestressing force is transferred to the concrete dependent on the bond between concrete and tendons. For post-tensioned prestressed concrete, stretching of steel tendons occurs in steel or plastic duct placed in the concrete. The concrete material is jacked with tendons anchored at the ends. In prestressed concrete, the entire section is efficient in resisting the applied moments, following to reduced deflections under service conditions [8].

Fully prestressed concrete structures utilize the cross-section efficiently. These structures are strongly resistible to shear forces controlled by the contribution of prestress, causing a reduction of principle tensile stresses. High-strength concrete in prestressed structures results in less shrinkage, cracks, and enhanced durability under aggressive environmental circumstances. Reduced creep, strain and high modulus of elasticity are additional factors for high-strength concrete, strengthening the concrete structures itself. Prestressed concrete structures are recommended for huge beam spans, especially related to long span bridges due to its high strength, fire resistance, cracking resistance, adaptability, and versatility. Figure 3 illustrates the principle of stress distribution from prestressing cable (P) and applied load, resulting to positive compression. A comparison to Figure 2 is that steel reinforcement is responsible for stress distribution [8].



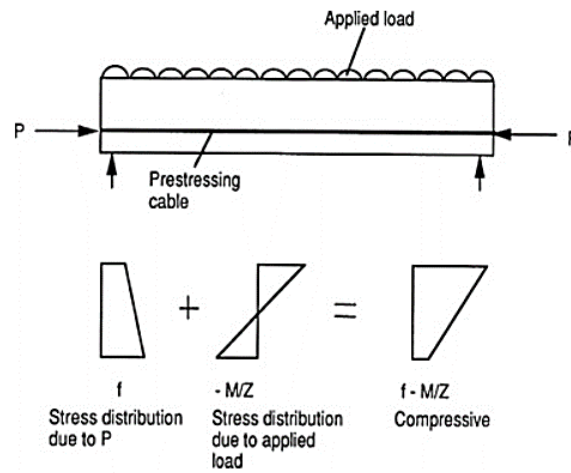


Figure 3 Stress distribution in prestressed concrete beam [8]

A challenge for prestressed concrete structures might be corrosion in tendons. Steel tendons are experiencing higher working stresses compared to non-prestressed steel, where contribution of corrosion can result to catastrophic failure. Based on previous reports, registered critical deteriorations and structural failures from corrosion of pre-tensioned concrete are relatively limited [9]. The main reason depends on dense and impermeable concrete cover. For post-tensioned tendons in ducts, high quality of grout contributes to fulfilling corrosion protection in critical environmental conditions. Corrosion in pre-tensioned tendons are divided in pitting type corrosion, stress corrosion and hydrogen embrittlement [10]. Pitting corrosion is described as an electrochemical process, resulting to “rusting” of the tendons. In addition, fracture of reinforcement and highly stressed strands act in pitting corrosion, minimizing the load-bearing capacity of the girders [11]. Prestressed concrete structures endure stress corrosion under high stress values, where hairline cracks will begin to form. These cracks will develop to sudden failure without any external warning in the structures. Hydrogen embrittlement gives failure affected by hydrogen sulfide. Chemical reaction of hydrogen sulfide changes the mechanical properties of the steel tendons [10].

Corrosive environments for prestressed concrete bridges are categorized in three different processes. The first process clarifies variations in the mechanical character of the concrete, and the second process increases the permeability of the concrete. The last process destroys the anticorrosive protective mechanism in the concrete. All these processes combined are related to prestressed concrete bridges exposed to marine environment. Corrosion hazards for the prestressing steel in a marine environment increase from its chloride content, chemical attack of sea water, freezing or thawing and abrasion of concrete by ice. Corrosion dominating environment takes place if high amount of deicer salts is applied to the prestressed roadway bridges. In a hot climate, piles and foundations reacting with high concentration of calcium, magnesium, potassium and sulfites endure corrosion attack [10].

Cracks in prestressed structures are mainly caused by corrosion, frost, deflection, shrinkage, and insecure aggregate-cement combination. Corrosion of reinforcing steel is the main source for internal pressure through volumetric changes, further developing to excessive cracking. The amount of corrosion depends on concrete's high quality, density, and capacity of hydrated cement paste. These are further related to permeability of the prestressed concrete structures, connected to porosity dependent on the material's size and distribution [10].

### 2.3 Deterioration of reinforced concrete structures

According to *chapter 2.4(1)* in *Eurocode NS-EN 1990* [12], a durable structure should be able to resist the deterioration over the design working life in a manner that does not affect the structure's capacity with regard to environment and the expected maintenance. *Chapter 4.1(1)* in *NS-EN 1990-1-1* describes that a durable construction should in its design working life fulfil the requirements of serviceability, strength, and stability without reduction in utility or need for extensive unforeseen maintenance [12].

There can be different factors causing deterioration, classified as physical, mechanical, chemical, biological, and structural induced deterioration. Figure 4 presents the cause of deterioration of concrete structures [13]. It is important to emphasize that corrosion of reinforcement does not only apply for reinforced concrete, but also prestressed concrete.

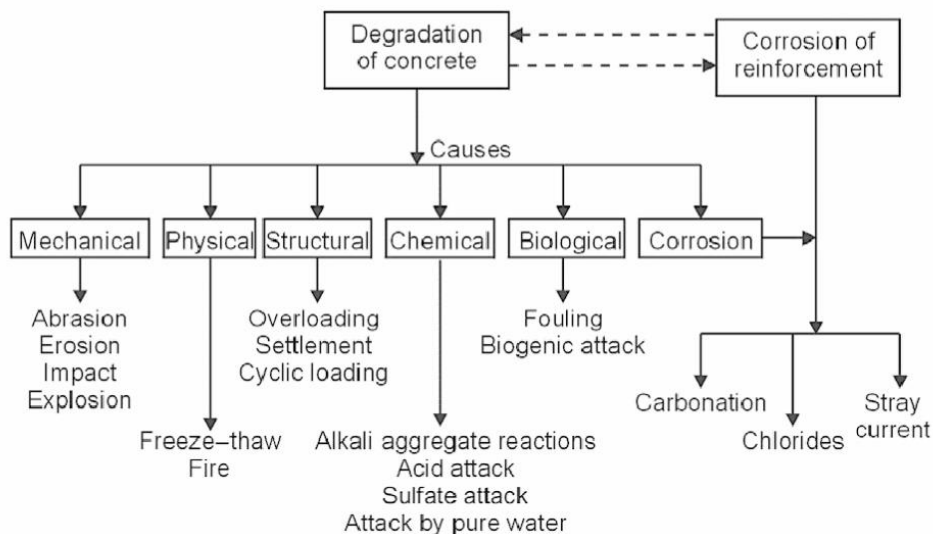


Figure 4 Causes of deterioration [13]

Corrosion of concrete structures is a major factor of deterioration, which is identified as carbonation induced corrosion and chloride induced. Still, chloride induced corrosion is one of the major causes of structural failure, as seen in Figure 5, showing the failure causes of German infrastructure.

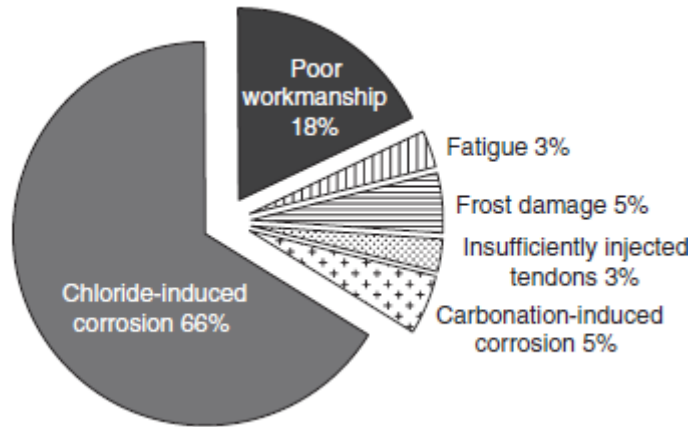


Figure 5 Cause of structural failure [14]

### 2.3.1 Cracking

The main cause of deterioration in reinforced concrete is due to the properties of the matrix and the ingress of aggressive agents from the environment. Generally, signs of deterioration in concrete appear often as cracks and is divided into structural and non-structural cracking. Structural cracking is often used to bring forth desired mechanical properties, and are easier to design and estimate, such as cracking of a beam to mobilize the tensile properties of steel reinforcement. On the other hand, the concrete involvement with the environment results in non-structural cracking [1]. Figure 6 illustrates some of the non-structural cracks, and Table 1 explains the non-structural cracks according to the Figure 6.

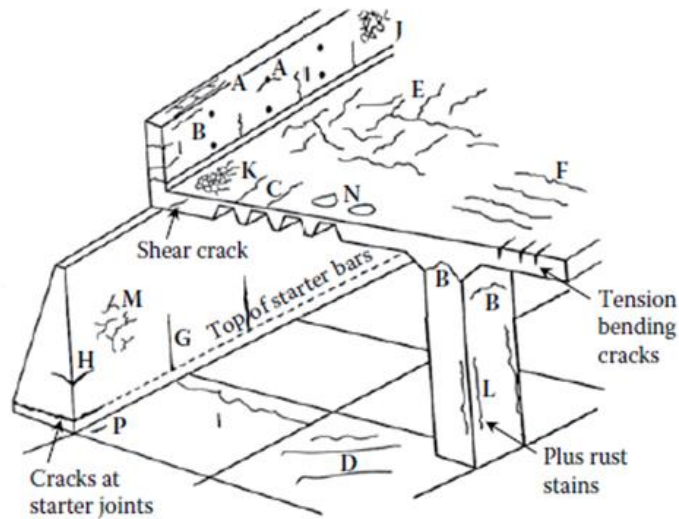


Figure 6 Illustration of non-structural cracks [1]

Table 1 Explanation of Figure 6

<b>Non-structural cracks</b>
Plastic settlement (A,B,C)
Plastic shrinkage ( D,E,F)
Early thermal contraction (G,H)
Long-term drying shrinkage (I)
Crazing (J,K)
Corrosion (L,M)
ASR (N)

Independent of cracking category and impact on the strength of the concrete structures, the cracks permit the transportation of aggressive agents into the material, for instance chlorides. These cracks have a great influence on the deterioration of the concrete, exposing the steel reinforcement that affects the durability and service life of the structure. Therefore, the impact of the concrete cracking is an important part of the service life prediction, where factor such as crack morphology, growth rate, permeability and transport properties are taken into account [15]. Figure 7 summarizes the main non-structural cracks. Cracks can also be divided into macro- and microcracks, associated with the size of the cracks and affecting the concrete properties and deterioration mechanism. The microcracks applies to the hardened cement paste with a size up to 30 microns, occurring due to the restraining of the aggregates, while macrocracks can have a size up to several millimeters occurring from load, drying shrinkage cracks or AAR [1].

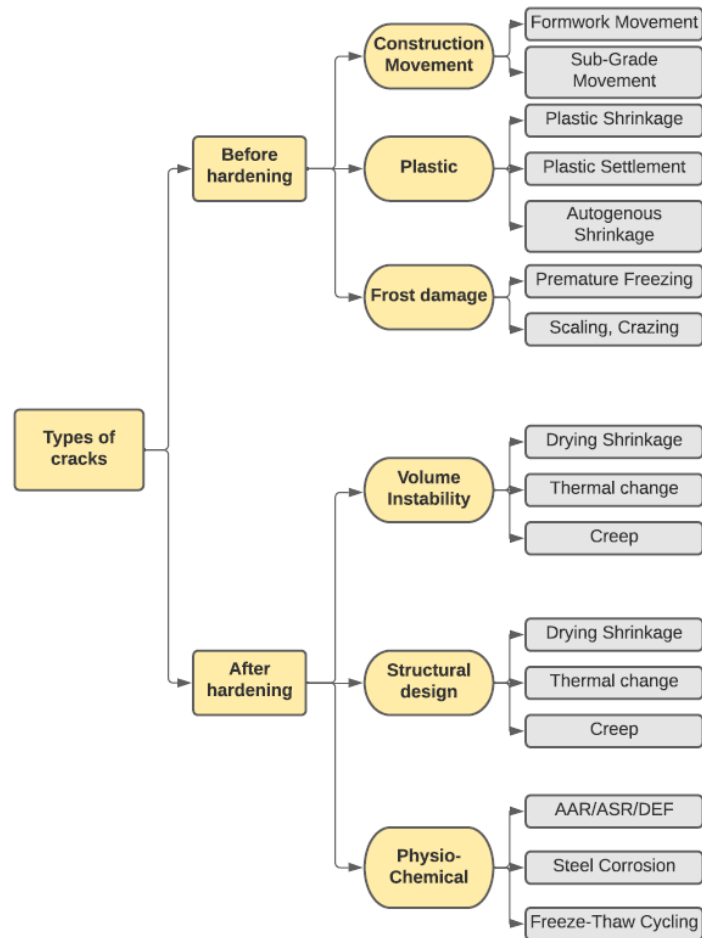


Figure 7 Causes and types of cracks [15]

### 2.3.2 Mechanical

Mechanical cause of deterioration is defined as concrete structures exposed to impacts, overloading, movements from settlement, vibration, blasting and other forms of loading [16]. The concrete structures ability to resist mechanical deterioration are associated with their structural integrity, reliant on the strength, toughness, and internal properties of the concrete related to its composition [1]. From an NDT point of view, the simplest way of assessing and detecting these damages is through VI. Some of these deterioration mechanisms are mentioned and illustrated in ACI 201.1R-08 [17].

#### Abrasion and erosion

Abrasion of concrete is caused by the structural lack of resisting friction, grinding, impact, overloading, and local crushing caused by movement of traffic on the surface, such as vehicles and pedestrians. The wear of the concrete cover results in loss of mass as the aggregates is exposed to further deterioration affecting the bond of aggregate and hardened cement paste. If no measures are implemented, the reinforcement will progressively be exposed, permitting corrosion and other deterioration mechanisms [1, 18, 19].

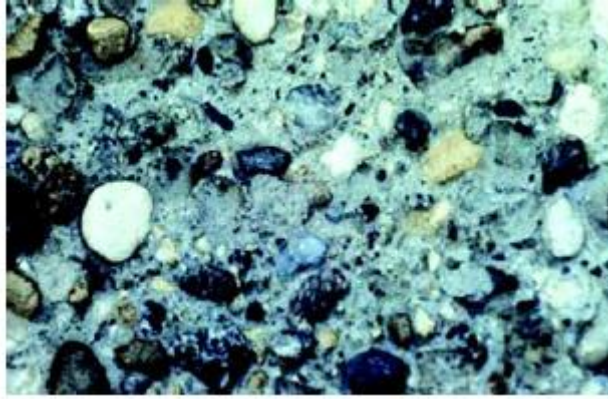


Figure 8 Deterioration due to erosion and abrasion [17]

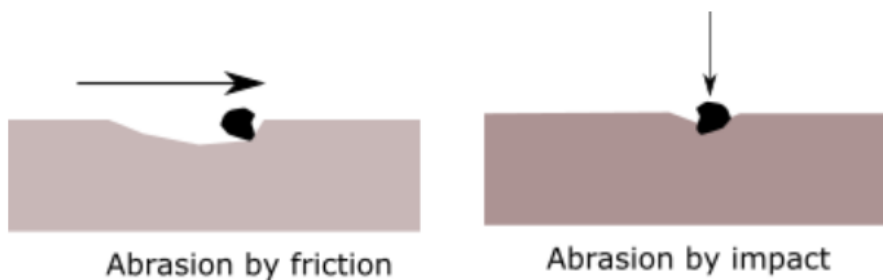


Figure 9 Schematic representation of abrasion due to friction and abrasion [18]

The mechanism and damage of erosion is identical to abrasion. However, the deterioration of the concrete surface is caused by fluids containing particles such as silt, sand, gravel, rock, and ice, and the damage is depending on the flow conditions. This form of deterioration is often observed in concrete tunnels, passages, channels, and conduits. The degree of abrasion and erosion is depending on the compressive strength of the concrete, including the hardness of cement paste and aggregate, the bond between these components, the size of aggregate, lower w/c ratio and curing time [1, 18, 19]. The following measures can be implemented to achieve a compact concrete and to increase the abrasion resistance [1, 18]:

- Increase the curing time
- Improve proportioning of aggregates and cement
- Cement replacements such as fly ash
- Consider fiber reinforcement

#### Impact and explosion:

Baeră et al. [20] defines impact as following:

*“Impact can be generally defined as a mass (i.e., the impacting mass) striking another mass (i.e., the impacted mass), under certain conditions of velocity, geometry and material properties of the impacting bodies”* [20, p. 240].

Impact load might be categorized as a single point impact loading or distributed impact loads. The single point impact may occur from a vehicular collision with a concrete supporting element such as a column, while a distributed impact load may arise from an explosion. Figure 10a illustrates the consequences of a single point impact on a concrete beam. The impact propagates compressive stress waves into the depth of the concrete, resulting in compression damages and spalling in the surface of the concrete. Other damages and failures that may occur are flexural, shear and flexure-shear failure as illustrated from Figure 10b - Figure 10e. Factors affecting the degree of damage are the impact intensity, confinement and the bond between the concrete and reinforcement [21].

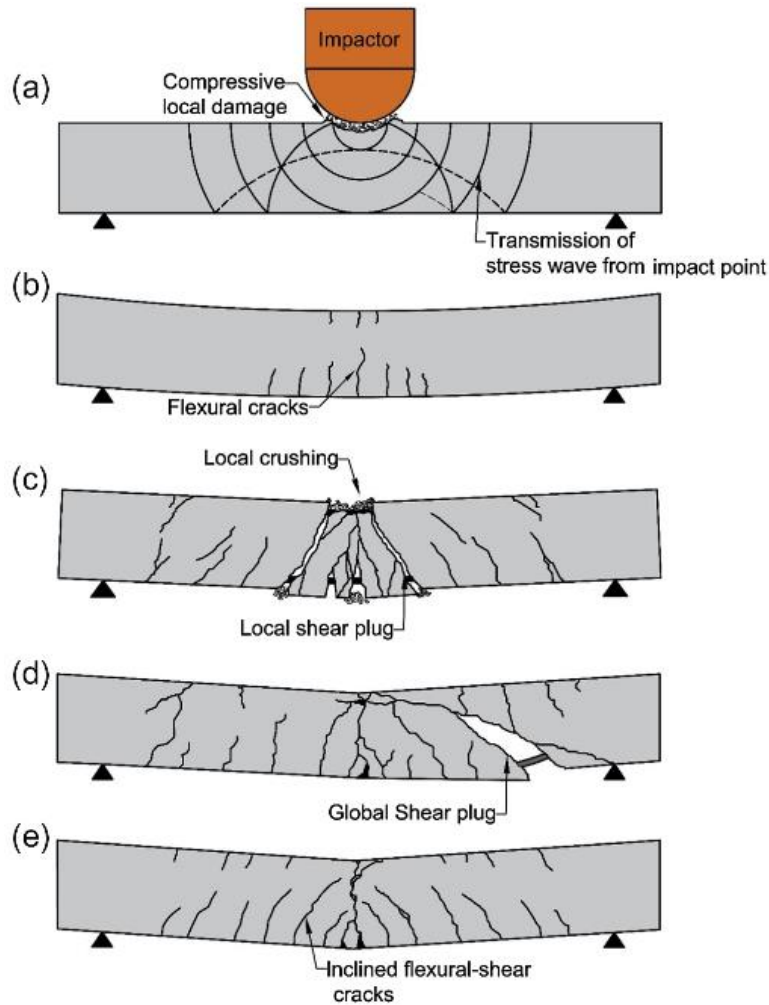


Figure 10 Effects of impact load on reinforced beam: (a) Local damage, (b) global flexural failure, (c) global shear failure, (d) global flexural-shear failure [21]

Explosion, also known as blast loading, is a major cause of damage affecting the structural integrity of the concrete structure due to the possibility of collapsing of the external and internal support system. The loading may arise from different sources such as a bomb, and the blast effects are classified as primary effects and secondary effects. Mainly, the damages from an explosion are caused by shockwaves increasing the pressure of the surrounding air, as seen in Figure 11. Other effects are ground shock in the form of vibration, heating that weakens the material or fragments from the explosion source hitting the structure [22].



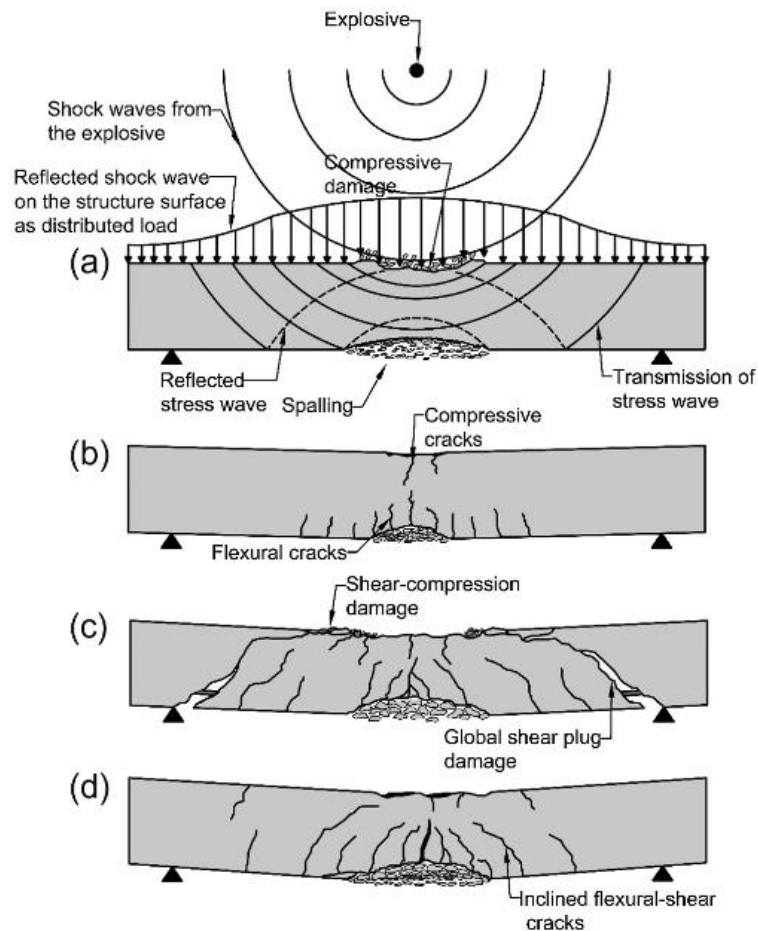


Figure 11 Effects of blast load on reinforced beam: (a) Local damage, (b) global flexural failure, (c) global shear failure, (d) global flexural-shear failure [21]

The blast load is applied as a distributed load and propagates in the depth of the concrete. This causes compressive damage at the surface of the concrete element and spalling and fragmentation on the tensile zone of the applied load, as illustrated in Figure 11a. The degree of damages is depending on the structural capacity of the concrete, for instance shear and bond resistance. Other damages and failures that may occur are flexural, shear and flexure-shear failure as illustrated from Figure 11b - Figure 11d [21].

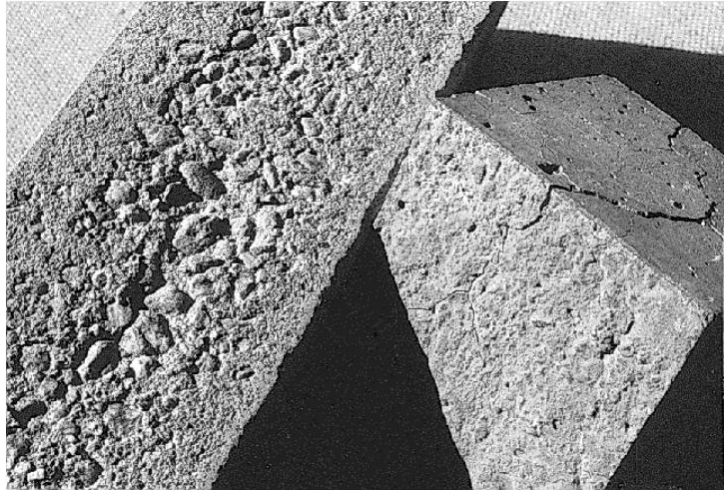
### 2.3.3 Physical

In the literature, the physical and mechanical causes of deterioration are often used interchangeably. A distinction to refer to is the influence of the environment on physical causes of deteriorations. The physical causes that will be addressed in this thesis are according to Figure 4.

#### Freeze-thaw

Freeze-thaw is a major source of deterioration characterized by surface scaling. Freeze-thaw is caused by temperature dropping to freezing point below 0°C. The tensile stress increases due to 9% volume expansion of frozen water in the pore system of the concrete, resulting in cracking or spalling in the outer layer of the material [13].





*Figure 12 Damage of different concretes due to freeze-thaw [23]*

The surface is usually more exposed to moisture and direct contact of water. In these circumstances, a pumping effect is created due to the freeze-thaw loads. The pore system in the surface acquires and increases moisture content. Therefore, the damage is initiated in the surface [24].

There are three properties that determines the degree of frozen pores [13]:

- The low thermal conductivity of concrete
- The concentration of ions in the pore water
- The diameter of pores affecting the freezing point

Generally, the freezing occurs in capillary pore water. Environmental conditions have an impact on the degree of deterioration, such as degree of water saturation, freeze-thaw cycles, freezing rate and the lowest measured temperature. The addition of salts in contact with concrete affects the material by lowering the freezing point, resulting in scaling and detachment of cement paste. The hydraulic pressure theory presents that the remaining liquid is pressurized by the expanding ice, and the pressure is depending on pore diameter and the moving distance of the remaining liquid. To release the pressure, there must be empty pores close to where the pressure is originating from. An increased pressure is achieved when the pore diameter is decreased and when the moving distance to empty the pores is increased [13].

The number of freeze-thaw cycles determines the frost resistance and degree of deterioration of concrete, in particular the saturation of the pores and the porosity of the concrete. A fully saturated pore under hydraulic pressure results in the microstructure expanding because of released pressure causing cracking. The porosity of the concrete is determined by the w/c ratio. Concrete with high porosity collects water lead from the capillary pores due to frozen water, which lowers the pressure and permits the growth of ice crystals. The degree of saturation increases for porous concrete, resulting in lower resistance against frost. Therefore, a lower w/c ratio results in higher frost resistance [13].

The main purpose of air-entrained concrete is to avoid generation of stress in the capillary pores when the water freezes. Etman and Ahmaed [25] proved that the use of air-entrained concrete provides a more durable concrete and showed that the optimal percent of air to obtain a better frost resistance is 0.15% of cement weight. It must be noticed that the air-entrained concrete has a lower compressive strength compared to no air-entrained concrete. To maintain the same strength as no air-entrained concrete, a lower w/c ratio should be considered [13, 23], as demonstrated by Shang and Yi [26]. Their experimental study showed that an air content of 5.5-6.5% and a w/c ratio of 0.36 provided the highest resistance against 400 cycles of freeze-thaw and a lower decrease in modulus of elasticity, compared to other samples.

Karakurt and Bayazit [27] studied the effect of air- and no air-entrainment, silica fume and fly ash on the freeze-thaw resistance. The degree of surface scaling on the different test specimen obtained from the paper is shown in Figure 13.

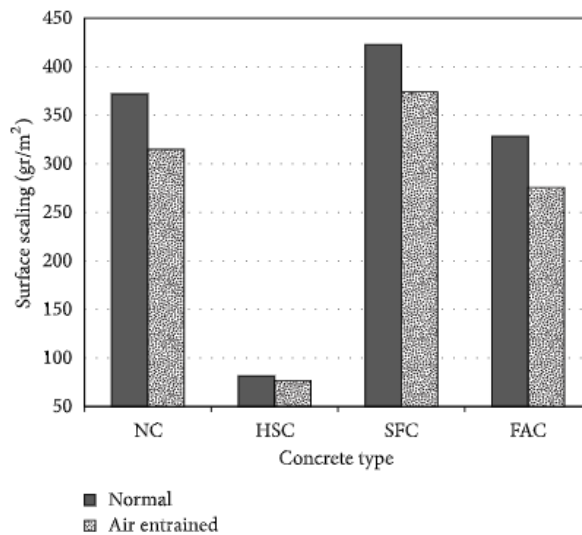


Figure 13 Surface scaling of normal concrete (NC), high strength concrete (HSC), silica fume concrete (SFC) and fly ash concert (FAC) [27]

From Figure 13, the surface scaling is demonstrated to be significantly lower in high strength concrete (HSC), consisting of silica fume and a w/c ratio of 0.30. This composition attributes a denser concrete with lower porosity. In contrast, other concrete specimen has a w/c ratio of 0.46, explaining the provided results. The entrainment of air is shown to result in lower surface scaling for all concrete types, thus providing lower compressive strength. The addition of silica fume was proven to result in higher degree of deterioration compared to other samples, due to reduction in workability and poorer compaction of the fresh concrete. Fly ash provided a better freeze-thaw resistance [27].

Musleh and Gutzwiller [27, 28] studied the effect of freeze-thaw on post-tensioned and reinforced concrete structures. When increasing the numbers of freeze-thaw cycles, the dynamic modulus elasticity decreased with maximum 10-25% for post-tensioned concrete, while a decrease of up to 50% were observed for reinforced concrete. The study also showed that the post-tensioned concrete withstands several cycles of freeze-thaw.

## Fire

In general, concrete has an excellent performance against temperature growth. However, when exposed to fire and high temperatures, a reduction in strength is experienced. The factors determining the fire resistance includes concrete cover, cross section of the element, material properties and the steel reinforcement [29]. The most common effect of fire in reinforced concrete is spalling of the surface, which is a result of the heating of the steel reinforcement. This damage of concrete cover exposes the reinforcement to high temperatures, as seen in Figure 14, affecting the structural integrity of the structure due to a decreased strength of the steel reinforcement. A reduction of the cross section of the element impacts the overall ability to support the imposed loads, resulting in skewed distribution of loads on the remaining structure. The heat from fire also generates thermal expansion and dehydration of the concrete and often result in cracking that permits the increasing of thermal stresses and additional cracking of the concrete [30].



*Figure 14 Spalling of concrete beam and column as a result of fire [31]*

According to Tufail et al. [32], the increasing of temperature e.g., fire, result in a decrease in various mechanical properties of concrete, such as the compressive strength, tensile strength, and modulus of elasticity. These properties showed an inversely proportional behavior in contrast to the temperature in the sense that these properties decreased with the increasing temperature. The study showed beneficial effects of granite as coarse aggregate, providing the highest compressive strength, tensile strength, and modulus of elasticity, while quartzite and granite provided the second-best results and the lowest values of these properties, respectively.

### 2.3.4 Structural Overload

Damage because of overloading may occur from different reasons, e.g. the structure being exposed to loads not designed for the purpose of the service or the structure is loaded before achieving the design strength. For instance, overload cracking can appear in post-tensioned constructions due to early release of strands [33]. Normally, the ductile of the concrete

prevents the structure from sudden failure and larger deflections and deformations is experience at overload as a safety precaution for possible collapse. Warner [34] remarks that ductility of concrete cannot be the only structural property considered to achieve a large deflection from an overloading, as this might not be the case in every scenario. Softening of the structure is necessary and desired for this behavior to occur.

### Settlement

Settlement is a described as a change in stress to the ground causing vertical movement of the earth occurring due to different reasons, such as increased stress from a structure. The movement of the ground results in loss of support beneath the concrete structure causing damage and distortion, affecting the performance and may result in failure. A common damage is cracking of slabs, as seen in Figure 15 [33].

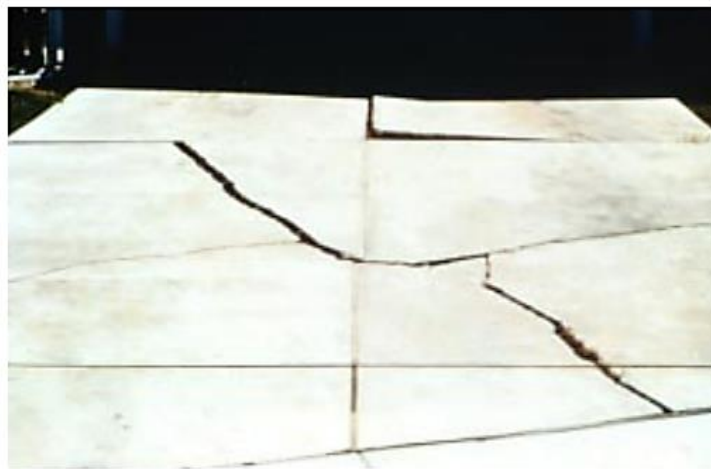


Figure 15 Cracking due to settlement [33]

### Cyclic loading

According to [35], cycling load is defined as following:

*“Cyclic loading is the application of repeated or fluctuating stresses, strains, or stress intensities to locations on structural components. The degradation that may occur at the location is referred to as fatigue degradation”*

The cyclic loading may arise from different sources, both structural and environmental, and accumulates microcracks which allows further deterioration of the concrete.

### 2.3.5 Chemical

#### Alkali–aggregate reactions

Alkali-Aggregate Reactions (AAR) is a generic term considering a chemical reaction due to accessible alkalis in the cement and aggregates. These types of reactions are known as the Alkali-Silica Reaction (ASR) and the Alkali-Carbonate rock Reaction (ACR). ASR occurs in the pore solution in which the alkalis react with some silica’s, causing the formation of extensive alkali-silica gel in the concrete. The moisture absorption causes expansion of alkali-silica gel



and results in microcracks of aggregate and cement [1, 36]. Figure 16 shows an electron microscope image of an internal cracking due to ASR. ASR is characterized by the reaction between alkali hydroxides and dolomite crystals in the clay matrix, causing expansion of the coarse aggregate particles [1].

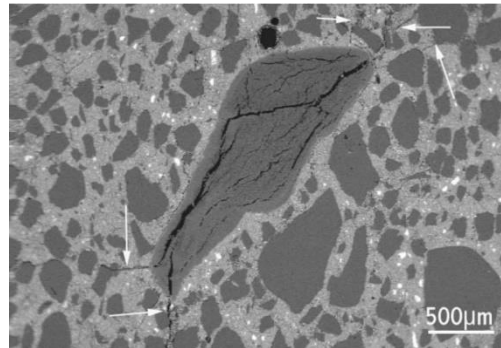


Figure 16 Electron microscope image of an internal crack due to ASR [37]

The ASR expansion results in visual cracking, expansion in the surface of the concrete structure and the characteristics of the cracks depend on the application of reinforcement in the concrete. The cracks appear as random patterns with several fine crack shapes resembling a map, illustrated in Figure 17. Therefore, named map cracking is known in non-reinforced concrete. However, cracks tend to reflect the rebars in reinforced concrete, as shown in Figure 18, where the cracking and expansion occur due to the restraining by the rebars. The cracks can also appear along the stress direction of columns and beams in case of heavily reinforced or prestressed concrete [38, 39].



Figure 17 Map cracking due to ASR [23]

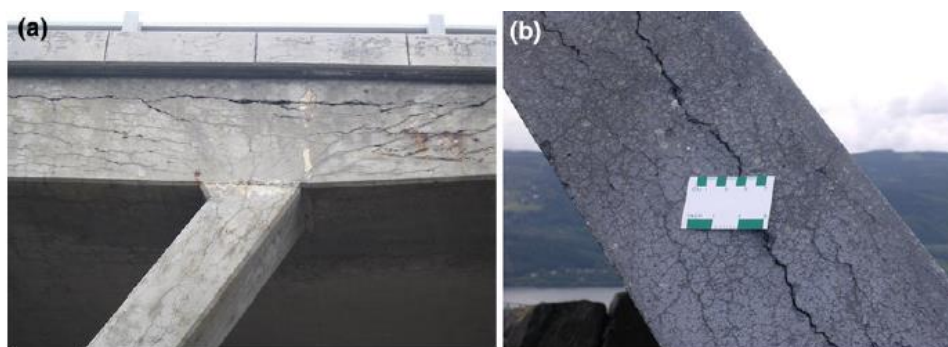


Figure 18 ASR induced crack pattern in reinforced concrete [24]

There are three requirements for ASR to occur in the concrete and if one of these components is removed, the reaction is prevented [40]:

- Presence of reactive silica (aggregate)
- High concentration of alkali is required
- Sufficient level of moisture

Further, factors that may influence the presence of ASR are stoichiometry, the properties of alkalis, reactive silica, humidity, temperature, concrete stiffness, or aggregate size [38]. Giaccio et al. [41] investigated the effect of ASR by using three different reactive aggregates and comparing these with normal concrete. This study shows no strength gain for the samples with reactive aggregates after 28 days, compared to normal concrete which has an increased compressive strength. The early internal crack due to ASR compared to normal concrete has a significant impact on the failure mechanism of concrete in compression, resulting in premature failure. Extensive cracking was also noticed from the load-deflection curve of concrete exposed to ASR.

Another research project examined a bridge demolished because of alkali-aggregate reactions. A part of the investigating was to replicate the concrete mix using the same aggregate as for the demolished bridge, and the aggregate were classified as reactive. Three concrete mixes were used in this investigation. Two of those had different cement contents, representing 0.5 kg/m<sup>3</sup> alkali content in difference, while the third mix were added fly ash to document the beneficial effect to prevent the development of ASR. The study showed that reactive aggregate in combination with higher temperature result in higher expansion in the concrete, except for the samples with fly ash demonstrating an insignificant expansion. For instance, the sample with 0.5 kg/m<sup>3</sup> higher alkali content and a temperature of 60°C resulted in 30% higher expansion the first year. A reduction of dynamic modulus of elasticity with increasing expansion were also observed, indicating the initiation of internal cracking in the concrete.

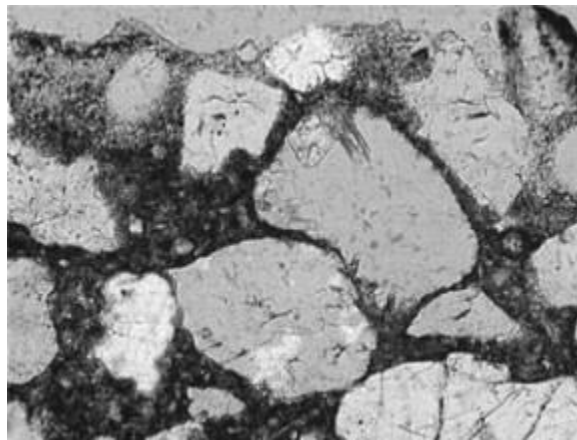
Tests were also conducted on field exposed concrete cubes added air-entrained admixture. These samples were compared to the samples from the original bridge, showing that the reconstructed samples had a considerable higher expansion. The explanation can be linked to the measured dynamic modulus of elasticity of the samples from the bridge, which are relatively low in value, indicating that the concrete had already developed internal cracking [42].

### Acid attack

Acid attack occurs when the liquid's pH value is below 6.5. A reaction between an acid and calcium hydroxide (Ca(OH)<sub>2</sub>) is active, producing a highly soluble calcium salt. Although, the soluble calcium salts are removed from the cement paste, reducing the paste structure. Acid attack can be divided in sulfuric, nitric, acetic, hydrochloric, and carbonic attack. Following attack on concrete is dependent on acid type and its concentration. Normally, Ca(OH)<sub>2</sub> in the hydrated cement and aggregate are influenced by acid attack. Amount of acid attack can be reduced by combining the Portland cement with Supplementary Cement Materials (SCMs) because this minimizes Ca(OH)<sub>2</sub> in the hydrated cement. Fly ash, ground granulated blast-

furnace slag (GGBFS) and silica fume are some SCMs contributors reducing the possibilities for acid attack [1].

According to Nijland and Larbi [43], acid attack on concrete results in loss of cohesiveness, reduced concrete strength and enhancement of capillary porosity. Figure 19 indicates a concrete surface affected by acid attack. There is clear sign of leaching from the cement paste matrix, resulting to reduction of matrix's cohesion and increased capillary porosity. The cement paste endures bonding loss to the aggregate but following aspect does not influence the microstructure and concrete quality. Therefore, acid attacks can be vulnerable for long-term durability [43]. Singh [44] emphasizes sulfuric acid attack, where production of gypsum attacks the cement paste. Following research paper clarifies that sulfuric acid attack results to weakness of the concrete micro-structure, reduction of size specimen, cement paste and compressive strength.



*Figure 19 Acid attack along the concrete surface from a micrograph [43]*

### Sulfate attack

Sulfate attack is defined as a progressive loss of cement paste strength based on the connection between hydration products. Sulfate attack is divided in an external and internal part. External sulfate attack controls ions that penetrates the concrete, reacting with cement matrix components to cause extensive chemical reactions. The brutality of external sulfate attack depends on sulfate concentration either in water or soil. To withstand external sulfate attack, concrete quality has a high significance. In addition, low permeability tolerates this type of sulfate attack by minimizing the sulfate penetration, which is dependent on blended cement and reducing w/c ratio. Blended cement is referred to either pozzolanic or blast furnace slag cement, minimizing  $\text{Ca}(\text{OH})_2$  content and refining the matrix's pore structure. A reduced amount of tricalcium aluminate ( $\text{C}_3\text{A}$ ) and calcium aluminoferrite ( $\text{C}_4\text{AF}$ ) is also dominant for the severity of sulfate attack. Three classes of aggressiveness that are related to sulfate attack are XA1, XA2 and XA3, briefly explained on the European standard EN 206-1, recommending minimum cement content, minimum strength and maximum w/c ratio for each classes [13, 45].

Internal sulfate attack, also known as delayed ettringite formation (DEF), occurs without exposure to a sulfate-bearing environment. The source of ions in internal sulfate attack is in the concrete itself, where higher presence of sulfates increases the possibility of internal sulfate attack. Extensive cracking of cement paste is related to internal sulfate attacks. Cracks are visible in and along the paste, and aggregate size is crucial for the crack opening in the paste. The probability of internal sulfate attack can increase depending on pre-existing damages of concrete, for instance freeze-thaw or ASR. To minimize the possibilities for internal sulfate attack, including cements with lower strength class are recommended. Simultaneously, cement containing either fly ash or slag may contribute to prevent internal sulfate attack [13].

#### Attack by pure water

Attack by pure water describes water amount with low dissolved solids. Calcium ions are familiar within dissolved solids, acting aggressively towards the concrete. Concrete permeability is an important factor for the degree of the attack by pure water. Lower amount of  $\text{Ca}(\text{OH})_2$  has impressive resistance against attack by pure water, such as blast furnace slag cement concrete. According to EN 206-1 [45], the aggressiveness of waters to concrete is decided from pH value, free  $\text{CO}_2$  content and sulfate ions. Attack of concrete by very soft waters is a form of pure water attack, dissolving free lime solubility of 1.7 g/l. Leaching of free lime are damaging other constituents of the cement paste, diminishing the concrete resistance [13].

### 2.3.6 Biological

#### Fouling

Biofouling in correlation with the marine environment is relevant for materials submerged in seawater, divided in microfouling and macrofouling. Microfouling specifies that the submerged concrete is quickly occupied by marine bacteria, establishing a bacterial biofilm. Macrofouling emphasizes occupation of bacterial biofilm by other micro- and macroorganisms. Biofouling includes an image-analysis-based method and wet/dry-weight biomass measurement, clearly illustrating the evolution of biofouling formation. Factors that can affect formation of biofouling are chemical composition, porosity, pH and roughness. In addition, chemical composition for a cement type is conclusive for biofouling's formation. For instance, Portland cement CEM I and slag cement CEM III are two influential binder types [46].

#### Biogenic sulfuric attack

Biogenic sulfuric acid attack (BSA) is a common form of biodegradation mechanism damaging the concrete, causing global infrastructure deterioration. This type of attack occurs normally in concrete sewers. Hydrogen sulfide is the main source for BSA, produced by sulfate reducing bacteria (SRB). According to Monteny et al. [47, 48], BSA causes higher deterioration based on microbial growth and movement in humid, porous and soft corrosion layer formed on concrete. On the other hand, Okabe et al. [49] emphasize that low amount of oxygen and reduced nutrients in the corrosion layers prevent the microbial succession in the corrosion layer. BSA can be described as a slow corrosion process from 1 mm/year to maximum 5 mm/year. At the same time, the risk of BSA is dependent on the relationship between bacteria



and the substratum. Related to BSA, the gypsum layer in concrete is regulating high humidity level in the environment, protecting the bacteria against dry conditions [47, 50].

### 2.3.7 Corrosion

Corrosion in steel is described as an electrochemical process consisted of cathodic and anodic areas. Electro-galvanic potential differences are developed on the steel surface, with concrete pore solution behaving as an electrolyte. The electrochemical process begins with an oxidation and electrons are consumed at the cathode by reduction and electrons transferred in the steel bars between anode and cathode producing a rust. In reinforced concrete, common explanations for corrosion are either carbonation or chloride-induced corrosion [1]. The modelling of corrosion is divided into initiation and propagation period, representing the time of depassivation and different stages of deterioration of the structure.

#### Carbonation of concrete

Carbonation is a major degradation of concrete due to its effects on corrosion of steel reinforcement. This mechanism is a result of a reaction between carbon dioxide from the air and calcium hydroxide in the hydrated cement paste.  $\text{CO}_2$  in the air diffuses into the concrete and reacts with pore liquid. The reaction produce carbonate ( $\text{CO}_3^{2-}$ ) that reacts with calcium resulting in calcium carbonate ( $\text{CaCO}_3$ ), known as carbonation. This reaction neutralizes the pore solution causing the pH value of the concrete to drop down to between 8 and 9. The process of carbonation is initiated in the concrete surface, as seen in Figure 20a, and will gradually penetrate the construction material, until reaching the steel reinforcement [13], [51].

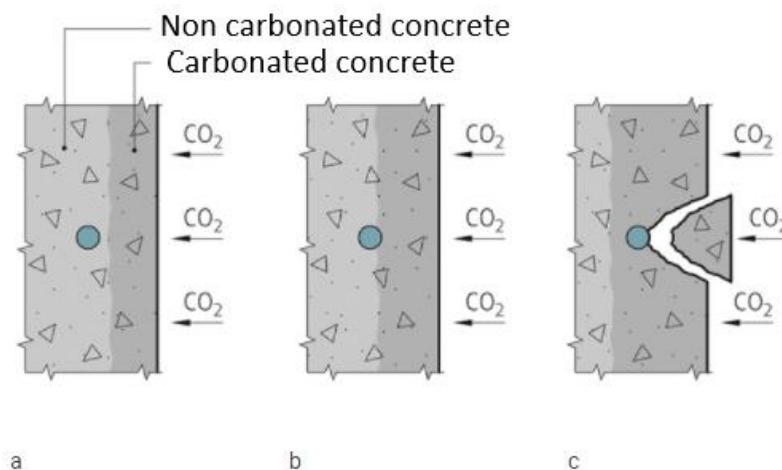


Figure 20 Representation of carbonation adapted from [51] ; a) carbonation of the concrete, b) carbonation reaching and depassivating the reinforcement, c) penetration of carbonation, initiating corrosion cracking and spalling the concrete

When reaching the steel reinforcement (Figure 20b) the pH value of the pore solution will passivate the reinforcement. Further, the carbonation will initiate active corrosion causing visual cracking and spalling of the concrete structure (Figure 20c). The concrete cover is the main factor determining the penetration of carbonation which is crucial in terms of durability and service life of the concrete structure. A method of detecting carbonation is through

spraying of phenolphthalein on the concrete which react and distinguishes carbonated concrete from normal concrete. The reaction appears as a pink color for concrete with a pH value greater than 9 [13, 51].

Several factors influencing the carbonation rate, mainly depending on the environment exposure and the concrete composition. The environmental factors that are important to address when considering carbonation are humidity, temperature, and concentration of CO<sub>2</sub>. Among the factors that may greatly affect the degree of carbonation ratio are relative humidity. Figure 21 represents that correlation between the carbonation rate and relative humidity, showing an increase in carbonation rate with increasing humidity [13],[51]. Elsalamawy et al. [52] also demonstrated the variation of humidity on carbonation. From the study, the carbonation depth increases with increasing humidity, and the highest level of carbonation is observed when the humidity is between 60-70%. Further, the degree of saturation and the presence of CO<sub>2</sub> are of great importance [52].

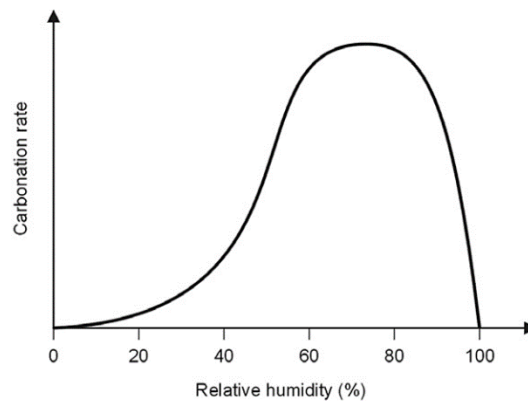


Figure 21 Carbonation rate as a function of relative humidity [13]

The carbonation rate and depth also increase with increasing CO<sub>2</sub> in the air, e.g., in motor vehicle tunnels [13, 51]. This was also proven by Cui et al. [53], however after the concentration of 20%, the increase rate of carbonation reduces to a great extent. The highest increase in carbonation was observed when CO<sub>2</sub> concentration increased from 2% to 10%. In this study, the scanning electron microscopy shows a denser microstructure in the concrete when the concrete is exposed to high CO<sub>2</sub> concentration. The reduction in CO<sub>2</sub> diffusion is due to denser surface with lower porosity as result of reduction of pore sizes and lower connectivity of the pores. The diffusion of CO<sub>2</sub> in the concrete increases in dry concrete due to air-filled pores, but the lack of water prevents the reactions [13],[51].

The effect of periodic wetting lowers the carbonation rate and decreases the carbonation depth. Further, the degree of this effect and its impact on the carbonation rate are dependent on wetting time, frequency, and duration of wetting-drying cycles. Frequent and short periods of wetting have a significant reduction on the carbonation penetration. Liu et al. [54] investigated the impact of temperature on carbonation. This study shows that higher temperature increases the carbonation depth, and the compressive strength decreases with the carbonation of concrete in a linear relation.

The parameters in concrete composition influencing the diffusion of CO<sub>2</sub> and carbonation rate includes cement type and concentration, curing time, w/c ration affecting the porosity of the concrete and admixtures. The influence of w/c ratio is shown in Figure 22, where the penetration of carbonation increases with increasing w/c ratio and the effect of different curing period demonstrates a decrease in carbonation depth. Balayssac et al. [55] investigated the importance of curing, but with the regard to cement content. For instance, after 18 months concretes with cement content of 420 kg/m<sup>3</sup> and 300 kg/m<sup>3</sup>, increasing the curing period from 1 to 3 days and 1 to 28 days, respectively, reduced the carbonation depth by 50% [55]. The reason for the difference is explained by the higher porosity of concrete with low cement concentration, and a longer curing time is therefore needed to obtain the same durability as for a concrete with high cement concentration.

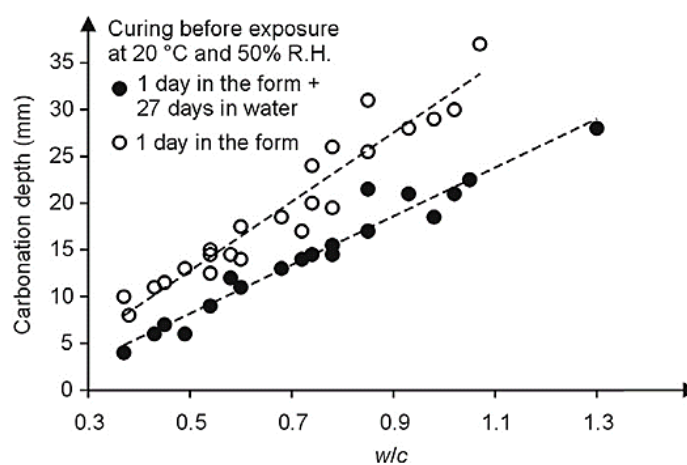


Figure 22 Influence of w/c ratio and carbonation depth [13]

The use of admixtures has been shown to have no beneficial effect on the carbonation rate. On the contrary Balayssac et al. [55] and Elsalamawy et al. [52] discovered that the addition of Ground Granulated Blast-furnace Slag (GGBS) resulted in higher carbonation depth, compared to concrete with Portland cement. Czarnecki et al. [56] discovered that the addition of fly ash increase the carbonation depth with 25%, compared to concrete with Portland cement. The replacement with silica fume only showed resistance against carbonation for w/c ratio exceeding 0.7. Therefore, the advantage of this binder is very limited. However, Elsalamawy et al. [52] showed that adding 10% silica fume with the combination of GGBS can possibly decrease the carbonation depth with 58%.

### Chloride induced corrosion

Chloride induced corrosion is a major cause of deterioration for reinforced concrete. Under normal condition, the presence of calcium hydroxide in hardened concrete dissolves OH<sup>-</sup> in the pore solution of the concrete. Depending on the concentration of this substance, the pH value in the pore solution of the concrete becomes alkaline (pH 12.5-14), which is to the advantage of the reinforcement steel from a durability point of view. In contact with the steel, the reinforcement becomes passivated due to protective layer of ferric oxyhydroxide between the steel and the environment [51].

There are two main reasons of depassivation and initiation of corrosion: the decrease of pH value of the pore solution due to carbonation or a certain concentration of chloride ions reaching the steel reinforcement. Regularly, the breakdown of the passive film occurs on a local level and the available chloride ions react with the surface of the steel. This weakened part of the reinforcement becomes an active zone in form of an anode, and the rest of the steel reinforcement still protected by the passive film acts as a cathode. The concentration of chlorides is increased to the anode due to the electrochemical reaction that induces a current from the anodic zone. Further, the corrosion occurs to the cathodic zone where reduction of oxygen takes place. Figure 23 illustrates the electrochemical reaction and the substances involved. The attack of chlorides is increased when  $\text{Cl}^-/\text{OH}^-$  in the pore solution is in contact with the steel reinforcement, resulting in pitting corrosion [13], [51].

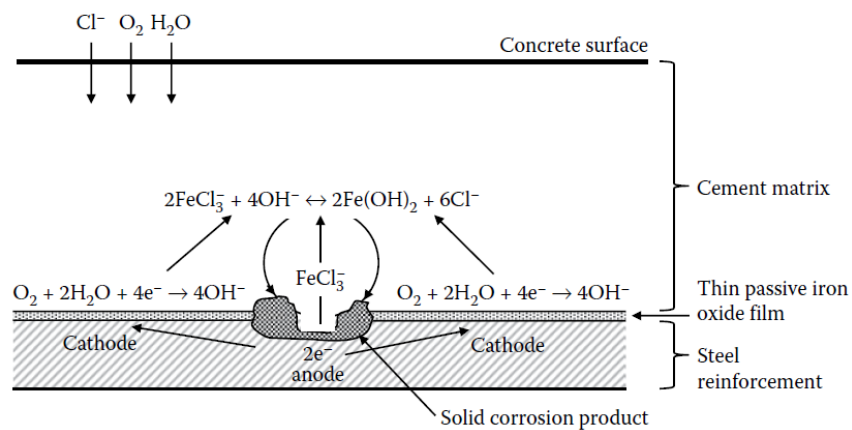


Figure 23 Chloride induced corrosion of reinforced concrete [1]

When addressing chloride induced corrosion of reinforced concrete, the parameter of critical chloride content or chloride threshold value is important to assess. This value is associated with the depassivation of reinforcement with the regard to the value of chlorides in the rebar and is an important parameter in service life design and service life prediction models. The properties affecting this threshold values are as following [1, 13]:

- Concrete cover thickness
- Temperature
- Relative humidity
- Electrochemical potential of the reinforcement
- Substances in the pore solution ( $\text{Cl}^-/\text{OH}^-$ )
- pH value of the pore solution
- Concentration of oxygen in contact with the steel reinforcement

The concentration level of chlorides to initiate corrosion is depending on the environmental exposure of the construction and the presence of oxygen that can reach the reinforcement. The corrosion of steel reinforcement affects the condition of the structure and the structural performance, from the esthetical appearance to serviceability and safety. The first signs of corrosion appear as rust spots on the surface of the concrete or as cracks on the concrete cover, which may result in spalling and delamination. The cracking is a consequence of the generated tensile stress from the volume expansion due to rust growth around the steel

reinforcement. Cracking increases the penetrability of the concrete cover layer, which is a main reason for rapid development of the corrosion process. When the reinforcement is subjected to direct environmental exposure because of damaged concrete cover, the serviceability and the safety of the structure is at stake. Further, the uniform or localized corrosion will have an impact on the properties of steel reinforcement, such as the load-bearing capacity due to the reduction in cross section of the reinforcement [13].

Almusallam [57], studied the effect of chloride induced corrosion on the mechanical properties of steel reinforcement. The load capacity had a significant decrease with the increasing degree of reinforcement corrosion as shown in Figure 24. This curve also shows that increasing degree of corrosion decreases the elongation before failure, indicating a brittle behavior of the steel bar. A loss in ductility and yield strain is noticed for corrosion higher than 12.6% [57].

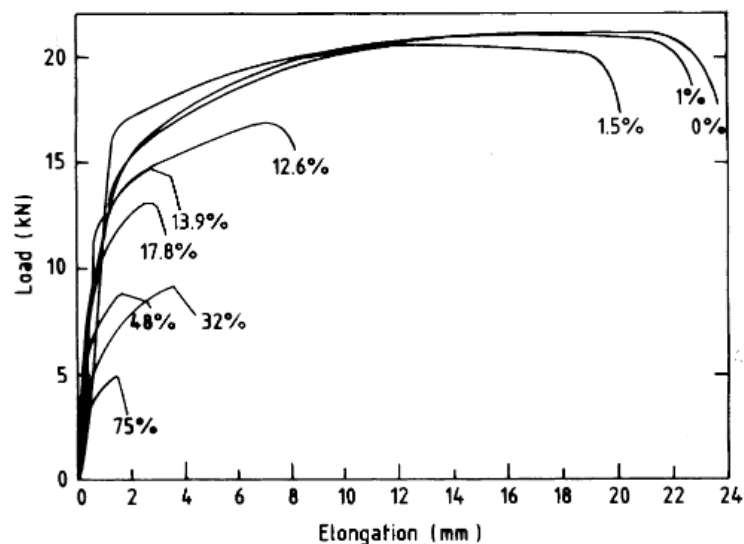


Figure 24 Load-elongation curve and different percentages of corrosion for 6 mm diameter steel bar [57]

Corrosion on the steel of post-tensioned concrete components may arise from the prestressing configuration and environmental exposure of the construction. This deterioration can be introduced during transport and storage from external sources such as moisture, sea spray and other contaminations. The presence of rust should not be the only factor of rejection of a strand because a small amount of rust does not affect the overall properties. However, the presence of pitting will have an impact on the loading and fatigue capacity, which may lead to failure and these strands should be rejected [58] [59].

After the application and tensioning of the strand in the concrete component, a time limit of 7 days is set for grouting in humid and marine environment to minimize the infiltration of aggressive substances. If contaminated water finds its way into the duct, initiation of corrosion is enabled with the presence of chlorides. This was the case during the construction of San Francisco-Oakland Bay Bridge. After 15 months 2% of the examined tendons showed moderate corrosion and few tendons indicated the initiation of localized pitting corrosion. Overall, only four samples failed to meet the requirements for minimum breaking strength and ductility [58] [60-62]. An important observation from this investigation is the importance

of grouting and the influence this consideration has on the integrity of the strands. This indicated that a longer period of ungrouted has the ability to propagate the corrosion which may result in a decrease of serviceability,

### 3. Assessment of concrete structures

The aspects of economy, history and serviceability have an important impact for the solution an engineer chooses when considering demolish, rebuild, or renovate a structure. These considerations have established the known methods of inspection, assessment, maintenance, repair, and rehabilitation of elderly damaged structures. This approach does not exclusively profit financially and extend the service life of a structure. The natural sources of this planet are additionally saved resulting in a sustainable gain. However, the existing concrete structures are showing increasing signs of deterioration even if building codes are considered, causing loss of serviceability and safety of concrete structures. Different reports uncover deterioration of concrete structures demanding high maintenance cost to improve the service life and performance level, and it is expected an increased need of rehabilitation work [16].

#### 3.1 Condition assessment of concrete structures

An assessment of concrete structures may be necessary for several reasons and is a crucial part of the long-term performance of the structure. Existing concrete structure is exposed to several deteriorations during the service life, as seen in chapter 2.3, causing various damages and distresses that influence the structure's integrity and durability. For that reason, condition assessment is an efficient approach to evaluating the extent of damages and implement measures to ensure safety and serviceability. The standard ISO 13822 [63] addresses the assessment of existing structures, providing principles and approaches considering structural reliability. A flowchart for this purpose is presented in Figure 25.

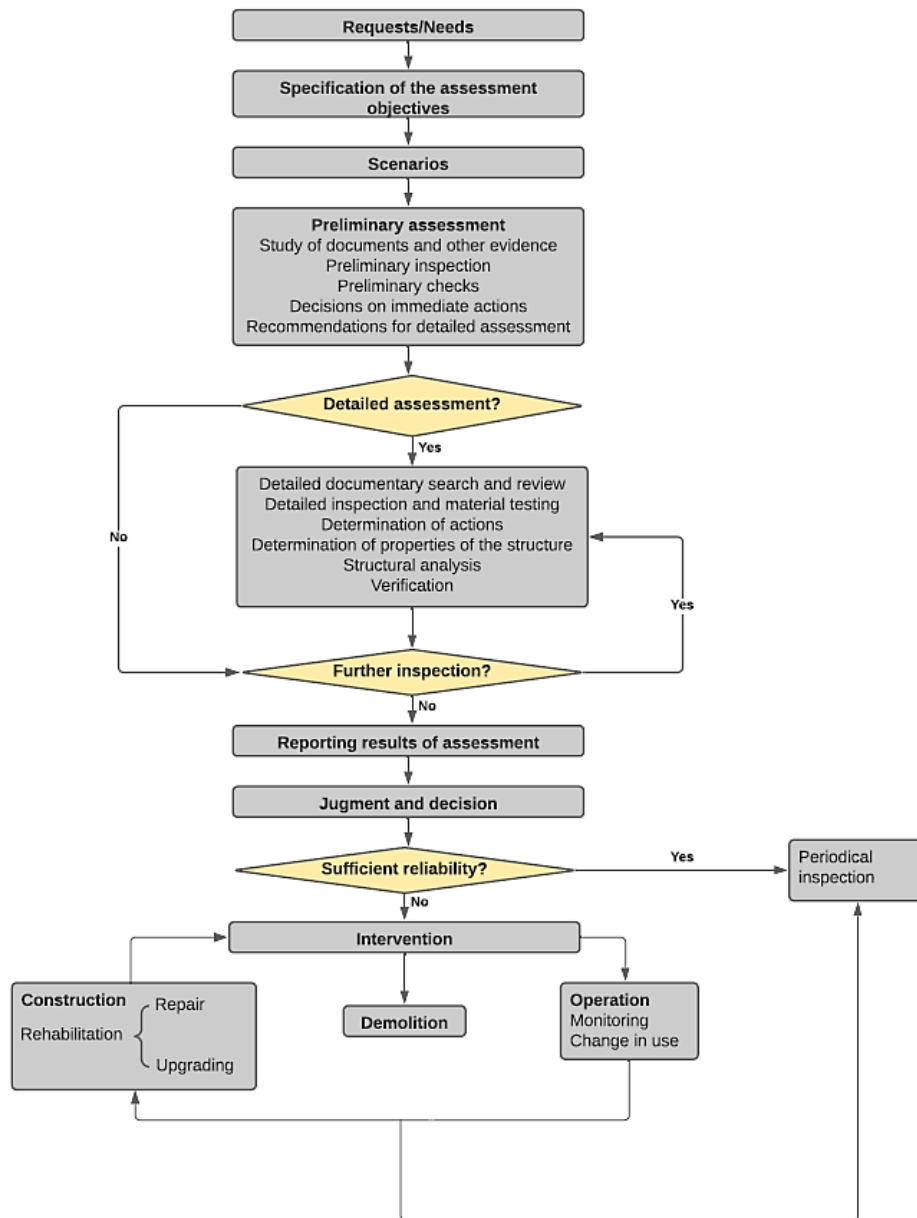


Figure 25 General flowchart for assessment of existing structures (ISO 13822) [64]

The purpose of the assessment is always the basis of the strategy that is proceeded. The various parts of the flowchart aim to identify and discover the cause of the structural condition and the extent of the problems. Implementation of various NDT methods is an important approach included to achieve the aim of the assessment. A part of the preliminary assessment is to map and clarify the possible causes of the deteriorations through a visual inspection. The preliminary assessment provides necessary guidance determining the applicable NDT methods that can be implemented in the detailed assessment for collecting crucial data to identify the extent of the problems. For this survey, several NDT methods may be applied to accomplish the aim of the investigation [63]. Figure 26 shows the essential parts of a detailed assessment. Under *determination of action*, an example of NDT methods is included that are relevant for several investigations.



A similar guideline for assessment of structures is ACI 364.1 R-94 [65]. Hence, this guide is specifically for concrete structures prior to rehabilitation and evaluates the necessity of rehabilitation based on the detailed investigation.

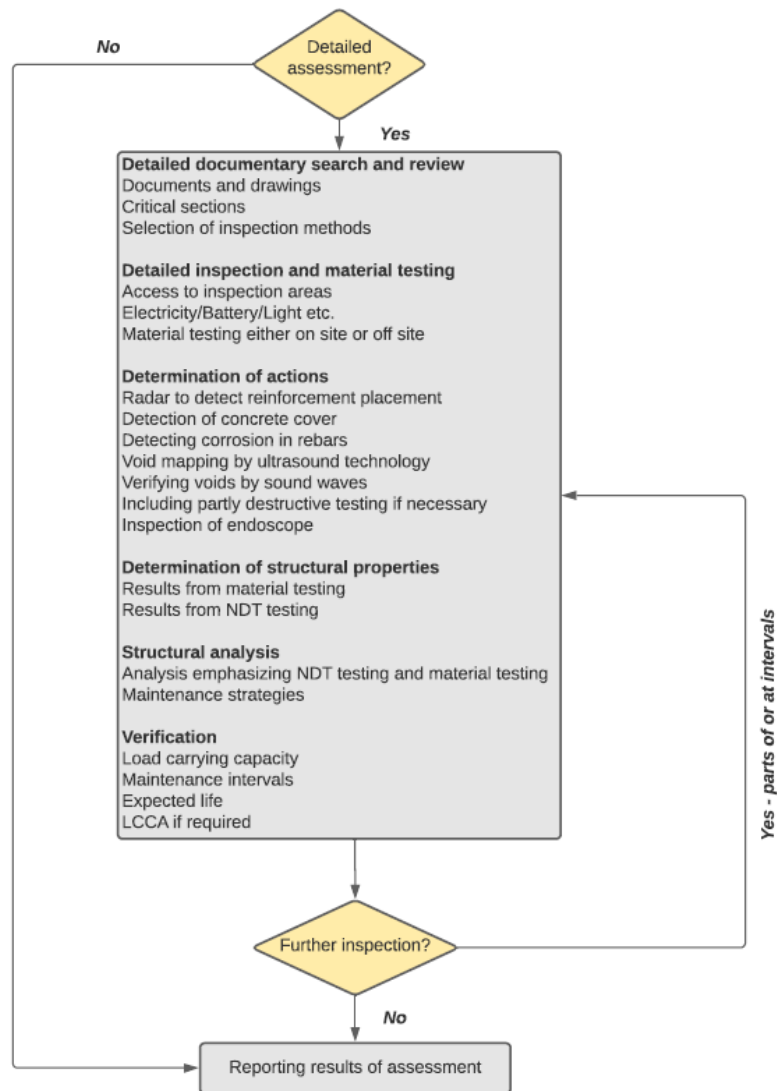


Figure 26 Flow chart for detailed assessment of concrete structures considering NDT methods [66]

An important guideline by the NPRA for assessing concrete bridges in Norway is manual V441 [67] and is specifically assessing bridges in general. However, it is interesting to evaluate the approaches included in this guideline. The purpose of the guideline is to evaluate the integrity and durability of the bridge from a safety point of view and addresses these steps of a bridge inspection: *planning, preparation, implementing, and follow up*. The *planning and preparation* are similar to the first phases included in ISO 13822 and considers the assessment strategy by an interval of inspection and the extent of the damage. A part of the strategy is evaluating the need for methods for data collection, including NDT methods. In *implementing*, the bridge damages are assessed by a preliminary inspection and NDT methods, according to damages described in the guideline. In *follow up* the collected measurements are analyzed and compared to documented data to identify the extent and

development of the damages. Based on these observations, measures are implemented to ensure the serviceability of the bridge [67].

### 3.2 Structural health monitoring (SHM)

Wan-Wendner [68] explains that the earlier lack of consideration of maintenance during the design of a new structure is one reason for the current state of the increasing deterioration of concrete structures. Long term maintenance strategies were absent, and cheaper design solutions were favored, neglecting the increasing maintenance costs during the lifespan of a construction. The concept of LCC has developed because of the old infrastructure, budgetary constraints, and aspect of sustainability. Several factors are considered during the different stages of a construction process due to the increased understanding of concrete as a construction material, such as load capacity, serviceability, initial costs, esthetics, durability, sustainability, and costs related to maintenance until the demolition of the structure and recycling [68]. The available standards are mainly based on long term experience that does not depend on accurate prediction models for time-dependent processes, often applicable for well-established materials and design situations. The most reliable approach for new constructions and maintenance of existing structures is models for time-dependent processes

The topic of structural health monitoring has a wide definition. Concise the term addresses the condition of a structure, considering the degree of damages during the service life. For this purpose, a condition assessment is conducted to map the performance of the concrete structure. The most optimal approach is to consider the entire construction. Thus this may be time-consuming, and often a more local inspection is chosen [13]. As seen in chapter 3.1, an important part of the assessment to achieve these considerations is the implementation of NDT methods. For visualizing the concept of SHM, Figure 27 illustrates the relation between SHM, assessment, and NDT. Monitoring the construction during the service life is one of the most essential phases to obtain the condition of the structure through regular recording of parameters. This information gives a perception of the structural behavior, as well enabling calibration of numerical models [69].

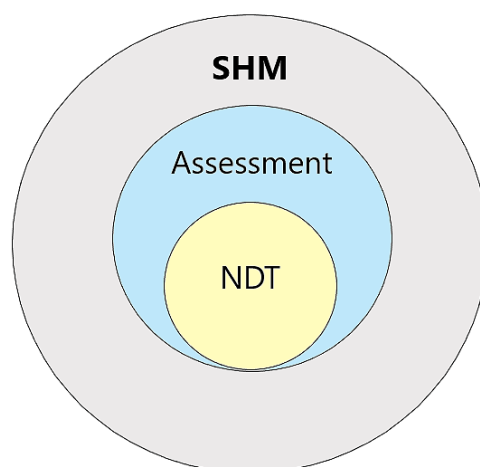


Figure 27 The relation between SHM, assessment and NDT

The data from monitoring is an important part from a managing point of view, where the data is used to optimize the operation, maintenance, and repair of the structure. The monitoring data can be assessed in structural management systems to obtain a survey of the state of the construction. Based on available information related to the condition of the structure, safety measures can be implemented. The utilization of better material properties, over design, and synergetic effects as part of safety measures in case of future deterioration, will maintain the design performance and extend the lifetime of the construction [69].

Digital twin is a part of SHM, developing digital profile which emphasize present behavior of either a physical object or process strengthening business performance. It considers real-time, real-world, and cumulative measurements based on an array of dimensions, establishing an evolving profile of either the object or process in the digital world that provides necessary information on system performance. Computer-aided design (CAD) and Internet of Things (IoT) comprise a constitutive part of digital twin, where CAD is related to a computer-simulated environment with success in modeling complex environments. IoT system measures position and diagnostics for a complete component, without considering full life cycle process and interactions between components. The real power behind digital twin is that it provides near-real-time connection between the physical and digital worlds, where digital twin contributes to richer models with more realistic and holistic measurements of unpredictability [70].

Digital twin predicts outcomes in much higher accuracy and is designed to model challenging processes interacting with their environment. Therefore, it is complicated to predict outcomes over a complete product life cycle. Digital twin in cooperation with NDT inspections are beneficial for systematical maintenance and rehabilitation processes. At the same time, these together minimize repair time and effort, estimating the remaining service life of a structure. In other words, the overall performance and sustainability will increase for following structure. NDT tasks performed by digital twin have an important place from the supplier to the costumer. Considering digital twin in NDT methods allows collection of high-quality data that can be integrated, interpreted, and analyzed [71].

An important area that forms digital twin is Building Information Modeling (BIM). BIM is a platform emphasizing interoperable and precise data of building information to improve planning, construction, and maintenance. BIM is responsible for merging the building's 3D CAD model with additional data connected to building specification, cost estimation, time schedule and maintenance management. In the field of manufacturing, building operation and maintenance, existing buildings suit from implementation of digital twin [72]. The connection between BIM and digital twin is dependent on Wireless sensor network (WSN), integration and data analytics. Different sensor networks are a part of digital twin to produce a real-time view of the asset, allowing real-time analytics, building efficiency, informed decision-making, and comfort, seen from Figure 28 [72, 73] .

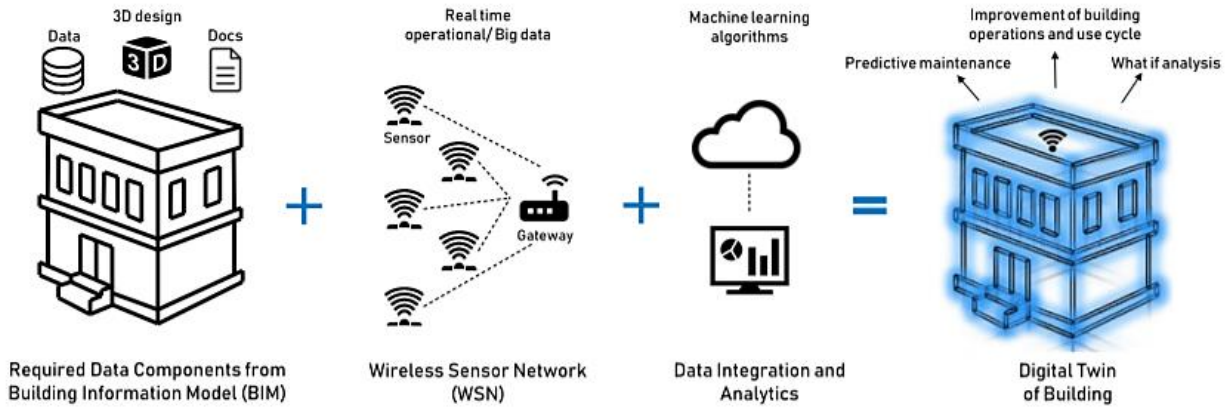


Figure 28 Necessary components to create a digital twin [72]

### 3.3 Non-destructive test methods (NDT)

In general, there is always a need to determine whether the concrete structure is designed properly and assess the structure's durability and structural integrity. Many properties of the concrete can be evaluated through NDT, such as mechanical parameters, the evaluation of the steel reinforcement and tendon ducts, and detection of damages and flaws [74]. The NDT methods provide important data to service life prediction and are a part of the assurance of the long-term performance of a concrete structure [15]. The NDT methods can be divided into several categories, and there are several available NDT methods for different purposes.

The stress wave method propagates stress waves which is a form of acoustic waves, and in contact with the concrete element, the test can provide information about the mechanical condition of the concrete. These waves pass through a concrete element, and the data involves the interpretation of waves reflected to a receiver. A change in the reflected waves can be noted depending on what the waves encounter, such as internal flaws, voids, steel reinforcement, and post-tensioned ducts, and are different for various materials. Furthermore, the acoustic NDT methods use different acoustic wave spectrum and frequency range, as seen in Figure 29 [15].

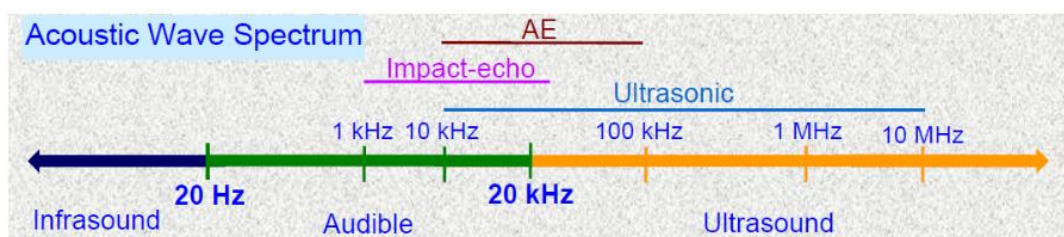


Figure 29 Acoustic wave spectrum and frequency for different NDT methods [15]

Radiographic methods use x-rays or gamma rays to evaluate a concrete structure for the identification of flaws and defects, where the element is placed between a radiation source and a film/detector. The radiation source penetrating the concrete and the radiation's attenuation depends on the density and thickness of the element due to absorption. The data is further recorded on a film or through an electronic means, and a benefit of radiographic methods is the detection of changes in thickness, corrosion, flaws, and density. Despite the benefits, there are considerable health risk related to this method as a result of the radiation from the test equipment [75].

The electromagnetic methods are based on the generation of electromagnetic waves. These waves penetrate the concrete element and are transmitted or reflected and are used to detect changes in the material properties of the concrete. Electrochemical methods use reference cells to get information about the chemical condition from the measured electrochemical potential [15].

The NDT methods that have been selected to investigate in this thesis are shown in Table 2.

Table 2 NDT methods [15, 76, 77]

NDT categories	
<b>Manual</b>	Visual inspection
<b>Stress wave method</b>	Rebound hammer
	Ultrasonic Pulse Velocity
	Ultrasonic Pulse Echo
	Impact Echo
	Impulse Response
<b>Radiographic methods</b>	Radiography
<b>Electromagnetic methods</b>	Ground-Penetrating Radar
	Concrete Resistivity
	Cover Meter
<b>Electrochemical methods</b>	Half-Cell Potential

In this thesis, some of the more common NDT methods will be addressed to evaluate the effectiveness and accuracy of the provided data. There are different NDT methods for the assessment of the various damages and flaws. The following parameters will be investigated:

- A. Cracks
- B. Delaminations
- C. Voids
- D. Corrosion of reinforcement
- E. Corrosion of post-tensioning strands
- F. Location of reinforcement
- G. Location of post-tensioning systems

The parameters A to E can be caused by several deterioration mechanisms and are, in general, some of the most common observed damages in existing concrete structures caused by this mechanism. It is important to emphasize that these can also be a result of the execution of the concrete. The ability of different NDT methods to detect the various damages and flaws will be addressed. The following assessment score is used:

- 0 – Not possible to detect deterioration
- 1 – Possible to detect deterioration, but not suitable
- 2 – Suitable, but there are limitations
- 3 – Suitable and preferable

### 3.3.1 Visual inspection

Visual inspection is recognized as the most important non-destructive test method, providing necessary information about the condition of the structure. A visual inspection is associated with structural serviceability, material deterioration and workmanship [74]. According to on ACI 201. 1R-08 [17], Guide for Conducting a Visual Inspection of Concrete in Service, the purpose of a visual inspection is to examine an existing construction to identify and determine the conditions the construction is subjected to during the service life. A visual inspection is often aimed for the surface of the concrete structure due to its visibility and is defined as an overview on performance and durability during the lifetime of the construction to detect possible distress and deterioration. When degradation is observed, further investigation through nondestructive test, destructive test and other methods are conducted to acquire information about the internal conditions of the concrete. Through these investigations, repair or rehabilitation can be considered, which is a more efficient approach. Thus, it is important that observations of environmental exposure, durability and performance are documented during the inspection.

For an engineer, it is important to separate between various signs of distress e.g., cracks, spalling, disintegration, and lack of uniformity. The visual inspection is specifically related to the investigated structure, including neighboring structures, climatic conditions, and surrounding environment. An important part of a visual inspection is to document the observations obtained during the investigation. Written description, sketches, photographs including dimensions and videos are essential parts of the documentation. An extensive description of damages is provided in ACI 201. 1R-08 to assist the investigator, with the cause of the deterioration and photos for illustration of different types of defects and distresses, for instance chemical attack, physical deterioration, mechanical damage, and weathering. A visual inspection is useful for existing structures, considering necessary parts of routine maintenance [17, 74]. A visual inspection form or a checklist is used during the inspection for documentation used in preparation of a report. An inspection form proposed by ACI 201. 1R-08 is found in Appendix 1. The report should include the following information [17]:

1. The name of the inspector(s)
2. Purpose of the inspection
3. Information about the available documentation of the structure
4. General description of the structure e.g., type, age and location
5. Inspection technique, the field test utilized and collected data
6. Filed observations and the part of the structure inspected
7. Conclusions and recommendation
8. Explanatory pictures and sketches

A recommendation is presented with description of testing and assessment necessary for a more comprehensive mapping of the observations. The visual inspection is always the first phase of an evaluation of a structure to determine the approach of a further inspection. The scope of the report should therefore be an instructive guidance for the determination of the

structural serviceability and safety of a concrete structure [17]. Table 3 provides a general overview of advantages and limitations associated with a visual inspection.

*Table 3 Advantages and limitations with visual inspection*

<b>Advantages</b>	<b>Result limitations</b>
Simple	Necessary of expertise
Inexpensive	Not applicable for internal condition assessment of concrete
Rapid	Does not detect small flaws
Detect distresses	Time consuming for larger concrete structures

Although a visual inspection is a rapid and inexpensive approach for the identification of apparent structural issues, detailed information about the interior defects is lacking. In addition, performing visual inspection on larger concrete structures is demanding and time consuming. Based on a study conducted by Federal Highway Administration (FHWA), 56 % of average condition ratings of concrete bridges were found incorrect where visual inspections accounted for 95% of the incorrect average condition ratings. Some challenges related to visual inspections emphasize that it is a single aspect of the total evolution plan. In other words, visual inspection is typically combined with other NDT methods to evaluate real condition of the structure [78].

Implementation of apparatus such as CCTV and endoscopes are preferred to access unseen parts and areas with limited access [79]. Another limitation is related to the detection and evaluation of small cracks. For this purpose, a crack width microscope (Figure 30) can be used enabling further assessment. The crack width microscope is a high definition tool for precise measuring cracks dimensions with the ability to magnify up to 40 times and a measuring range of 4 mm. This tool improves the performance of a visual inspection and is priced from \$598.00 [80].



*Figure 30 Crack width microscope [80]*



A recent method for visual inspection is to include drone equipped with 360° camera. Drone inspection is mostly adapted for bridge structures and high-quality camera is necessary to detect bridge damages contributing to localize bridge deterioration depending on time, load capacity, load frequency and environment. According to Humpe [81], drone inspections lower the economic costs and makes the inspection process more effective. Drones for bridge inspections can cause less disturbance and minimize safety-connected issues for manual inspections. This approach provides detection of challenging parts of the bridge structure, such as bridge corners, ceiling and arches [81]. Figure 31 illustrated a drone inspection.



Figure 31 Drone inspection of the Daniel Carter Beard Bridge [82]

The ability of a visual inspection to detect various deteriorations is listed in Table 4. In general, many of these parameters can be observed from the surface and can indicate the cause of deterioration. However, a visual inspection cannot evaluate the internal condition of the concrete and this consideration has been accounted when giving scores.

Table 4 Assessment score of a VI

Parameters	Assessment score
Cracks	1
Voids	0
Delamination	0
Corrosion of reinforcement	1
Corrosion of post-tensioning strands	1
Location of reinforcement	0
Location of post-tensioning systems	0

### 3.3.2 Ultrasonic method

#### Ultrasonic Pulse velocity

There are several standards related to Ultrasonic Pulse Velocity (UPV) methods, such as *EN 12504-4*, *ASTM C 597-02* and *ASTM E 114-95*. *EN 12504-4* [83] describes a standardized method for propagation waves of ultrasonic longitudinal waves in hardened concrete, useful for several applications. UPV equipment consist of an electrical pulse generator, several transducers, an electronic timing device and an amplifier. An electro-acoustical transducer produces a pulse of longitudinal vibrations, which is held in contact with one part of the concrete surface during the test. The pulse vibrations are transmitted by using a liquid coupling material such as cellulose paste or grease. The vibration pulses are converted into electrical signals by a second transducer after travelling a defined path length in the concrete. In addition, the pulse transit time is measured by enabling electronic timing circuits. The stress waves consist of both shear and longitudinal waves propagating through the concrete [74, 83].

The time interval is measured from the transmitting transducer to the receiving transducer. Calibration is provided to detect information about the velocity measurement. According to *EN 12504-4*, two variants of the electronic timing apparatus are oscilloscope and an interval timer. In an oscilloscope, the first front of the pulse is indicated in comparison to an appropriate time scale. An interval timer emphasizes a direct reading digital display. Major requirements for UPV performance are specified in this standard, where it should measure transit times in the calibration bar to a limit aberration of  $\pm 0,1 \mu\text{s}$  and an accuracy of 2 %. The frequency range for the transducers should be between 20 kHz and 150 kHz. Determination of pulse velocity is dependent on various factors that can affect the measurements. Some of the factors described in *EN 12504-4* are moisture content, concrete temperature, path length, geometry, steel reinforcements, cracks, and voids [83]. Figure 32 illustrates a schematic representation of the pulse travel path from the transmitter to the receiver in relation to cracks, voids/delaminations and sound concrete.

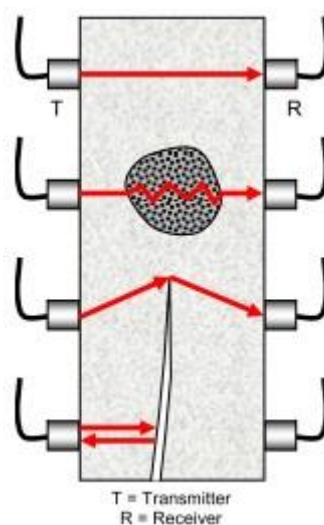


Figure 32 Pulse travel path from transmitters to receivers in concrete based on UPV [84]

According to EN 12504-4 transducers in the UPV method can be organized in direct transmission, semi-direct transmission, and indirect transmission (Figure 33). In direct transmission, the transducers are placed opposite of each side of the concrete, meanwhile semi-direct transmission illustrates adjacently placing of the transducers on the surface of the concrete. In indirect transmission method, transducers are placed on the same surface of the concrete. Malhotra [85] explains that direct transmission provides more accurate and meaningful results compared to semi-direct and indirect transmission. The angles of the transmitters contribute to decent measurements of maximum pulse energy, where the travel path is simplified. Semi-direct transmission is adequate when the angle of the transducers and path length is not too large. Indirect transmission gives uncertain results because the amplitude contribution is ineffective. The amplitude of received signal in indirect transmission could be less than 3 % compared to a received signal of direct transmission, mainly caused by the pulse propagation [85, 86].

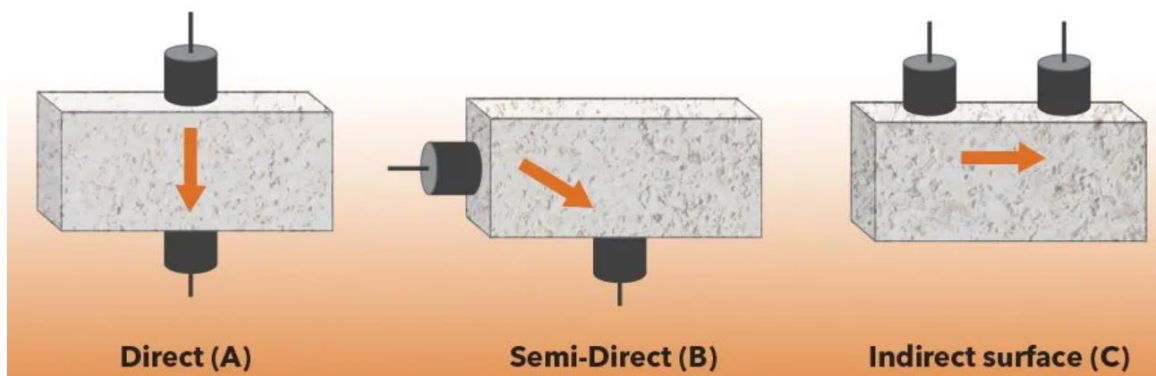


Figure 33 Type of UPV measurements (a) Direct, (b) Semi-Direct, (c) Indirect [87]

EN 12504-4 emphasize the common method is to place the transducers in a direct form. However, description of path length measurement is different for each transducer arrangement. The path length is defined as the shortest distance between the transducers for direct transmission, where the accuracy of path length measurement is  $\pm 1\%$ . The path length measured from the center to center of the transducer faces is sufficient for semi-direct transmission. Nevertheless, the size of the transducer in comparison with center to center distance is conclusive for the accuracy. Path length is not measured for the indirect transmission. However, the standard recommends various measurements with different distances between the transducers. A test report for following NDT method can contain many elements, for instance identification of concrete structure, location and date for test performance, concrete age, concrete temperature, details of transducers and many more [83].

Measuring the velocity of longitudinal vibrations contributes to acquiring important mechanical properties, such as modulus of elasticity, dynamic Poisson's ratio of concrete and compressive strength, addressing the uniformity of concrete. The implementation of UPV contributes to efficient examination of heterogeneous areas in the concrete [74]. According to Lorenzi et al. [88], UPV methods can provide condition assessment of the concrete structure during the entire structure service life. *ASTM E 114-95* clarifies that UPV methods are perfect quality control for detection of defects, material characterization and thickness

measurement of concrete. UPV tests are also used for analyzing internal depth of imperfections, estimating deformation values, and monitoring variations from compressive strength. Changes in the concrete density and soundness can contribute to sensitive influences. Factors affecting the concrete strength and density are w/c ratio, cement type, molding procedure, sample size and type of aggregate. In other words, concrete quality is dependent on the velocity value in UPV as seen in Table 5.

*Table 5 Quality of concrete as a function of UPV from BS [89]*

<b>Pulse velocity (m/s)</b>	<b>Concrete quality</b>
Above 4500	Excellent
3500 to 4500	Good
3000 to 3500	Medium
Below 3000	Doubtful

Table 6 provides a general overview of advantages and limitations associated with UPV.

*Table 6 Advantages and limitations of using UPV method [15]*

<b>Advantages</b>	<b>Result limitations</b>
User-friendly and simplified	Requires surface preparation
Detects concrete uniformity and quality outstandingly	A point measurement technique à time consuming
Measures thick members and large areas rapidly	Expertise from structural engineers for interpretation of results
	Better workability on homogenous materials
	Assessment of each side of the concrete element
	Presence of steel reinforcement
	Attendance of moisture
	Type and amount of aggregates

The ability of UPV to estimate cracks is an efficient method as seen in [90, 91] and an important condition for this to apply is if the right transducer is used, due to the variety of transducers. There are different methods used for the estimation of crack width and depth, as presented by Pinto et al. [90]. The paper refers two methods with different approaches. Figure 34 illustrated the principal of the measurement method. According to the paper, these methods can estimate the crack with an error of 15%.

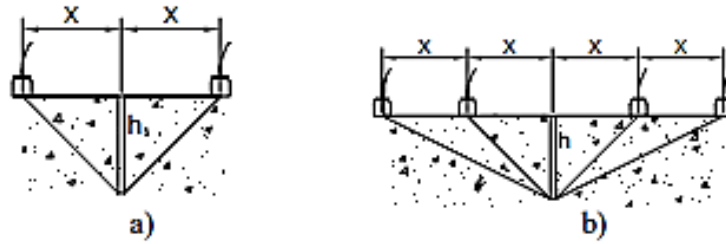


Figure 34 Principles of crack estimation by a) Bungey and b) BS 1881

Two methods were also proposed in the paper and the principal of the methods is illustrated in Figure 35, based on BS 1881. Method A (Figure 35a) consider four locations for the velocity measurements, while Method B (Figure 35b) can be used for cracks close to a specimen edge. These methods were shown to be more efficient with an error of 10%.

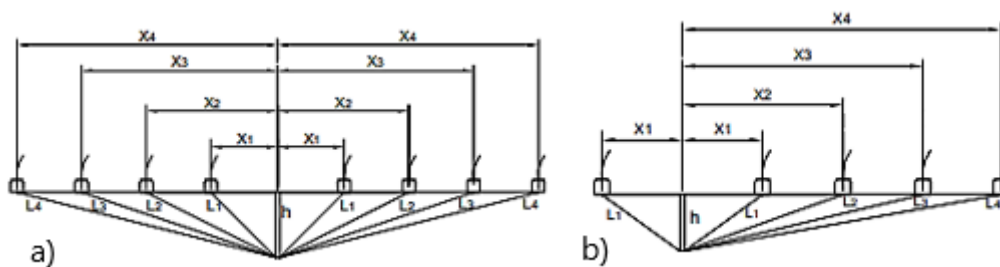


Figure 35 Principles of crack estimation by a) Method A and b) Method B

Kumar and Santhanam [92] demonstrated the influence of the distance between the transducers for crack detection. A high degree of accuracy for depth detection of vertical cracks with UPV were shown to apply for distances of under 100 mm. For horizontal cracks, this distance can be measured with reasonable degree of accuracy for distances 100 – 200 mm between the transducers. For a distance <100 mm the surface waves are registered before the compression waves, while for a distance >200 mm several reflections may occur. The measurements of mechanical properties of the concrete with UPV can possibly detect crack propagation in concrete. For void detection, a lower velocity is registered as presented by Garg and Misra [93]. However, the presence of voids in post-tensioning ducts decreases the velocity due the increasing steel strands and the interpretation of data is more challenging.

The effect of different causes of deterioration is detectable with the UPV e.g., depth of concrete damage due to freeze-thaw, as presented in [77]. There is a disagreement whether UPV can be an accurate for the assessment of ASR damage. For instance, Sargolzahi et al. [94] presented a low sensitivity of UPV by comparing the variation of pulse velocity and expansion due to ASR. However, the measurement of modulus of elasticity by UPV was confirmed to be an efficient approach for the determination of ASR damage, as seen by Diab et al. [95]. Their investigation demonstrated a rational correlation between UPV and ASR expansion. UPV have also proven the ability of evaluating corrosion.

Although UPV is a user-friendly method for evaluation of concrete structures, several research studies are critical to the reliability of the results. Adamatti et al. [96] clarified that



correct choice of test parameters is vital to obtain correct interpretation of UPV results from concrete structures. The UPV equipment in following research gave decent results by comparing a smooth concrete surface with a rough concrete surface, clearly seen from Figure 36. In other words, adequately UPV velocity values were obtained from the smooth surface in comparison to the rough surface. The red areas indicate low UPV velocity values, meanwhile the blue areas symbolize UPV zones with high velocity values. In addition, presence of reinforcement has a major impact on interpretation of UPV results. UPV equipment is clearly visualizing the color differences between the different cases, where reinforced concrete obtains lower UPV velocity values compared with the concrete wall without steel reinforcement, seen from Figure 37.

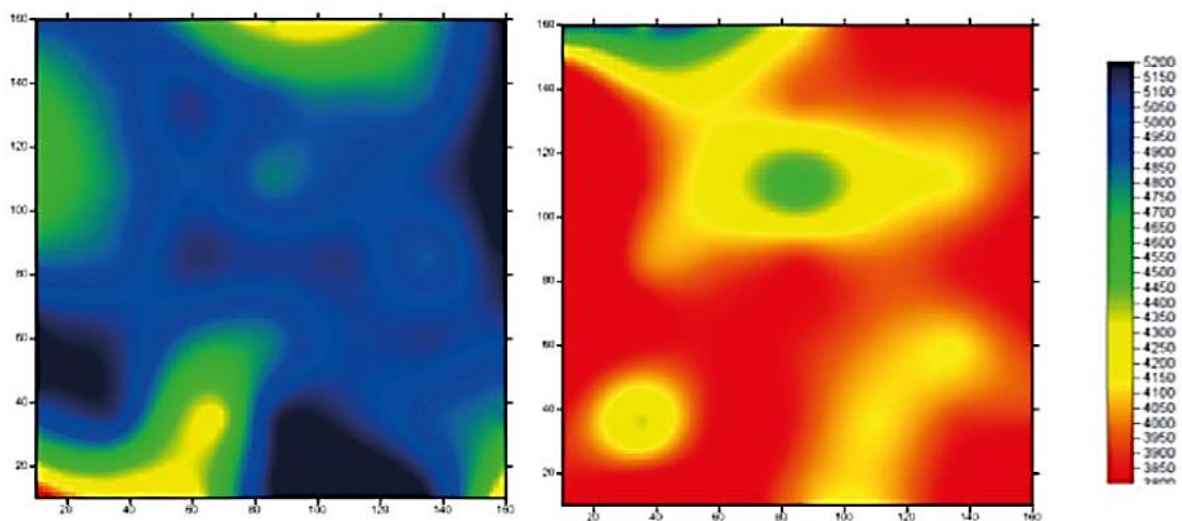


Figure 36 Smooth surface concrete wall vs rough surface concrete wall [96]

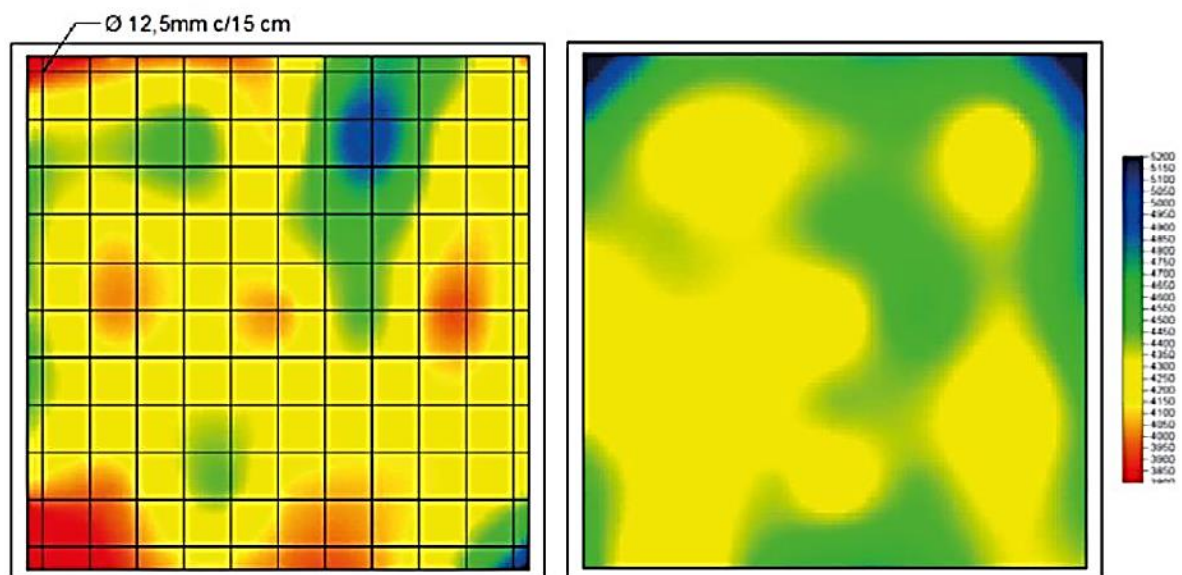


Figure 37 Concrete wall with and without reinforcement [96]


Komloš et al. [97] emphasize that there are certain areas of application where UPV can be improved. The most reliable application of UPV tests is for evaluating the uniformity of



concrete without reinforcement. UPV detects strength estimation within a  $\pm 20\%$  accuracy, where obtained strength level accuracy is accomplished from an established calibration curve. Furthermore, combining UPV with rebound hammer does not improve the strength accuracy. In addition, detection of defects and crack depth measurement are even less reliable applications of UPV. The same paper requires an improvement on the international standards related to UPV tests.

Many UPV equipment are available in the market, such from the manufacturer Proceq. Pundit Lab (+) offer a digital screen and is a simpler equipment compared to the Pundit 200 touchscreen unit and does not offer scan modes for on-site analysis of 2D visualizations of raw signals. However, USB connection to a PC allow a further analysis of the obtained data [98].

Olson Instruments offers the NDT and evaluation equipment Freedom DATA PC (FDPC) and NDE 360, which are platforms for multiple evaluation and data processing. These platforms are supplied with add-on systems, allowing multiple NDT evaluations such as UPV, Impact Echo and Impulse Response. The Freedom Data operates by stress waves and provides a software managing collection of data and analysis of the mentioned NDT methods through instrument modules, and several evaluations can be conducted simultaneously. The NDE 360 is a more compact instrument providing mobility in the field inspection and a memory flashcard is included for storing collected data and an upgrade of the flashcard memory provides extension of NDT evaluations. The data from the NDE 360 is further downloaded to a PC for analysis and processing. The add-on systems will be addressed further in the respectively chapters [99, 100]. Table 7 provides a general overview of the mentioned products and the relevant details.

Table 7 Different UPV equipment from Proceq [99-101]

Product	Product details
<p data-bbox="395 1339 542 1373">Pundit 200</p> 	<ul style="list-style-type: none"> <li data-bbox="807 1346 1331 1435">• Calculates the surface velocity automatically considering standards</li> <li data-bbox="807 1462 1430 1615">• Scan modes: Line Scan, Area Scan, Modulus of elasticity measurement, Data logging and compressive strength correlations</li> <li data-bbox="807 1641 1377 1731">• 2D-visualization color classification with Area Scan</li> <li data-bbox="807 1758 1142 1792">• Estimates crack depth</li> <li data-bbox="807 1818 1331 1852">• Transducer Frequency: 20 – 500 kHz</li> <li data-bbox="807 1879 1246 1912">• Measuring Range: Up to 15 m</li> <li data-bbox="807 1939 1150 1973">• Price - \$3,389.00 [102]</li> </ul>

<p style="text-align: center;">Pundit Lab(+)</p> 	<ul style="list-style-type: none"> <li>• Eliminates external amplification when used with exponential transducers</li> <li>• Estimates crack depth</li> <li>• Transducer Frequency: 20 – 500 kHz</li> <li>• Measuring Range: Up to 15 m</li> <li>• Price - \$3,910.00 - \$4,925.00 [103]</li> </ul>
<p style="text-align: center;">UPV-1 Model</p> 	<ul style="list-style-type: none"> <li>• Detect cracks, delaminations, honeycomb</li> <li>• Transducer Frequency: 50 kHz</li> <li>• 2D and 3D Tomographic velocity images</li> </ul>

### Ultrasonic Pulse Echo

Another ultrasonic method is the Ultrasonic Pulse Echo method (UPE). The principal of this method is based on the introduction of a stress pulse to a surface of a concrete element and the changes in acoustic impedance through the reflection from flaws and interfaces are measured [15]. UPE apparatus is commonly measuring the slab thickness and placement of voids and delamination. The longitudinal waves and the transverse waves are applicable in the UPE method. Reflection of the ultrasonic waves is depending on the acoustic impedance, which describes percentage of transmitted and reflected energy [104].

The UPE method is mainly divided into three systems and techniques: (a) pulse-echo, (b) pitch-catch and (c) phased array. The principal of these techniques is illustrated in Figure 38. The pulse-echo has a single transducer acting as transmitting and receiving transducer. The transmitter converts electrical pulses to ultrasonic waves and the ultrasonic waves are reflected reliant on localized cracks and end surface. The system of pitch-catch uses a separate receiving and transmitting transducer. The travel time is applicable for determination of the reflection depth when knowing the wave speed of the material [15, 77].



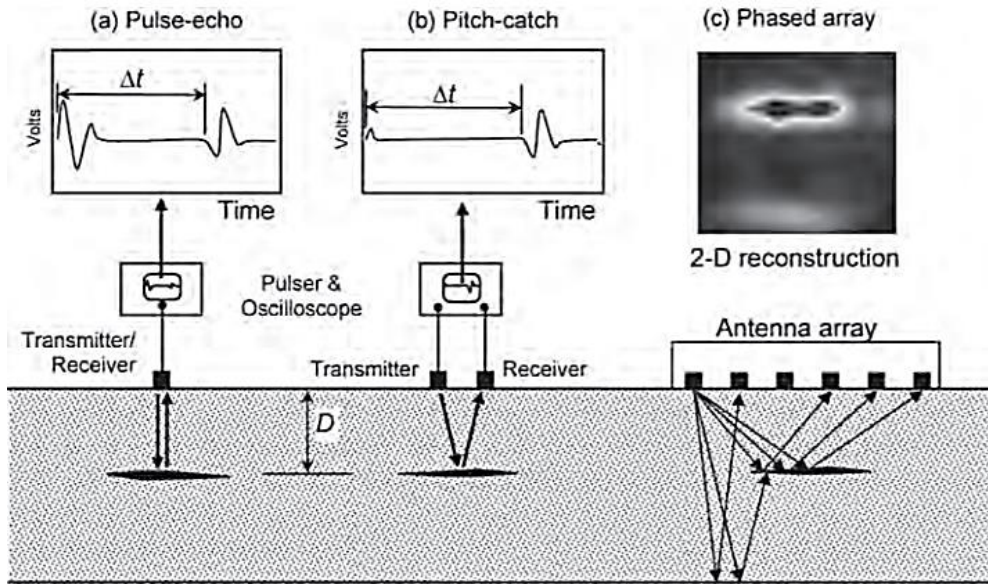


Figure 38 Schematic of UPE methods: (a) pulse-echo, (b) pitch-catch and (c) phased array [77]

The phased array system is a development of the pitch-catch principal based on array of transducers allowing several pitch-catch measurements sequentially. For the transducers to have the function of transmitting and receiving in a predefined sequence, the phased array system uses a computer software program. The synthetic aperture focusing technique (SAFT) processes the signals from reflected interfaces generated from the travel time measurements and reconstructs internal images of the concrete object. A mesh system is used for the object to identify the location of the transducer pairs and the SAFT algorithm provides a 3D image for the possibility of different view planes. This method is often known as ultrasonic tomography [77]. UPE provides data in colors, depending on the intensity and amplitude of reflection of the waves and is influenced by the damage or flaws in the concrete. The amplitude is presented in a color scale in the following manner: blue, green, yellow and red, where the reflection increases in that order indicating the presence of air [105].

Table 8 provides a general overview of advantages and limitations associated with UPE.

Table 8 Advantages and limitations of using UPE method [15, 77]

Advantages	Result limitations
Inexpensive, portable and user-friendly	Expertise from structural engineers for interpretation of results
Demands one accessible surface	Demands technical knowledge for inspections
Reconstruction of 3D tomographic images	Unsuitable for not homogeneous parts and irregular shape
Penetrates efficiently to detect deep flaws	Requires surface preparation

Exceptionally determine the thickness and internal flaws depth
Estimates the shape, size and orientation of defects

For a reliability assessment of UPE, Beutel et al. [106] demonstrated that several UPE systems are sufficient for locating shallow thickness sections and tendon ducts. Dimensions with small deviations were considered, which gave promising accuracy for UPE tests. Small grid size is also an important parameter for improved accuracy. In following research paper, ultrasonic echo managed to determine the depth and the concrete cover over the ducts. Another research paper from Krause et al. [107] adds that reliability of UPE is dependent on source to first receiver distance, boundary conditions and spacing of the receivers. Most importantly, ultrasonic echo specified a clear difference between air filled and well grouted parts. Furthermore, these results allow the distinguishing between reflection of steel and reflection of air. Faster performance of UPE measurements is available by applying dry contact transducers, known as air-coupled ultrasonic (ACU).

There are many UPE equipment available in the market, such as from the manufacturers Proceq, Elop and Germann Instruments. Proceq offers several variants of the Pundit model with new generation and design-protected touchscreen units, mainly measured from a single side transducer. The main difference with the different model is related to the technology and detection measurements by different modes. Elop Insight is a new revolutionary NDT scanner allowing accurate inspections, management, and structural health monitoring of concrete structures. Ultrasonic waves are transferred through the material while the scanner rolls over the concrete surface. Gathered information for this scanner is transferred and located automatically in the cloud, simplifying the inspection [66].

According to Wagle [108], Elop Insight is more than 10 times quicker than conventional scanning methods, accomplish a speed up to 50 cm/s. Germann Instruments offers MIRA Tomographer, an equipment used for the assessment of the internal condition of the concrete and creates 3D images of defects. The equipment is based on the phased array system and dry point contact transducers consisting of 48 transducers.

The UPE equipment from the manufacturers offer various visualization features to provide an easier analysis: 3D visualization, B-scan, C-scan and D-scan. The three last mentioned scans are based on a coordinate system, which are perpendicular to the cross section of the investigated object, as seen in Figure 39 [109]. B-scan provides a scan vertically, C-scan provides a scan horizontally and D-scan provides a scan in the profile plane.

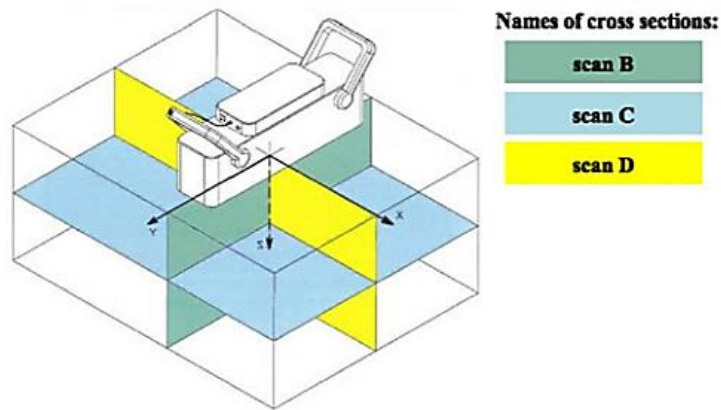
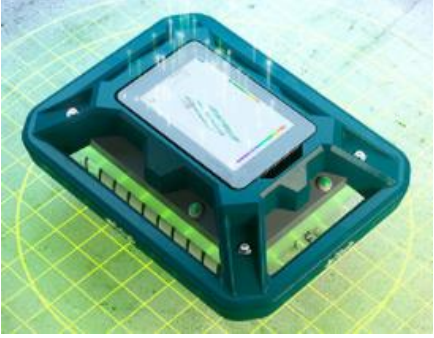





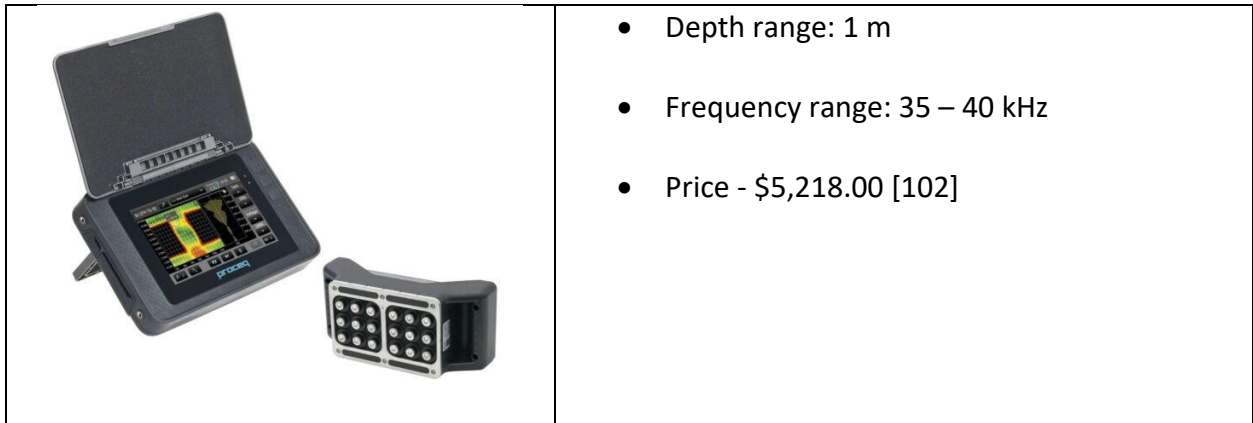
Figure 39 Illustration of the B-, C- and D-scan [109]

Table 9 provides a general overview of the mentioned products and the relevant details.

Table 9 Different UPE equipment from Elop, Germann Instruments (MIRA) and Proceq [101, 105, 110]

Product	Product details
<p data-bbox="391 864 547 898">Elop Insight</p> 	<ul style="list-style-type: none"> <li>• Detects voids, delamination and non-vertical cracks</li> <li>• Easily rolled over the surface</li> <li>• Visualizes and detects rebars, material thickness, backwall, honeycombing and grouting defects in the tendon ducts</li> <li>• Effective and rapid structural imaging of huge areas</li> <li>• Live 3D visualization, B-scan, C-scan and D-scan</li> <li>• Depth range: 2 m</li> <li>• Frequency range: 50 – 200 kHz</li> <li>• Price – Unknown</li> </ul>
<p data-bbox="432 1659 505 1693">MIRA</p> 	<ul style="list-style-type: none"> <li>• Detects cracks, flaws, slab thickness, honeycombing, voids and grouting defects in post tension ducts efficiently</li> <li>• Possible to detect reinforcement</li> <li>• 3D visualization, B-scan, C-scan and D-scan</li> <li>• Depth range: 2.5 m</li> </ul>

	<ul style="list-style-type: none"> <li>• Frequency range: 25 – 80 kHz</li> <li>• Price – Unknown</li> </ul>
<p>Pundit PD8000</p>  <p>The image shows the Pundit PD8000 ultrasonic testing device. It consists of a black main unit with a color LCD screen on top displaying a blue-toned scan image. Two black transducer probes are attached to the sides of the unit. The brand name 'pundit' is visible on the front panel.</p>	<ul style="list-style-type: none"> <li>•</li> <li>• Dominates superior depths with image clarity and geometrical accuracy</li> <li>• Localizes grout defects in tendon ducts</li> <li>• Detects delaminations, honeycombing and voids</li> <li>• Live 3D visualization with B-scan, C-scan and D-scan</li> <li>• Depth range: 2 m</li> <li>• Frequency range: 20 – 80 kHz</li> <li>• Price – Unknown</li> </ul>
<p>Pundit 250 Array</p>  <p>The image shows the Pundit 250 Array ultrasonic testing device. It features a grey and black ruggedized design. A color LCD screen is integrated into the top section, displaying a scan image. A black transducer probe is connected to the front of the device. The brand name 'pundit' is visible on the front panel.</p>	<ul style="list-style-type: none"> <li>•</li> <li>• Localizes grout defects in tendon ducts</li> <li>• Detects delaminations, honeycombing and voids</li> <li>• B-scan available in panorama mode</li> <li>• Depth range: 1 m</li> <li>• Frequency range: 35 – 40 kHz</li> <li>• Price - \$24,380.00 [111]</li> </ul>
<p>Pundit 200PE</p>	<ul style="list-style-type: none"> <li>• Detects delaminations, honeycombing and voids</li> <li>• Rapid availability of B-scan as the scan is carried out</li> </ul>



To summarize, UPV and UPE equipment are useful for quality assessment of concrete. The frequency range has a huge influence on the equipment interpretation of cracks, delaminations, honeycombing, voids, and other type of concrete damages. Some equipment has the possibility to localize grout defects in tendon ducts. Irrespective, UPV and UPE technology are recommended to use in combination with other NDT methods. The results obtained from UPV and UPE measurements are demanding interpretation, and expertise from structural engineers is required to maintain the tests credibility. The rebound hammer is often used in combination with UPV, where concrete strength measurement from rebound hammer and internal damages detected from UPV contribute to promising structural evaluation.

The ability of UPV and UPE to assess the listed parameters is shown in Table 10. The uncertainties related to the method has been considered when giving scores.

Table 10 Assessment score of UPV and UPE

Parameters	Assessment score	
	UPV	UPE
Cracks	3	2
Voids	2	3
Delamination	3	3
Corrosion of reinforcement	1	0
Corrosion of post-tensioning strands	0	2*
Location of reinforcement	0	2
Location of post-tensioning systems	0	2

\*The UPE cannot directly detect corrosion of strand, however the presence of voids in post-tensioning ducts can be a possible indication of deterioration

### 3.3.3 Impact echo (IE)

Impact echo (IE) detects structural flaws in concrete with elastic waves after mechanical impact instead of ultrasonic sound waves. IE develops high-energy pulse that penetrates deeply into concrete. Impact on the surface creates longitudinal waves and shear waves travelling into concrete specimen, meanwhile surface waves (R-wave) travels in the opposite direction of the impact point. Internal defects reflect longitudinal and shear waves, and these waves create displacements measured by a receiving transducer. The following principle is illustrated in Figure 40, where a pattern of surface and longitudinal displacement is shown. Initially, surface waves lead to high downward displacement. When longitudinal waves are introduced, the displacement has lower amplitude with repeating downward displacements induced by multiple reflections between the surface and the internal void [112].

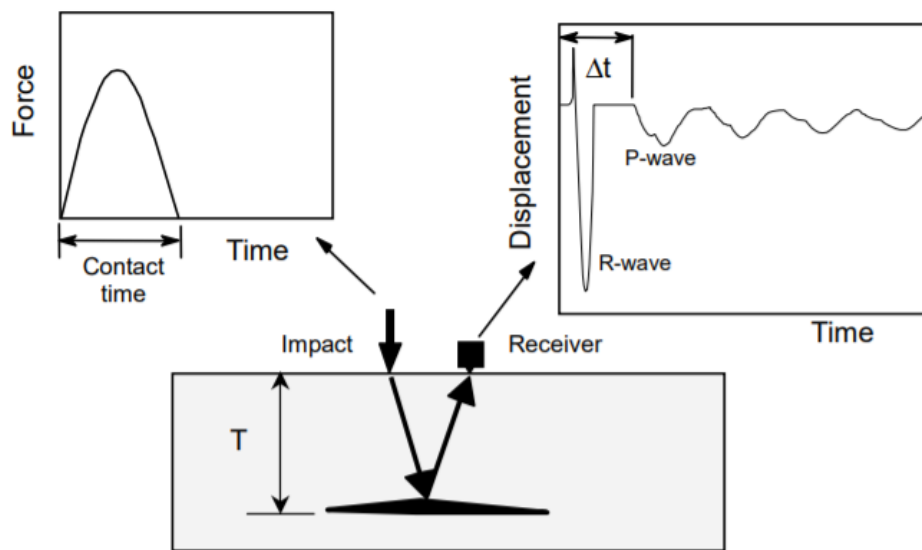


Figure 40 The coherence between mechanical impact and elastic waves [112]

The principle of frequency analysis is major part of IE. Longitudinal waves created by the impact endures multiple reflections between the top and bottom of the concrete specimen. A close distance between the receiver and impact point corresponds to a round trip travel distance  $2T$ .  $T$  can be defined as the distance between the test surface and reflecting interface. In several cases, understanding amplitude spectrum is necessary for determining dominant frequencies. For concrete specimens with either reinforcement or ducts, the thickness frequency is defined as the dominant peak in the spectrum [112].

The standard *ACTM C 1383, "Standard Test Method for Measuring the P-Wave Speed and the Thickness of Concrete Plates Using the Impact-Echo Method"* considers the *IE* method. According to following standard, the scope specifies procedures for determination of concrete slab thickness, bridge decks, walls, pavements, or other plate-structures. *IE* is mainly divided into *procedure A* and *procedure B*. Procedure A measures the concrete longitudinal waves (P-wave) speed, which is dependent on the measured travel time of waves from a known distance path between two transducers. Following procedure is suitable for dry concrete, where a high surface moisture content influences the obtained results. On the other hand, procedure B determines the thickness frequency evaluated from *IE* method. The plate

thickness from procedure B is calculated from registered P-wave speed. Procedure B is appropriate on concrete plates in connection with permeable asphalt concrete or lean Portland cement concrete. Figure 41 illustrates both procedures for plate thickness according to ACTM C 1383 [112] [113].

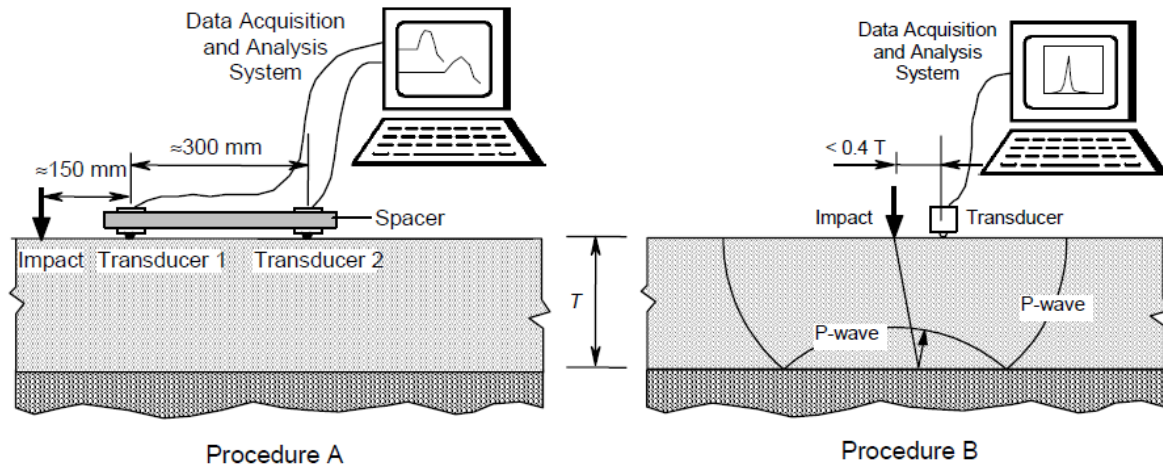


Figure 41 Procedure A and procedure B according to ACTM C 1383 [112]

ACTM C 1383 emphasize that a dry test surface is recommended. Facing a rough surface creates complications on achieving decent contact between the concrete and transducer. In addition, loose material on the surface must be removed based on adequately coupling between the surface and transducers. The IE equipment should be properly placed on the concrete surface, where the position of the impactor strikes between two transducers at a distance of  $150 \pm 10$  mm. ACTM C 1383 clarifies that preparation of correct data acquisition parameters is necessary for obtaining correct data, mainly focusing on sampling rate and voltage range [113].

Table 11 shows a general overview of advantages and limitations associated with IE measurements

Table 11 Advantages and limitations of using IE [15, 77]

Advantages	Result limitations
Portable and user-friendly	Expertise to optimize testing parameters and interpret results
Only one surface is needed for the investigation	Time consuming when assessing bigger concrete structures
Applicable for post-tensioned ducts	Results can be affected by small flaws, type of flaw, orientation, depth and contact time of
No interference of the steel reinforcement on the results	Depth precision of 1 m
Possible to locate different defects	




Cheng and Sansalone [114] suggested that a crack width of 0.1 mm or higher does not transmit stress waves by short duration impacts. Following paper emphasizes that IE method managed to detect signals from reinforced concrete plates containing delamination. However, detecting shallow cracks or delamination in concrete are more challenging than deeper cracks or delaminations. Delamination depth, lateral dimensions of delamination and elastic properties of concrete are decisive for damage evaluation. IE detected that increasing dimensions of delamination resulted in lower value of frequency. Jaeger et al. [115] have based on numerical, laboratory and field studies demonstrated that IE outstandingly detects both complete and partial voids in grouted tendon ducts. A total number of 14 tendon ducts were evaluated, where 11 ducts were detected as fully grouted, meanwhile 3 ducts contained voids. Frequency peak values obtained in the amplitude spectrum showed promising sign of voids in the ducts.

Krüger et al. [116] clarify that IE is a valuable NDT technique to measure cracks. Cumulative energy of the transmitted signal contributed to promising results. The signal peak energy travelling across a crack is delayed, causing a lower overall energy. A part of the impact energy is reflected at the crack surface, automatically detecting the cracks. However, the system of cumulative energy demands a more reliable impact generation.

The Freedom DATA PC (FDPC) and NDE 360 addressed earlier also have the ability of conducting Impact Echo evaluation with the following test heads; IE-1 Model, IE-2 Model and IES. The IE-2 Model includes an accelerometer providing an enhance depth precision compared to the IE-model. The Concrete Thickness Gauge 2 (CTG-2) is another independent device by Olson Instruments, which is a handheld device with an integrated software that can be connected to a tablet or PC for analysis of the collected data. Table 12 provides a general overview of the mentioned products and the relevant details.

Table 12 Different Impact Echo equipment for Olson Instruments [99, 100, 117, 118]

Product	Product details
<p style="text-align: center;">IE model</p> 	<ul style="list-style-type: none"> <li>• Compatible with the FDPC and NDE 360</li> <li>• Detect cracks, delaminations, honeycomb, voids</li> <li>• Determines thickness of concrete members with accuracy of <math>\pm 2\%</math></li> <li>• Applicable for RC and PT concrete</li> <li>• Monitor waveform on-site</li> <li>• Depth range: <ul style="list-style-type: none"> <li>– IE-1 Model: 81 mm – 1.8 m</li> <li>– IE-2 Model: 3.6 m</li> </ul> </li> </ul>



### The Impact Echo Scanning (IES)



- Compatible with the FDPC and NDE 360
- Used for investigation of larger areas
- Detect cracks, delaminations, honeycomb, voids
- Determines thickness of concrete members with accuracy of  $\pm 2\%$
- Applicable for RC and PT concrete
- Locate PT systems
- Rolling displacement transducer recording data every 25 mm
- Provides 2D and 3D images of obtained data
- Depth range: 1 m

### CTG-2

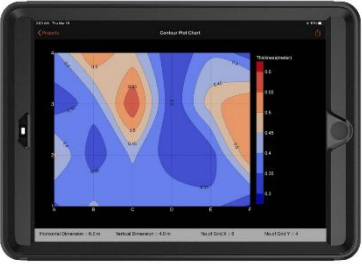


- Detect cracks, delaminations, honeycomb, voids in concrete
- Determines thickness of concrete members with accuracy of  $\pm 2\%$
- Frequency Resolution: 10 Hz
- Depth range: 81 mm – 1.8 m

### MIRADOR 2



- Measures thickness and detects voids, delaminations and honeycomb
- Frequency Resolution: 40 Hz
- Determines thickness of concrete members with accuracy of  $\pm 2-4\%$
- Price – Unknown

<p style="text-align: center;">FPrimeC Impact Echo</p> 	<ul style="list-style-type: none"> <li>• Measures thickness and detects voids, delaminations</li> <li>• Frequency Resolution: Unknown</li> <li>• Determines thickness of concrete members with accuracy of <math>\pm 2-4\%</math></li> <li>• Price – Unknown</li> </ul>
--	---

To summarize, the IE methods provides a reliable assessment of different concrete flaws and defects. The NDT method has an enhanced ability to determine the geometry of different flaws, such as cracks, delamination, and voids accurately. In addition, the IE has been proven to be a great method of locating ducts, evaluating the internal condition of the tendon ducts through detecting voids and to determine the level of grouting. This detection contributes to indicate the possible degradation of the tendons, such as corrosion. The ability of IE to assess the listed parameters is shown in Table 13. The uncertainties related to the method has been considered when giving scores.

*Table 13 Assessment score of IE*

Parameters	Assessment score
Cracks	2
Voids	3
Delamination	3
Corrosion of reinforcement	0
Corrosion of post-tensioning strands	1
Location of reinforcement	0
Location of post-tensioning systems	2

### 3.3.4 Impulse response (IR)

The Impulse Response (IR) method sends stress waves through tested elements based on low-strain impact. An instrumented hammer is used to measure the impact force. *IR* method is based on the long-duration impact, meaning that the structural element responds to the impact in a bending vibration mode. Application areas for *IR* are voiding beneath concrete pavements, delaminations of concrete around steel reinforcement in slabs and honeycombing and cracking in concrete structures. A mechanical impact from transient stress pulse takes place on the surface, where an analyze of the resultant bending behavior is active to characterize the integrity of the element. Velocity transducer (geophone) response and time records for the hammer force are included in the field computer by considering the fast Fourier transform (FFT) algorithm. Frequency and mobility are essential for describing IR sound response, where mobility emphasizes information on the integrity and condition of concrete [77].

According to ASTM C1740 [119], the purpose of the Impulse response method is to assess the structural condition of slabs in concrete. The configuration of IR method and the included components are shown in Figure 42. As seen in the figure, the obtained data is described in form of frequency (x-axis) and mobility (y-axis), and after processing the data a contour plot of the mobility is generated. ASTM C1740 requires that the hammer strikes  $100 \pm 25$  mm from the transducer, and an accuracy of  $\pm 5\%$  between the first and second average mobility value.

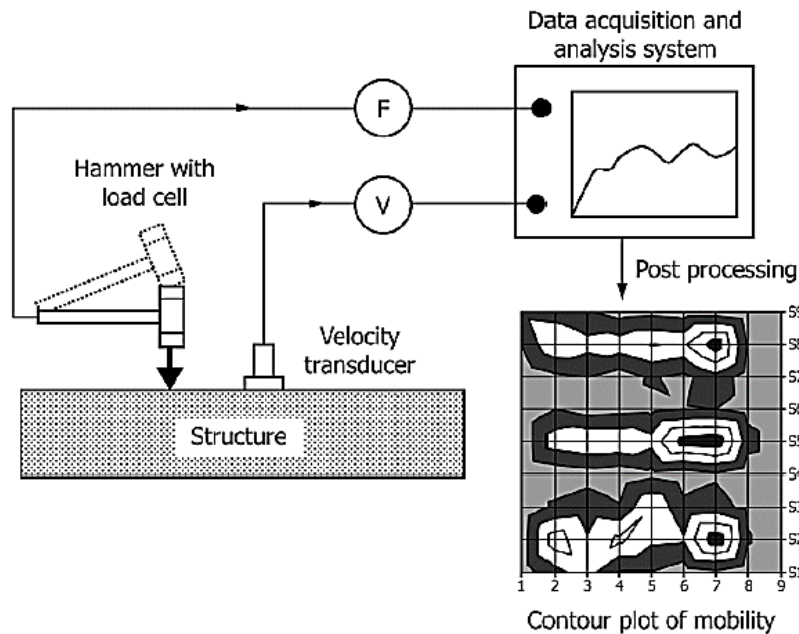


Figure 42 Principal and set-up of the IR method

IR mobility is depending on dynamic stiffness, damping and peak/mean mobility ratio. Dynamic stiffness defines the inverse of the compliance, known as the slope of the mobility plot under 0.1 kHz. The thickness of the plate, density, elastic modulus, and the support conditions are decisive for the dynamic stiffness. The impact-generated elastic wave is damped by the element's intrinsic rigidity, more familiar as body damping. Any cracking or honeycombing in the concrete minimizes both the body damping and stability of the mobility plots. If delamination or debonding occurs in the concrete structure, *IR* is controlled by the response behavior of the uppermost layer. Peak/mean mobility ratio defines the presence of either debonding, voiding or support loss [77].

Normally, results from average mobility, stiffness, mobility slope and peak-to-mean mobility ratio are presented in form of a contour plot. Figure 43 shows an example of a contour plot for average mobility, testing a slab-on-ground floor. The darker area in the following figure identifies higher mobility, which were dominant at the corners of the slab. A possible theory is that the slab has lifted off the ground at the corners [77].

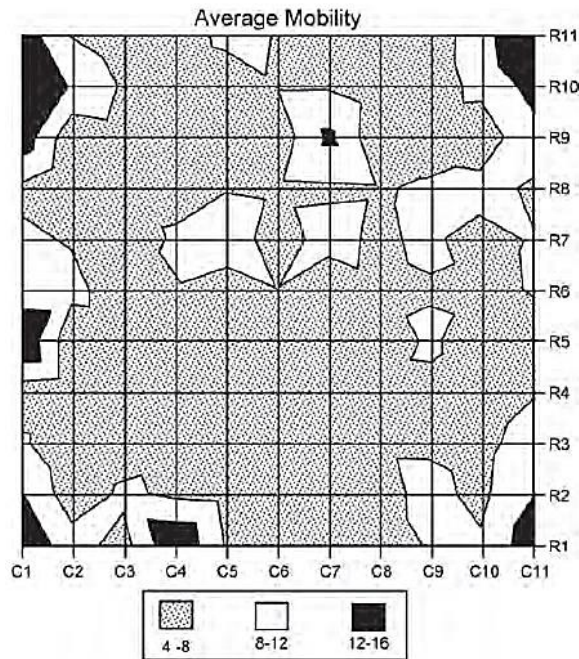


Figure 43 Contour plot from a concrete floor slab showing average mobility values [77]

Table 14 shows a general overview of advantages and limitations associated with *IR* measurements.

Table 14 Advantages and limitations of using *IR* [77]

Advantages	Result limitations
Demands only access to one face	Requires experienced operator
Does not require coupling materials	Thickness limit to 1000 mm
Covers large area in short time	Uncertain results
	Limited to slabs of concrete structures


According to Davis [120], *IR* test method has a significant role in evaluation of reinforced concrete structures e.g., for floor slabs, bridge decks, piers, and pavements. *Freedom Data PC* (FDPC) and *NDE 360* are modern computer data storage and analysis facilities, contributing to quick evaluation of large concrete structures during *IR* testing on site. Therefore, *IR* allows immediate identification of critical zones within the structure for more detailed investigation. Obtained results from *IR* measurements boost the confidence and economic advantage for engineers. By using low-strain impact to send stress waves through the concrete material, promising *IR* results have been registered for different case studies in North America. From following research paper, a 120 m long reinforced concrete bridge deck in Washington State was emphasized. In this case, *IR* measurements were performed to interpret the integrity of the concrete below the asphalt. No signs of concrete delamination were indicated in the deck, where peak/mean mobility ratios had lower numbers than the critical value [120]. Nazarian


et al. [121] emphasize that detecting voids are possible with the IR method. Nevertheless, thickness size of the concrete is significant for especially corner voids .

On the other hand, Sajid and Chouinard [122] are emphasizing the research directions for IR condition assessment of concrete structures. Grid size for the *IR* test is an important factor to evaluate the effect of hammer impact duration and influence zone, but improvements here is still possible. In addition, quantifying *IR*'s reliability for the test results are recommended in the future. Although *IR* is a wave reflection technique, following NDT method contributes to clarify defects in the material that are greater than the wavelength of the elastic-stress wave. The lack of reliability for *IR* is especially related to correct detection of a defect and the probability of false detection. Otherwise, following research paper defines *IR* method as an extensively NDT method used for condition assessment of concrete structures and in combination with other NDT methods. The *IR* method has also been proven to detect the depth of ASR and is mentioned as a secondary method for assessing freeze-thaw in [77].

For the Impulse Response evaluation, The Slab Impulse Response (SIR) system is connected to the Freedom DATA PC (FDPC) or NDE 360. The system is available in two models, SIR-1 and SIR-2, where the difference is related to the area of application. The SIR-1 Model include a vertical geophone transducer while the SIR-2 Model has an additional omnidirectional velocity transducer enhancing the ability of testing slabs and ceiling of concrete structures. For the processing of data, a software is used for the evaluation of the integrity of the concrete structure. Counter plots are also generated for simplifying the interpretation of the collected data. Table 15 provides a general overview of the mentioned products and the relevant details.

Table 15 Different IR equipment from Olson Instruments and FPrimeC [123, 124]

Product	Product details
<p data-bbox="400 1301 536 1330">SIR model</p> 	<ul style="list-style-type: none"> <li data-bbox="807 1301 1374 1330">• Compatible with the FDPC and NDE 360</li> <li data-bbox="807 1361 1414 1447">• Detect delaminations, voids and soft/weak areas in RC slabs</li> <li data-bbox="807 1478 1235 1507">• Monitor waveform of on-site</li> <li data-bbox="807 1538 1310 1568">• Provides 2D maps of obtained data</li> <li data-bbox="807 1599 1219 1628">• Depth range: Up to 600 mm</li> <li data-bbox="807 1659 1310 1809">• Area of application: SIR-1 Model: Slabs SIR-2 Model: Slab, walls and ceiling</li> </ul>

<p style="text-align: center;">FPrimeC i.Pile</p> 	<ul style="list-style-type: none"> <li>• Evaluate the depth of concrete piles</li> <li>• Locates defects, delaminations and voids in piles</li> <li>• Sampling frequency: 40 kHz</li> <li>• Price – Unknown</li> </ul>
---	--

Overall, *IR* method is efficient to include in combination with other NDT method, identifying critical concrete damages such as voids, cracks, honeycombing and delaminations. *FDPC* and *NDE 360* are available *IR* products in the market together with an instrumented hammer. The instrumented hammer covers large area in a short time, and the setup for *IR* method does not demand coupling materials. At the same time, *IR* method requires only access to one face. However, this method is often limited to concrete slabs and the result from an *IR* is in need of comparison to other NDT method for verification. In addition, *IR* method has a thickness limitation up to 1000 mm, which is less beneficial in comparison to other NDT methods. However, this NDT method is extremely useful for voids detection in floor slabs, bridge decks, piers, and pavements, describing its value in the market. The ability of *IR* to assess the listed parameters is shown in Table 16. The uncertainties related to the method has been considered when giving scores.

*Table 16 Assessment score of IR*

Parameters	Assessment score
Cracks	1
Voids (internal)	2
Delamination (internal)	2
Corrosion of reinforcement	0
Corrosion of post-tensioning strands	0
Location of reinforcement	0
Location of post-tensioning systems	0



### 3.3.5 Ground-penetrating radar (GPR)

According to *ASTM D6432*, a transmitter and receiver antenna, suitable data storage, display devices and a radar control unit are active elements in a GPR setup. EM waves are detected by the receiving antenna, where the EM signals are transferred to the control unit. There are different radar penetration depths for GPR, but a range from less than 1000 mm to greater than 30 m is usually common [125]. GPR waves travel through concrete dependent on admixtures, w/c ratio, air bubbles and aggregate size. The electrical conductivity of the material is dominant for GPR waves, especially water. Wetter concrete gives higher electrical conductivity and lower penetration [126]. The GPR technology includes high-frequency-pulsed EM waves between 10 MHz and 3000 MHz to acquire subsurface information. Transmitting antenna is responsible for propagation of energy downwards to the concrete, later reflected to a receiving antenna. The reflected signals are contributing to either scan production or trace of radar data. Relative permittivity and radar propagation of materials are emphasized in the standard. For concrete, the relative permittivity is between 5 and 10 K and pulse velocities are between 0.134 and 0.095 (m/Ns). The penetration depth is decided by the radar signal attenuation, where EM signals are converted to thermal energy through either dielectric relaxation, electrical conduction, or magnetic relaxation losses [125].

ASTM D6432 [125] specifies that alignment parallel with rebar increases the ability of rebar mapping, meanwhile alignment perpendicular to the rebar decreases rebar scattering reflections. Based on the last scenario, it may be challenging to see through or past the rebar with hope of evaluating concrete thickness. However, following standard highlights that a successfully complete GPR survey entails theory understanding, field procedures and interpretation methods of GPR data. The accuracy of GPR survey is dependent on the reflection depths. Lateral resolution and vertical resolution are major considerations for proper GPR scans. Lateral resolution is controlled by the antenna frequency, antenna speed and station spacing. On the other hand, vertical resolution is dependent on small change in GPR depth and detection of a thin layer [125].

Using GPR technology for bridge decks is a huge advantage related to unrequired removal of an existing asphalt overlay. Two types of GPR antennas are available: air-launched (1 – 2 GHz) and ground-coupled antennas (15 MHz – 2.5 GHz). The air-launched antennas are located 0.15 – 0.3 m above the surface of the investigated concrete surface and offers a faster scan attached to a vehicle, while ground-coupled antennas are used directly in contact with the surface of the concrete element. The ground-coupled antennas have the ability of a more enhanced concrete penetration, greater than 1 m, providing a higher resolution scan [127].

The main factors influencing the reflected signals from the assessed concrete are the speed of the signal, amplitude, attenuation, signal polarity and wavelength. Due to the variation in electrical properties of the layers in the concrete, a difference in the signal response will be registered detecting reinforcement, voids and cracks. The electrical conductivity determines the penetration of the EM waves, while relative dielectric permittivity affects the speed of EM waves. The deflection of rebars in a GPR scan is because EM waves cannot be penetrated through metals. The presence of moisture and chlorides will attenuate the GPR signals and therefor the GPR can indicate corrosion induced deterioration in the concrete [128].

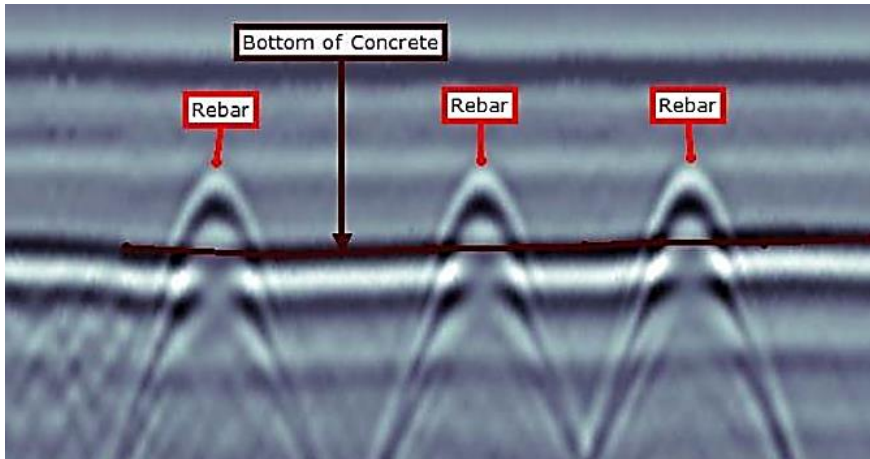


Figure 44 Rebars in GPR [129]

Figures 44 and 45 illustrate GPR with the reflection of different elements in the concrete. Strong reflection is observed of rebars as hyperbolas in the top layer of the concrete, while rebars in the underlying layers are reflected as secondary hyperbola. In Figure 44 the GPR scan of the bottom of a concrete element is shown and this reflection can provide estimation of the thickness of the slab. This also applies for the measurement of rebar spacing [129].

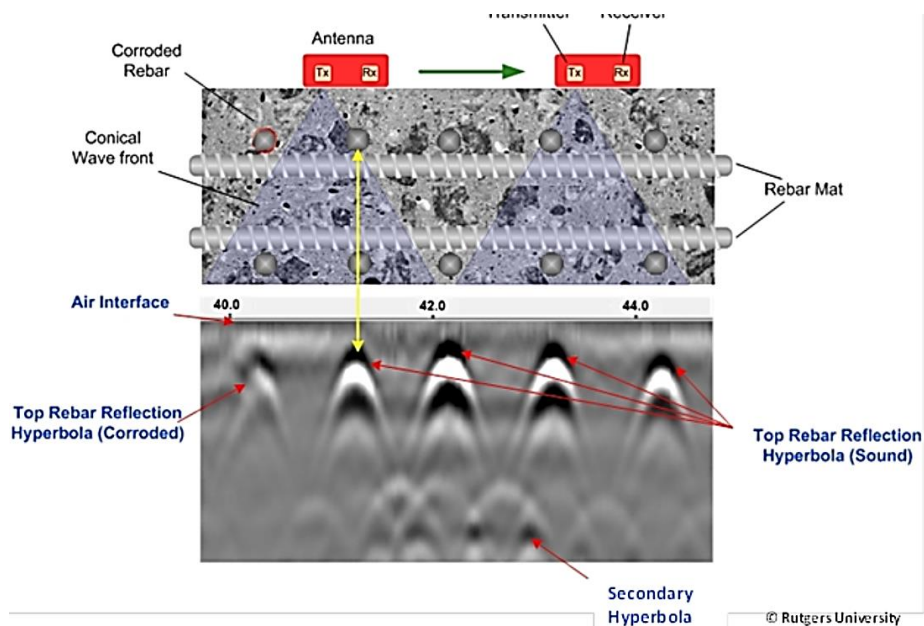


Figure 45 Illustration of GPR signals [128]

As mentioned, in the event of corrosion GPR signals will be attenuated around the area of the deterioration. This attenuation is clearly seen in Figure 45 and 46, where Figure 46 is from a GPR scan of a bridge deck inspection. Often the rebar amplitude values are processed into signal attenuation map images. Figure 47 shows a Deterioration Index map used to evaluate asphalt-covered bridge decks. Signs of deterioration, such as corrosion are marked in the red areas which is a consequence of lower amplitude as discussed earlier [130].



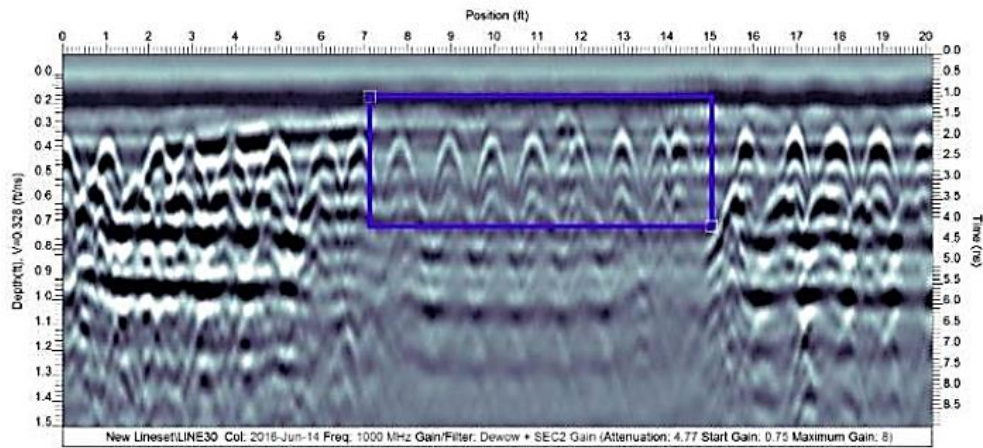


Figure 46 Detection of potential corrosion in a bridge deck [129]

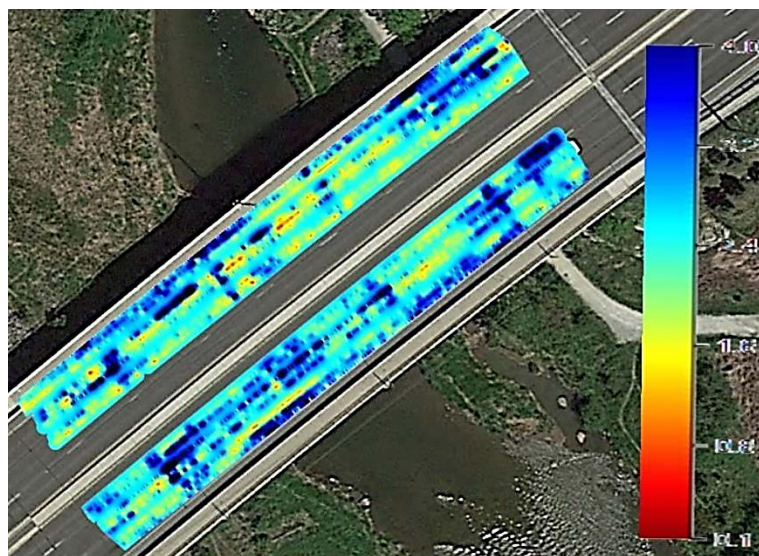


Figure 47 Deterioration Index map [130]

The detection of voids is often observed through strong reflection of the GPR signals due to the difference in properties between the concrete and the void filled with air/water, as seen in Figure 48. GPR is also a useful method for locating post-tensioned ducts (Figure 49) and are often used in combination with other NDT methods for the investigation of post-tensioned strands [129]. Garg and Misra [93] demonstrated that the GPR has the ability of detecting voids in post-tensioning plastic ducts, depending on the diameter of ducts and numbers of strands. The performance of detection increases when these parameters increase. However, this is not a suitable method for steel ducts.

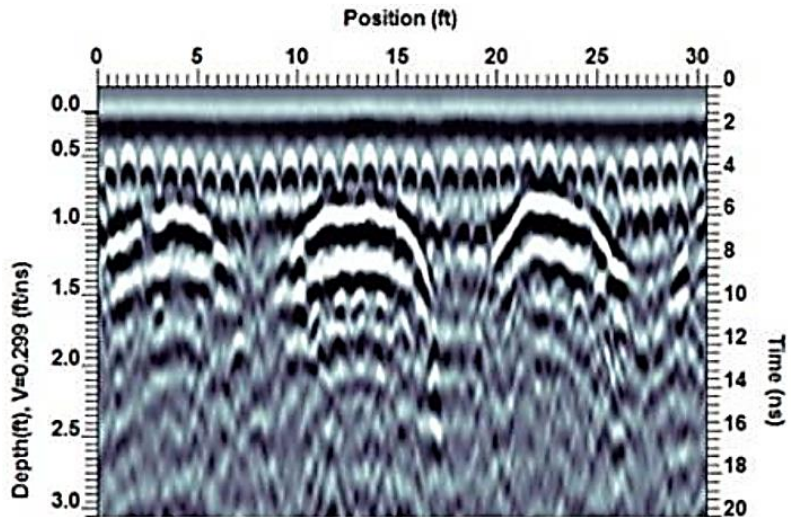


Figure 48 The reflection of voids [129]

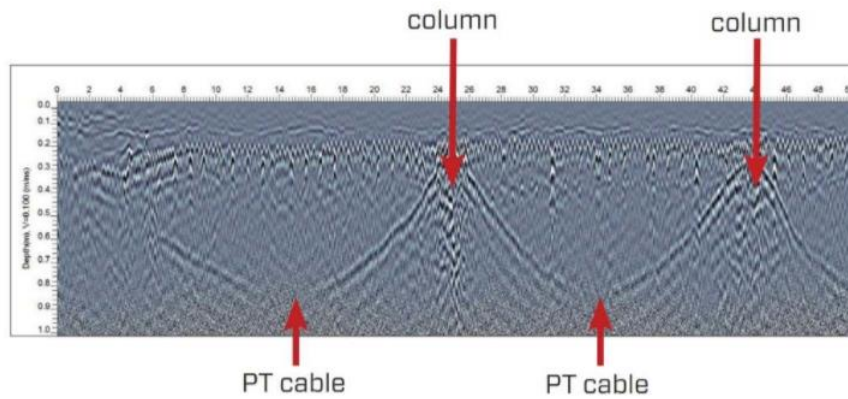


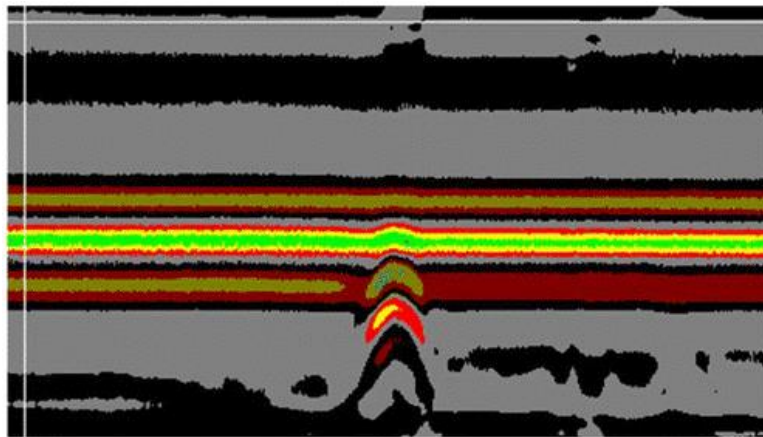
Figure 49 Location of post-tensioned ducts [129]

Table 18 show a general overview of advantages and limitations associated with ground-penetrating radar.

Table 17 Advantages and limitations of ground-penetrating radar[76] [15]

Advantages	Result limitations
Easily assess larger areas	Requires knowledge about physical principals of GPR and defect in concrete to interpret results
Detects location of reinforcement, voids and cracks	Signals from small objects are difficult to detect in the depth
	Possible difficulties with validation of corrosion
	Cannot detect defects on strand in post-tensioned concrete
	Difficult to detect objects under a lot of steel reinforcement

For estimation of cracks, Rhazi et al.[131] demonstrated that GPR can detect deep lateral internal cracks of a width between 0.5 and 3 mm. However, with a frequency of 400 MHz the reflection of the cracks was attenuated, and cracks were not possible to detect. Data processing was necessary and the GPR data was applied a low pass filter (25 – 100 MHz) for the cracks to be visible. For crack depth measurements with GPR, there are adapted antennas available for assessment of crack. Forest [132] proved that crack depths between 25 to 160 mm can possibly be detected with GPR. Still, the investigation emphasizes the challenges related to the interpretation of cracks with the GPR. The reflections of cracks from a GPR signal are observed in form of hyperbolic waves, as seen in Figure 50. Due to the disparity of crack geometry, a hyperbola will be reflected for every change of direction of the crack.






*Figure 50 GPR of a concealed crack [133]*

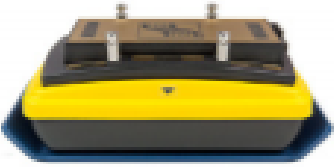

Among the researchers, there are a consensus that the GPR provide sufficient information about the location of the steel reinforcement and the concrete cover. Still, there are disagreements about the ability and reliability of detecting delamination in the concrete, as stated by Sultan et al. [134]. On one side, some researchers suggest that the GPR does not have the capability to fully detect delaminations and instead only indicates the possibility of corrosion due to presence of moisture and chlorides. These researchers have concluded that lower degree of deterioration gives less possibility to detect delaminations. On the other side, researchers including international standards organizations, suggests that the GPR shows promising result indicating the great potential of detecting delaminations. According to these researchers, the GPR has a great accuracy, where high reliability levels are presented [134].

There are many manufacturers of GPR products in the market, such as Proceq, Sensors & Software and Hilti. The Proceq models are based on “Stepped Frequency Continuous Wave” radar technology, which implies that the device separately has a large frequency range. Sensors & Software offers several types of GPR for different purposes, from assessing a concrete element to more complex concrete constructions such as bridges. All of the mentioned products are ground-coupled antennas and offer software for management, processing, and interpretation of the collected GPR data [135-137]. Table 19 provides a general overview of the mentioned products and the relevant details.



Table 18 Different GPR equipment from Proceq, Sensors & Software and Hilti [135-137]

Product	Product details
<p data-bbox="405 389 608 421">Proceq GP8800</p> 	<ul data-bbox="884 389 1406 1010" style="list-style-type: none"> <li>• Locates rebars, tendons, ducts and objects</li> <li>• Small size which allows inspection in tight spaces and close to concrete elements</li> <li>• An app to access data from a device</li> <li>• Provides 2D and 3D images of data</li> <li>• Penetration depth: 65 cm</li> <li>• Frequency range: 0.4 – 6 GHz</li> <li>• Price - \$3,135.00 - \$6,740.00 [138]</li> </ul>
<p data-bbox="405 1023 608 1055">Proceq GP8000</p> 	<ul data-bbox="884 1023 1449 1576" style="list-style-type: none"> <li>• Locates rebars, tendons, ducts and objects</li> <li>• Investigate pavement and bridge decks</li> <li>• An app to access data from a device</li> <li>• Provides 2D and 3D images of data</li> <li>• Penetration depth: 80 cm</li> <li>• Frequency range: 0.2 – 4 GHz</li> <li>• Price - \$9,875.00 - \$11,975.00</li> </ul>
<p data-bbox="395 1621 617 1653">CONQUEST® 100</p> 	<ul data-bbox="884 1621 1458 1973" style="list-style-type: none"> <li>• Locate rebars, post-tensioned cables and voids</li> <li>• An app to access data from a device</li> <li>• Investigate floors, decks, columns, walls and ceilings</li> <li>• Provides 2D and 3D images of data</li> </ul>

	<ul style="list-style-type: none"> <li>• Penetration depth: 30 cm – 91 cm</li> <li>• Antenna frequency: Up to 1 GHz</li> <li>• Price - \$14,899.00 [139]</li> </ul>
<p style="text-align: center;">NOGGIN® 1000</p> 	<ul style="list-style-type: none"> <li>• Investigation of e.g., pavements and bridges</li> <li>• Assessment of larger areas</li> <li>• Provides 2D images of data</li> <li>• Penetration depth: 25 m</li> <li>• Antenna frequency: 1 GHz</li> <li>• Price - \$7,425.00 [140]</li> </ul>
<p style="text-align: center;">PS 1000-B X-SCAN</p> 	<ul style="list-style-type: none"> <li>• Locate rebars, tendons, voids and cavities</li> <li>• Inspection of floors, decks and slabs</li> <li>• Depth accuracy: <math>\pm 0.5 - 15\%</math></li> <li>• Accuracy of locating rebars/tendons: <math>\pm 10</math> mm</li> <li>• Penetration depth: 30 cm</li> <li>• Antenna frequency: 1 – 4.3 GHz</li> <li>• Price – \$24,629.00 [137]</li> </ul>

To summarize, GPR appears to be an effective NDT method to locate and collect information about reinforcement and post-tensioning ducts embedded in the concrete. The disagreements about the evaluation of delamination may indicate that the detection is depending on the GPR equipment used in the assessment due to a variety in the frequency range as seen in Table 20. Further, the algorithms and user interface have a great impact on for the interpretation of the results and may vary among the manufacturers, as stated by [76]. One of the greatest challenges with the GPR is related to the interpretation of data. A thorough assessment of the data is necessary for the determination and distinguishing of

different deteriorations. The ability of GPR to assess the listed parameters is shown in Table 20. The uncertainties related to the method has been considered when giving scores.

Table 19 Assessment score of GPR

Deteriorations and other parameters	Assessment score
Cracks	2
Voids (internal)	3
Delamination (internal)	2
Corrosion of reinforcement	2
Corrosion of post-tensioning strands	1
Location of reinforcement	3
Location of post-tensioning systems	3

### 3.3.6 Concrete Resistivity (CR)

An NDT method of assessing corrosion is the CR method, a fast, simple, and cheap method of detecting corrosion. The electrical resistivity determines the current level between anodic and cathodic sites. The microstructure is an important factor affecting the electrical resistance of concrete of a concrete object, e.g., the conductivity of the pore solution and degree of saturation. For instance, a higher electrical resistance will be observed for a denser saturated concrete (low w/c ratio) than a porous concrete microstructure. The CR method can be divided into two systems: the four-electrode method and the two-electrode. The more recognized system is the four-electrode method used for in situ concrete. Meanwhile, the two-electrode method is considered a less accurate system [15, 77].

The most well-known four-electrode system is proposed by Wenner. The principle of this method is presented in Figure 51. The system provides information about the CR quickly and of four electrodes equally spaced in line at the concrete surface. A source of alternating current sends a low frequency between the two outer electrodes, and the voltages are measured in the inner electrodes through a voltmeter [15, 77].

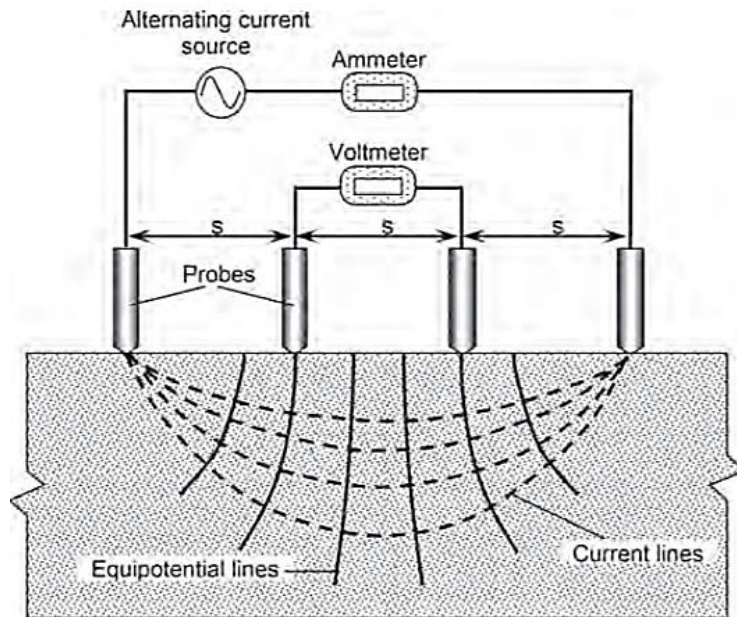


Figure 51 Principal of Wenner four-probe method [77]

An important variable affecting the CR measurements is the spacing of the electrodes. The spacing is mainly dependent on the maximum size of the aggregates because of the difference in resistivity and should be enough that a representative average of resistivity of the concrete is obtained. Normally, the electrodes have a spacing of 50 mm, reducing the degree of scattering, and can obtain accurate measurement up to 200 mm. For ideal measurements, wetting or conductivity gel is applied before pushing the electrode against the concrete surface resulting in better electrical contact between the electrodes and the concrete [15, 77].

Other factors influencing the CR are moisture, salt content, temperature, and mix properties. In general, the CR is often combined with HCP measurements for the assessment of corrosion rate. It is important to emphasize that there is no direct connection between resistivity and corrosion rate. Still, there are available guides for the interpretation of the possibility of corrosion. For instance, Table 21 is considered in combination with HCP readings indicating possible corrosion [15].

Table 20 Guide for interpretation of CR [15]

Resistivity (ohm cm)	Likely Corrosion Rate
Less than 5,000	Very high
5,000 – 10,000	High
10,000 – 20,000	Low/Moderate
Greater than 20,000	Negligible

Table 22 shows a general overview of the advantages and limitations associated with the CR method.


Table 21 Advantages and limitations of using CR method [77]

Advantages	Result limitations
Portable apparatus	Lack of standardization
Simple	Assumed models is the basis of measured values
Inexpensive	Expertise needed for testing and interpretation of results
Indicates relative corrosion rate when active corrosion is present	Some systems demand access to reinforcing bars for electrical contact

Nonetheless, as discussed, many uncertainties and factors are affecting the CR measurements. It is important to emphasize that the CR method cannot determine the corrosion rate unless the reinforcement is depassivated. ACI 228.2R-13 [77] points out that small spacing between the electrode may result in an error in the measurement due to a poor representation of the overall resistivity, often very high. With larger spacing, on the other hand, reliable measurements can be provided. However, there is a risk of the measurements being influence by the steel reinforcement due to the conductivity. The steel reinforcement's impact on the resistivity mostly depends on the concrete cover, especially for lower concrete covers and smaller bar spacing. ACI 228.2R-13 [77] also points out the possibility of difference in resistivity in the layers of the concrete due to the variation of aggregate size and resistivity (particularly in the concrete surface), and the CR measurements may not result in a good representation of the concrete [77].

Table 23 provides a general overview of the available products by Proceq and the relevant details.

Table 22 Different methods for corrosion by Proceq and other companies [141, 142]

Product	Product details
<p>Resipod</p> 	<ul style="list-style-type: none"> <li>• Water-proof construction</li> <li>• Accurate, standardized and reliable test method</li> <li>• Estimates corrosion rate and concrete resistance to aggressive agents</li> <li>• Visualize concrete homogeneity</li> <li>• Price – From \$3,450.00 [143]</li> </ul>

The CR method evaluates of probability of corrosion rate through the measurement of concrete resistivity. Guides for interpretation of concrete resistivity according to corrosion rate has been developed to confirm the HCP measurements suggesting corrosion. However,



several factors must be considered for the inspection to obtain more reliable measurements as discussed, thus expertise is required when conducting this test. The ability of CR to assess the listed parameters is shown in Table 24 . The uncertainties related to the method has been considered when giving scores.

Table 23 Assessment score of CR

Parameters	Assessment score
Cracks	0
Voids	0
Delamination	0
Corrosion of reinforcement	2
Corrosion of post-tensioning strands	0
Location of reinforcement	0
Location of post-tensioning systems	0

### 3.3.7 Cover meter (CM)

Cover meter (CM) is an electromagnetic method visualizing the steel reinforcement in x-, y- and z-direction and defines the thickness of the concrete cover. The following NDT method is described as useful, cost-effective, accurate and simple. Nevertheless, *CM* is not recommended to use in locating post-stressing tendons, dependent on the amount of reinforcement. The *CM* has difficulties locating rebars and tendon ducts because of limited depth range, compared to other NDT methods. However, the *CM* is a necessary part of inspections based on the accuracy of localization, usually in the range of 1 – 4 mm and the accuracy range is influenced by concrete cover [76].

The British standard *BS 1881-204* includes recommendations on using electromagnetic *CM*. The principle is to decide bar position, depth, size and accuracy from electromagnetic devices. Application areas for *CM* are quality control of correct location and reinforcement cover. *BS 1881-204* emphasize that the concrete surface is scanned with the search head, where the *CM* detects proximity of reinforcement either by analogue or digital devices. The standard requires the *CM* to have a concrete cover accuracy, depending on the largest value, of either  $\pm 5\%$  or  $\pm 2$  mm. Further, the standard classifies *CM* tests as method A, B or C, depending on the concrete quality. Method A is utilized for cover at 12 mm or above. For smaller cover, method B or C is recommended. The search head should not be subjected by rapid movement, which can influence the calibration mark. *BS 1881-204* also highlights that a report related to *CM* testing must be included [144].

*CM* emphasizes the interaction between the reinforcing bars and low-frequency electromagnetic field. In other words, understanding the operation of *CM* depends on the basic relationship between electricity and magnetism. Electromagnetic induction is a significant principle in *CM*, defined as a magnetic field intersecting an electrical circuit that induces an electrical potential, connected to the Faraday's law. According to ACI 228.2R-13 [77] commercial *CM* is normally divided into two different systems: *magnetic reluctance*

meters and eddy-current meters. Figure 52 perfectly describes a simplified schematic of *CM* dependent on the variations in the reluctance of a magnetic circuit either with or without steel bar [77].

A ferromagnetic U-shaped core called yoke, an excitation coil and a sensing coil is included in the magnetic reluctance meter. A current from the excitation coil creates the magnetic flux, and in the absence of steel bar, a high reluctance is registered between the yoke and concrete. In addition, the amplitude of the magnetic flux between excitation coil and sensing coil is small, illustrated in Figure 52a. In Figure 52b, the reluctance decreases, and the magnetic flux amplitude increases. This clarifies that the sensing coil current will also increase, dependent on if the steel bar is present. However, the reluctance is strongly dependent on the distance between the bars and yoke poles [77].

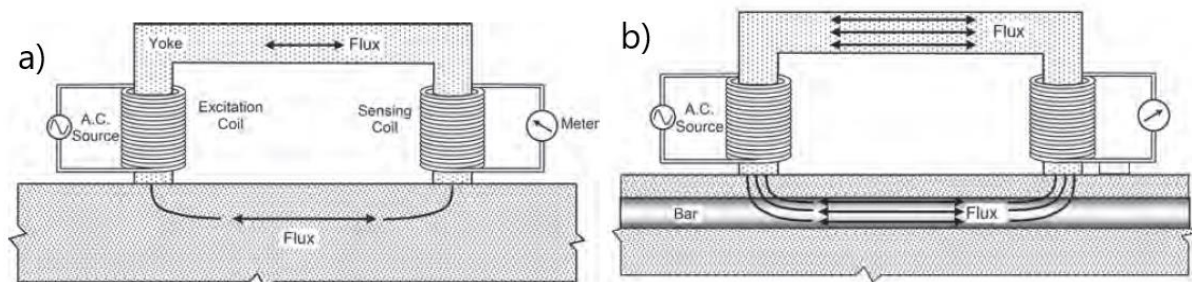


Figure 52 Illustrations of magnetic reluctance meters for: a) small current induced in sensing coil without bar; b) enhancement of current in sensing coil with bar [77]

Eddy-current *CMs* define circulating currents at the magnetic field and occurs when an alternating current is approaching near an electrical conductor and is divided in two different categories. The first category considers the continuous excitation of the coil by an alternating current, meanwhile the second category is dependent on pulsed excitation. Figure 53a shows eddy-current *CM* without reinforcing bar. When bringing the coil near the reinforcing bar, alternating eddy currents are active on the bar surface. Therefore, eddy currents are described as additional source for an alternating secondary magnetic field, inducing a secondary current in the coil. Figure 53b points out eddy-current *CM* with reinforcing bar. Depth and size of the steel bar are factors influencing the induced current amplitude [77].

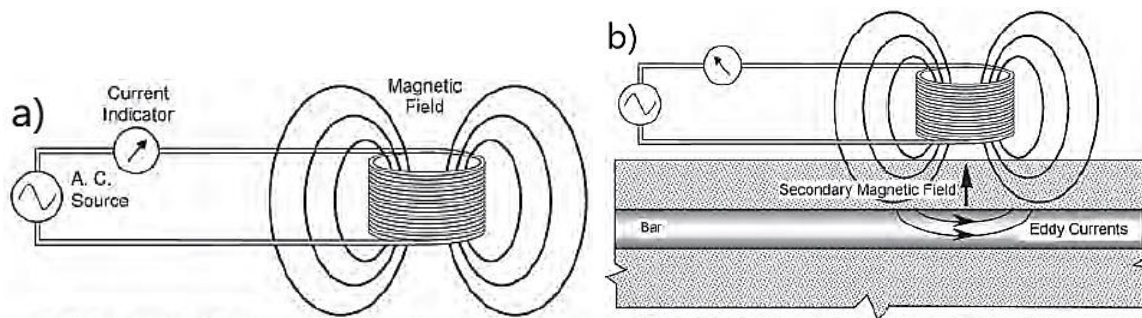


Figure 53 Illustrations of eddy-current meters for: a) a characteristic current amplitude; b) differences in current amplitude interacting with reinforcing bar [77]

Maximum response is obtained when the search head is placed directly above the reinforcing bar, as shown in Figure 54a. The relationship between meter amplitude and the horizontal distance is significant for *CM* measurements, identified from the center of the steel bar to the

center of the search head. Figure 54b pinpoints diversification in amplitude by considering the horizontal distance, identifying a magnetic reluctance  $CM$ . The cover depth was equal to 21 mm, meanwhile the size of the steel bar is 19 mm. Following figure has attributes related to a bell-shaped curve. Figure 54c shows the relationship between amplitude and horizontal distance for an eddy-current meter, emphasizing two different search heads. By comparing both search heads, one of them has smaller area of influence, which is an advantage for detecting individual bars that are closely spaced. This type of search head is known as focused search heads. Nevertheless, focused search heads have less penetrating ability, unable to localize bars with deep cover. Both search heads in Figure 54c consider the same bar size (19 mm), but cover depth for search head 1 is defined as 21 mm, meanwhile cover depth for search head 2 is 59 mm [77].

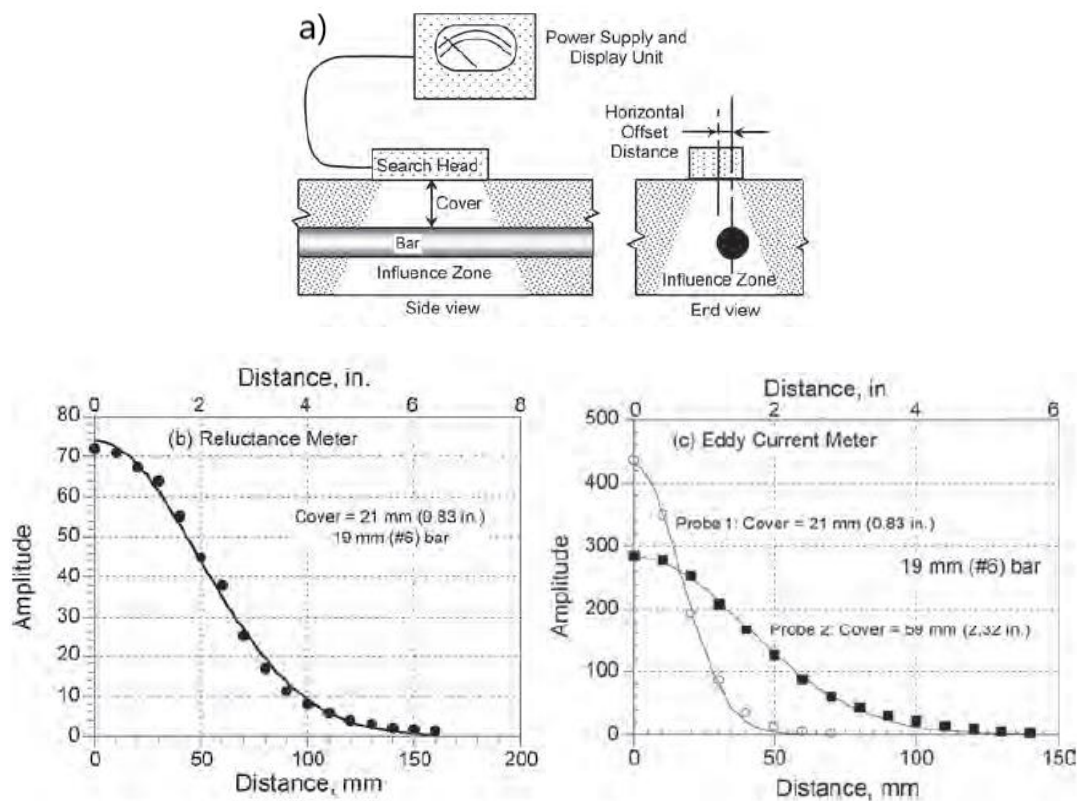


Figure 54 Zone of influence for: a) the search head; b) magnetic reluctance  $CM$ ; c) eddy-current  $CM$  [77]

Table 25 shows a general overview of advantages and limitations associated with the  $CM$  test.

Table 24 Advantages and limitations of using  $CM$  test [77]

Advantages	Result limitations
Locate reinforcing bars	Bar size and spacing affect cover depth accuracy
Portable and easy to use	Difficult to bar diameters with precision
Lightweight	Does not identify presence of second layer of reinforcement


Estimates cover depth	Limitation of maximum penetration and dependent on meter design
-----------------------	---




Algernon et al. [145] demonstrated an excellent accuracy of CM measuring concrete cover with different distances between the reinforcement and diameter, providing an accuracy of  $\pm 1$  mm. However, considering an additional layer of reinforcement had a negative influence on the accuracy. Larger diameter and close spacing between the steel bars in the crossing layer are influential for doubtful measurements. Different CM equipment are available in the market from the manufacturers Proceq, such as various Profometer models and Profoscope(+). Hilti and Elcometer, also offer the Ferroskan PS200 and various models of Elcometer 331, respectively. Different search heads are supplied providing a variety of depth range and the main difference of the models is related to the ability for multiple NDT evaluation, such as HCP.



For instance, Hüblová et al. [146] demonstrated the Profometer 630 AI has the possibility of analyzing uninterrupted linear scans up to 15 m. The equipment provided promising results for determining reinforcement diameter with an accuracy of  $\pm 1$  mm. However, Cikrle et al. [147] showed some challenges with the Profometer 630 AI. Detecting closely placed rebars with CM is a challenge, regardless if the rebars are behind or next to each other. In addition, measurements deeper than 100 mm can influence obtained CM results. Although the distance of the bend from the abutment was measured with an accuracy of  $\pm 10$  mm, Profometer 630 AI managed easily to locate bends in reinforcement.

Table 26 provides a general overview of the available products by the manufacturers and relevant product details.

Table 25 Different CM equipment from Proceq and other companies [148] [149]

Product	Product details
<p>Profometer 650 AI</p> 	<ul style="list-style-type: none"> <li>• High quality of cover measurement through Artificial Intelligence (AI) feature</li> <li>• Measure rough surfaces and wide areas</li> <li>• Provides 2D and 3D imaging of rebar arrangement</li> <li>• Cover measuring: 185 mm</li> <li>• Cover measuring accuracy: <math>\pm 1</math> to 4 mm</li> <li>• Diameter measuring: Up to 63 mm</li> </ul>

	<ul style="list-style-type: none"> <li>• CM principal: Eddy current</li> <li>• Price - \$8,180.00 [150]</li> </ul>
<p>Profometer 630 AI</p> 	<ul style="list-style-type: none"> <li>• High quality of cover measurement through Artificial Intelligence (AI) feature</li> <li>• Measure rough surfaces and wide areas</li> <li>• Depth measuring range: 185 mm</li> <li>• Cover measuring accuracy: <math>\pm 1</math> to 4 mm</li> <li>• Diameter measuring: Up to 63 mm</li> <li>• CM principal: Eddy current</li> <li>• Price - \$6,635.00 [150]</li> </ul>
<p>Profometer 600</p> 	<ul style="list-style-type: none"> <li>• Measure rough surfaces</li> <li>• Depth measuring range: 185 mm</li> <li>• Cover measuring accuracy: <math>\pm 1</math> to 4 mm</li> <li>• Diameter measuring: Up to 63 mm</li> <li>• CM principal: Eddy current</li> <li>• Price - \$5,085.00 [150]</li> </ul>
<p>Profoscope(+)</p> 	<ul style="list-style-type: none"> <li>• Includes single handed operation</li> <li>• Checks spot on rebar cover</li> <li>• Depth measuring range: 185 mm</li> <li>• Cover measuring accuracy: <math>\pm 1</math> to 4 mm</li> <li>• Diameter measuring: Up to 63 mm</li> </ul>

	<ul style="list-style-type: none"> <li>• CM principal: Eddy current</li> <li>• Price - \$2,465.00 - \$2,620.00 [151]</li> </ul>
<p style="text-align: center;">Ferrosan PS200</p> 	<ul style="list-style-type: none"> <li>• Measure rough surfaces and wide areas</li> <li>• Provides 2D and 3D imaging of rebar arrangement</li> <li>• Depth measuring range: 180 mm</li> <li>• Localization accuracy: <math>\pm 3</math> mm</li> <li>• Minimum distance detection of objects: 36 mm</li> <li>• CM principal: Eddy current</li> <li>• Price - From \$6,800.00 [152]</li> </ul>
<p style="text-align: center;">Elcometer 331 Models</p> 	<ul style="list-style-type: none"> <li>• Easy to transport and store with single handed operation</li> <li>• Depth measuring range: 180 mm</li> <li>• Diameter measuring: 8 – 40 mm</li> <li>• CM principal: Eddy current</li> <li>• Price - \$1,250.00 - \$2,549.00 [153] [154]</li> </ul>

To summarize, *CM* is an efficient NDT contributor controlled by either magnetic reluctance meters or eddy-current meters. There are many *CM* products that are available in the market and all of the *CM* equipment consider eddy-current principle rather than magnetic reluctance principle. The explanation is that magnetic reluctance detects only ferromagnetic objects, limiting the detection of rebars to certain types of steel reinforcement. Overall, *CM* equipment are contributing to decent accuracy of reinforcement diameter, which allows correction in the distance of adjacent rebars. Simultaneously, fast and accurate results on measuring cover depth are obtained from *CM* equipment. However, using *CM* is a challenge for measuring an additional layer of reinforcement crossing the layer, where the accuracy decreases. In the crossing layers, large diameter and close spacing between steel bars are affecting the measurements negatively. Nonetheless, the *CM* cannot directly indicate any deteriorations or provide an evaluation of the internal condition of a concrete. The ability of



CR to assess the listed parameters is shown in Table 27. The uncertainties related to the method has been considered when giving scores.

Table 26 Assessment score of the CR method

Parameters	Assessment score
Cracks	0
Voids	0
Delamination	0
Corrosion of reinforcement	0
Corrosion of post-tensioning strands	0
Location of reinforcement	3
Location of post-tensioning systems	0

### 3.3.8 Half-Cell Potential (HCP)

Half-Cell Potential is an acknowledged NDT method in the field to estimate steel corrosion in concrete structures. For corrosion detection and corrosive environmental detection, HCP measurements are preferred. HCP is described as cost-effective and rapid, contributing to secure concrete repair and rehabilitation. Evaluation of steel corrosion is measured from the coherence between corrosion potential and steel corrosion rate. A standard portable half-cell and a standard reference electrode are active to measure the potential difference. Different reference electrodes used in the set-up of HCP are copper-copper sulfate and silver-silver chloride/potassium chloride. The reference electrode is attached to the positive pole of the voltmeter, and the steel reinforcement is connected to the negative end, shown in Figure 55 [155, 156].

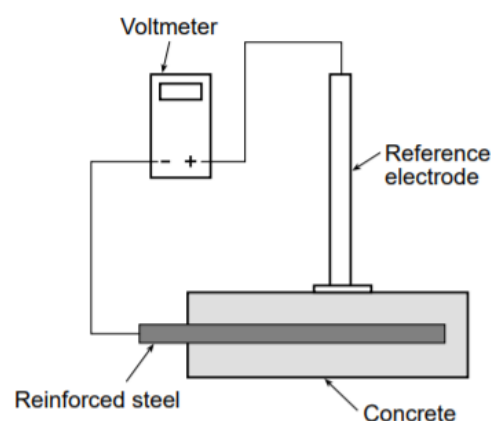


Figure 55 Schematic setup of HCP in reinforced concrete [155]

The different factors influencing the test result readings of the HCP method are oxygen level, chloride concentration, concrete electrical resistance, and concrete cover. A reduction in oxygen concentration on the steel reinforcement gives higher negative corrosion potential values. However, the probability of steel corrosion is still less because corrosion is affected by

permeability. For instance, porous concrete with higher permeability has less negative corrosion potential than a dense concrete cover with low permeability. Concrete carbonation decreases the pH value of steel reinforcement, enhancing the probability of steel corrosion. The following case gives more negative corrosion potential values, which is related to enhancement in the rate of corrosion [155].

Higher chloride ion concentration gives significant steel corrosion in reinforced concrete and a more negative corrosion potential value. Simultaneously, a dense concrete cover gives a decent physical barrier defending the steel from chloride-induced corrosion. The reinforced concrete has a relatively low oxygen level, where the corrosion potential shifts towards negative potential values. High concrete resistance is conducive for significant errors in HCP data. The potential between the two ends of the voltmeter's resistance describes the measured half-cell potential. If the potential resistance is greater than the concrete resistance, the measured HCP value is approximately identical to the steel reinforcement's corrosion potential. The accuracy is increased by wetting the concrete surface, which decreases the concrete resistance. Another possibility is to include a voltmeter with high internal resistance greater than 20 M $\Omega$  [155]. Table 28 presents the probability of corrosion from HCP measurements.

*Table 27 Probability of corrosion based on HCP method [155]*

<b>HCP readings (Cu/CuSO<sub>4</sub>)</b>	<b>Corrosion activity</b>
Less negative than -0.200 V	90% probability of no corrosion
Between -0.200 V and -0.350 V	An increasing probability of corrosion
More negative than -0.350 V	90% probability of corrosion

The purpose of ASTM C876 [156] is to determine the corrosion activity of the reinforcing steel. The HCP method is applicable to different members irrespective of their size or concrete cover depth. A concrete cover above 75 mm can lead to loss of the ability to detect variation in relative corrosion activity. In addition, either engineers or technical specialists with massive experience in concrete materials and corrosion evaluation in the fields should interpret the potential measurements. Other vital data such as carbonation depth, delaminations, corrosion rate, and environmental exposure conditions are contributing to formulating conclusions regarding corrosion activity of embedded steel and its influence on the structure's service life. Data presentations are either available as equipotential contour maps or cumulative frequency diagrams. A contour map contributes to a graphical illustration of concrete areas where corrosion activity occurs. The cumulative frequency diagram indicates the concrete's magnitude of the influenced area. Localizing corrosion pinpoints differences in potential over relatively short distances. Another condition with the demand of experienced engineers is the evaluation of the carbonated depth of reinforcing steel. Irrespective, corrosion potentials are neither nor an indication of corrosion current [156].

Table 29 shows a general overview of the advantages and limitations associated with the concrete resistivity method. with HCP method.




Table 28 Advantages and limitations of using HCP method [15]




Advantages	Result limitations
Portable apparatus	Indirectly indicate corrosion
Simple	Minimal information of the corrosion rate
Inexpensive	Experienced operator required
Straight forward data analysis	Demands access to reinforcing bars for electrical contact
	Decreases test accuracy dependent on concrete moisture and temperature

When addressing the efficiency of the HCP method there are some uncertainties related to the measurements. As explained by Gu and Beaudoin [155], even if lower negative values are obtained from the HCP method there are several factors affecting the measurements and increasing the probability of corrosion. Not all of these factors are directly related to induction of corrosion and the HCP measurements can be misleading as an evaluation. It is therefore important to emphasize that this test method only indicate the probability of corrosion. This was clearly shown in the investigation of Frølund et al. [157], where the HCP measurements were concluded to be misleading in three out of four case.

There are different HCP equipment available in the market, with varying specifications and features. Some of the manufacturers Proceq, Elcometer and Jet materials. Table 30 provides a general overview of the available products by the manufacturers and relevant product details.

Table 29 Different methods for corrosion by Proceq and other companies [141, 142]

Product	Product details
<p>Profometer Corrosion</p> 	<ul style="list-style-type: none"> <li>• Advanced processing and reporting tools</li> <li>• Effective productivity with wheel electrodes</li> <li>• Cover meter functionality available for combined testing</li> <li>• Price - \$4,090.00 - \$5,780.00 [143], [158]</li> </ul>

<p>CANIN+ (discontinued)</p> 	<ul style="list-style-type: none"> <li>• Quick presentation of test area</li> <li>• Cost effective approach</li> <li>• Detects active corrosion in reinforcement</li> <li>• Wheel electrodes available for increasing testing speed</li> <li>• Price – Unknown</li> </ul>
<p>Elcometer 331 model</p> 	<ul style="list-style-type: none"> <li>• Easy to transport and store with single handed operation</li> <li>• Quickly and accurately locate the orientation of rebars in harsh environments</li> <li>• Up to 32 hours battery use</li> <li>• Price - \$1,250.00 - \$2,549.00 [153] [154]</li> </ul>
<p>COR-MAP® SYSTEM</p> 	<ul style="list-style-type: none"> <li>• Locates corroding steel reinforcement easily and economically</li> <li>• Designed electrodes available for horizontal, vertical, and inverted positions</li> <li>• Price - \$1,614.00 [159]</li> </ul>

Based on these facts and the addressed literature, it is recommended that HCP should be combined with other NDT tests to increase the accuracy and the probability of detection of corrosion, due to the fact that there are many factors affecting the HCP measurements. However, one should not ignore the fact that HCP can be a great approach for assessing and indicating the possibilities of corrosion, but further investigation is required for validation. The concrete resistivity method is a great and easy NDT test in combination with HCP. Guides for interpretation of concrete resistivity according to corrosion rate has been developed to confirm the HCP measurements suggesting corrosion. However, several factors must be considered for the inspection to obtain more reliable measurements as discussed, thus expertise is required when conducting this test.

Table 30 Assessment score of HCP

Parameters	Assessment scores
Cracks	0
Voids	0

Delamination	0
Corrosion of reinforcement	2
Corrosion of post-tensioning strands	0
Location of reinforcement	0
Location of post-tensioning systems	0

### 3.4 Combining NDT methods in field tests

When a concrete structure is investigated, an assessment strategy for NDT methods is prepared. The NDT methods used in the investigation must be selected based on the purpose of the survey and their usefulness. There are several NDT methods and techniques enabling the detection of different defects and flaws, and many of these NDT methods are combined to gain an enhanced insight of the condition of the structure. Including multiple NDT methods are a secure way of realizing and managing durability conditions of reinforced concrete. In addition, combining NDT methods is a common approach in different field tests presented in the literature, and will be briefly described in this chapter.

#### 3.4.1 Field test of Farris bridge in Larvik

The following field test is presented from the NPRA report elaborated by DEKRA Industrial and Täljsten [76]. The purpose of the field test of the Farris bridge was to detect partial and fully grouted ducts by combining several NDT methods. NDT methods that were combined for the Farris bridge are CM, GPR, and UPE. CM was used to localize the first layer of rebars with concrete cover around 16-25 mm, meanwhile GPR localized the tendon ducts in the segments. Placement of tendon ducts and the mesh visibility were possible with an area scan, seen in Figure 56. The following figure for segment 1 clarified ducts at a depth around 150 mm, visible from the red arrows. Segment 2 had difficulties verifying the ducts because of duct placement at a greater depth. The ducts placed with a depth around 350 mm in segment 2 were impossibly detected by GPR technology, clearly shown in Figure 57. Results from the GPR are dependent on the quality of concrete and the signal speed [76].

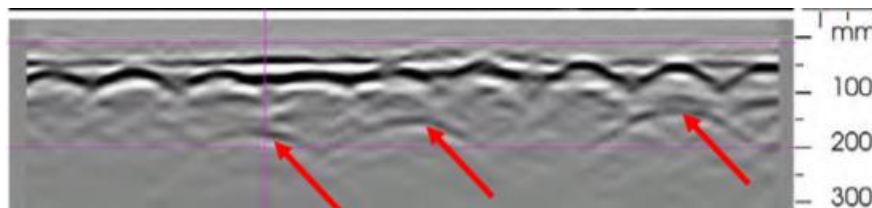


Figure 56 Tendon ducts marked with red arrows in segment 1 [76]

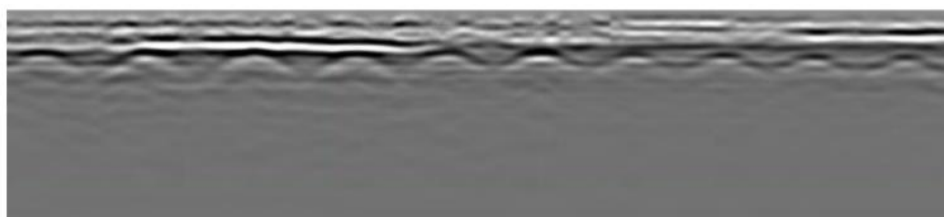


Figure 57 No sign of tendon ducts in segment 2 [76]

Together with CM and GPR, UPE scans were performed on the ducts for both segment 1 and segment 2. The red arrow in Figure 58 showed clear visibility of coherent tendon duct 3 with an average depth of 150 mm. Figure 59 identified the same tendon duct 3 (red arrow) at a depth between 165-450 mm. From Figure 59, localization of the ducts was complicated in segment 2 because of the higher depth value. Therefore, examination of results in the computer and extensive data processing were recommended for segment 2. According to

DEKRA and Täljsten, signals were weak because of a placement with a depth from 200-450 mm. Another reason may be that the grout in ducts is partly injected [76].

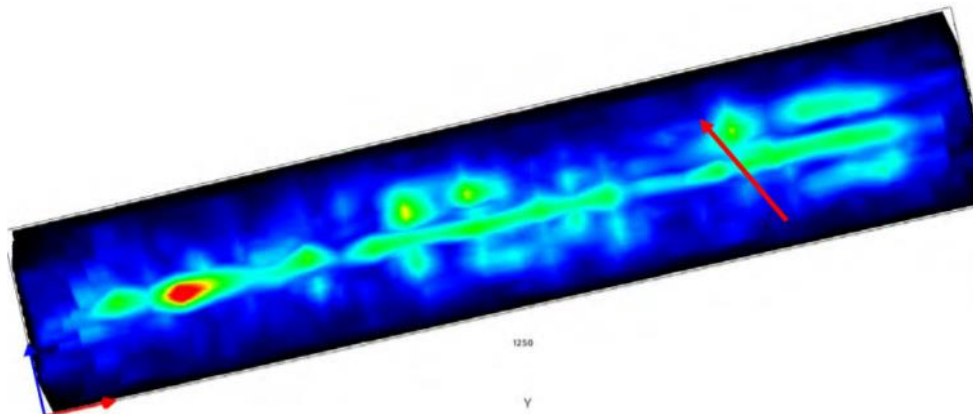


Figure 58 Tendon duct 3 at a depth around 150 mm (segment 1) [76]

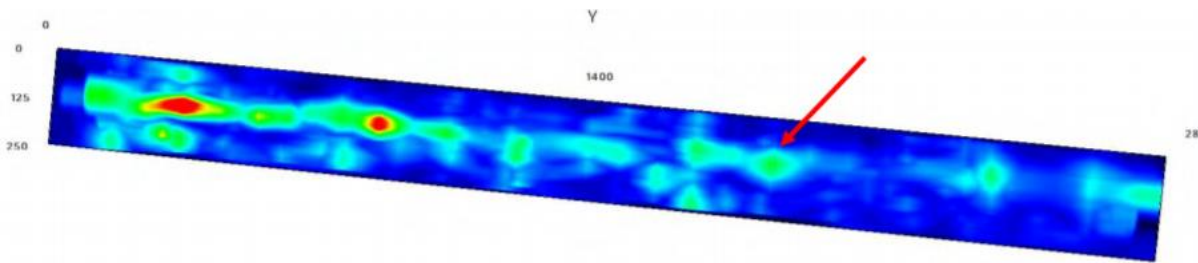


Figure 59 Tendon duct 3 at a depth between 165-450 mm (segment 2) [76]

Obtained results from the Farris bridge were valuable to understand better how combining NDT methods work together. CM is a quick learnable NDT method with less knowledge required. However, CM has a limit of 80 mm, making several challenges to locate the tendon ducts. In addition, CM has difficulties distinguishing between reinforcement and tendon ducts. Therefore, combining CM with GPR can be efficient regarding depth measurement for tendon ducts. Uncertainties may arise considering the interpretation of CM and GPR. Including UPE, CM, and GPR show a clearer indication of the cavity in concrete [76].

### 3.4.2 Field test of Herøysund bridge

A field test was conducted in the Herøysund bridge by DEKRA Industrial and Täljsten [76] to investigate the condition of the tendon ducts in the bridge. This test was a part of concrete repair work, and an NDT inspection was conducted to detect voids inside the ducts and other defects to assess the bridge's safety.

A combination of different NDT tests was preferred to achieve the best possible results. The NDT tests emphasized in this field test were the CM, GPR, UPE, IE, and VI. The case study highlights that experience is needed when investigating tendon ducts and determining the degree of grouting. Combining NDT methods and drilling holes into the duct is a required NDT approach to inspect and verify the condition of the strands in terms of corrosion and breakages in the wires. Tendon ducts tend to be located deep into the concrete, and with this shortcoming, there are difficulties for the CM to locate tendon ducts. On the other hand, GPR

serves more efficiently for this task with a depth precision of up to 200-250 mm. These two methods are combined in the sense that the information about the location of rebars and concrete cover from the CM is used to calibrate the GPR to gain accurate results. The GPR locates and marks the tendon ducts on the concrete structure to facilitate the UPE to detect voids. Further, the IE method is used to verify the data from UPE [76].

Different locations of the tendon ducts on the bridge were chosen for investigation, as seen in Figure 60.

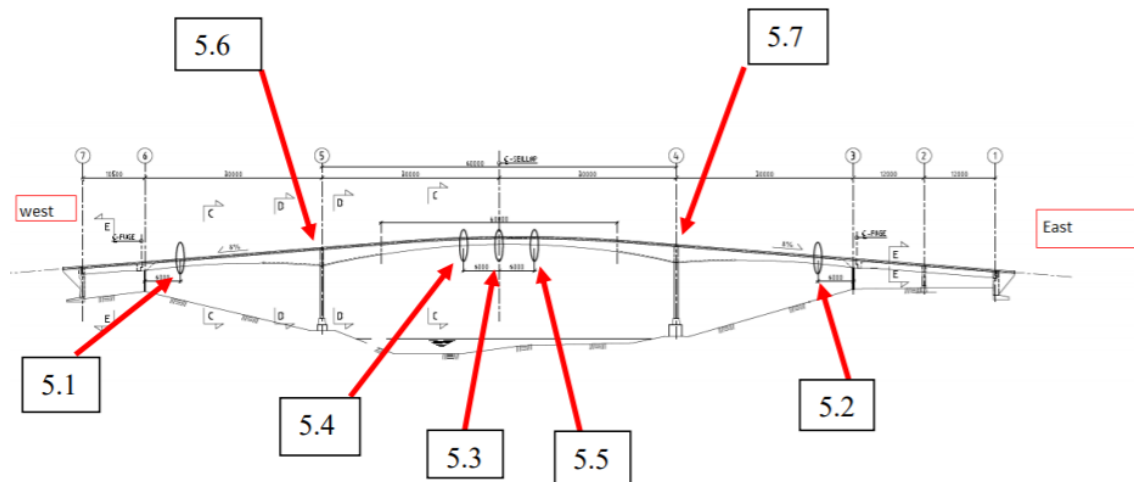


Figure 60 Test areas of the bridge [76]

On a general basis, the NDT tests were a great approach and revealed that all the 8 ducts in both girders had missing grouting in some investigation points. For simplicity, only some of the results of this inspection will be addressed. For instance, the North grid of point 5.1 did not detect any voids in the ducts. Nonetheless, on the South grid, the UPE indicated both small voids (2S) and missing grout (3SA), as seen in Figure 61 in red. The location of the ducts in the GPR is shown in Figure 62 [76].

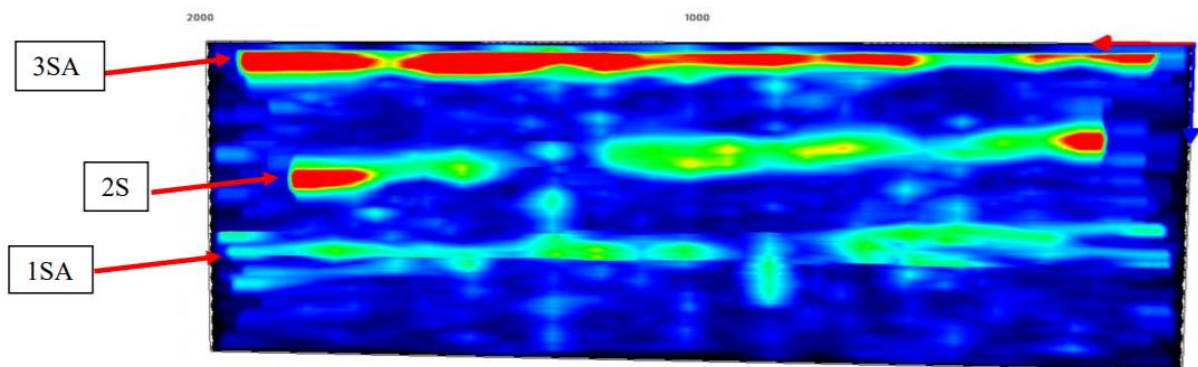


Figure 61 UPE scan from point 5.1 South girder [76]

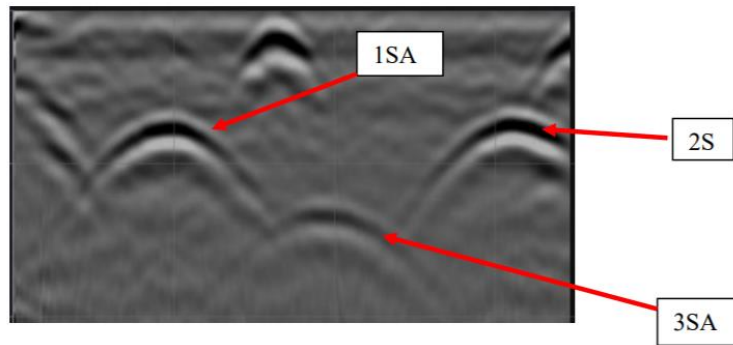


Figure 62 GPR from point 5.1 South girder [76]

For point 5.2 Southern girder, three holes were drilled as a visual check to confirm the results from the UPE. The location of the holes and the results from the UPE scan is shown in Figure 63. The moderate scan signals are seen from tendon ducts 1SC and 2S, indicating no missing grouts or air voids. Strong signals are seen through the whole tendon duct 3SC, indicating an air-filled duct. Another scan over a longer span was conducted for duct 3SC to assess the grouting. Figure 64 reveals that strong signals along the whole duct, indicating missing grout [76].

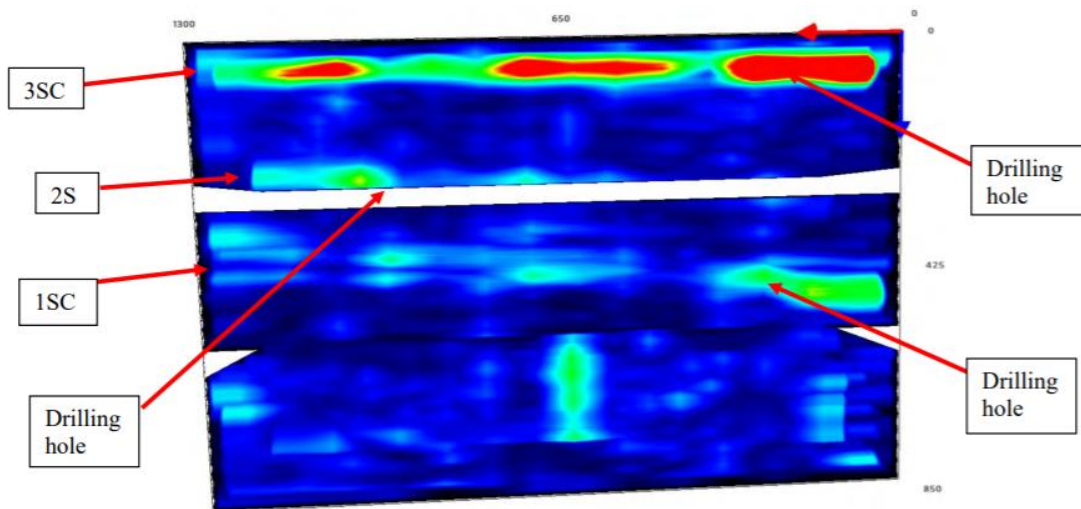


Figure 63 UPE scan from point 5.2 South girder [76]

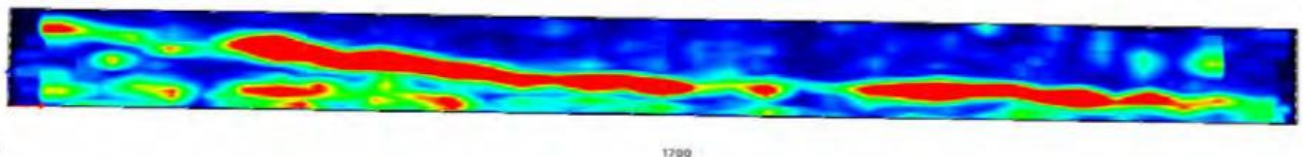
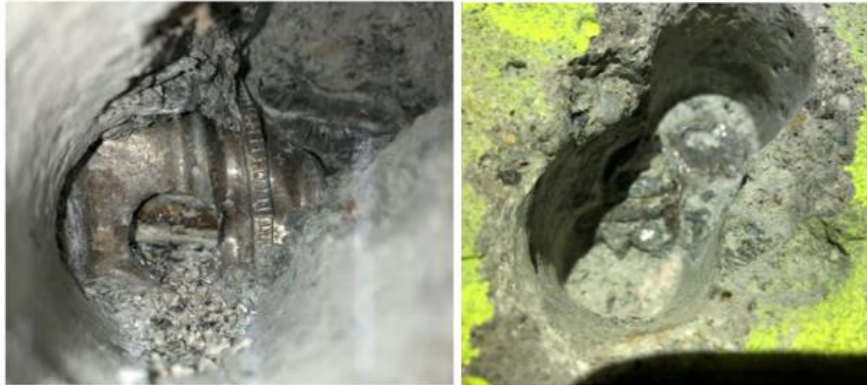


Figure 64 UPE scan of tendon duct 3SC [76]



The holes drilled in tendon duct 1SC and 2S confirm the grouting, as seen in the results from the UPE. For tendon duct 3SC, the drilling revealed missing grouting as expected. However, breakage in three wires was also detected. The breakage of wires is a consequence of air in the tendon ducts, which induces corrosion [76].



*Figure 65 Drilling and visual check of 1SC (left) and 2S (right) [76]*



*Figure 66 Drilling and visual check of 3SC [76]*

In point 5.3 Northern girder, no voids were detected. However, 1 m from the middle in both directions revealed voids and missing grouting. In the Southern girder, three of four cables had voids and missing grouting. The results from UPE for point 5.5 are shown in Figure 67, where the tendon duct 1NB and 2N do not show any strong signals. However, duct 3ND suggests missing grout or partially grouting due to the variation in signals, and tendon duct 4NB indicates missing grouting due to the continuous strong signals [76].



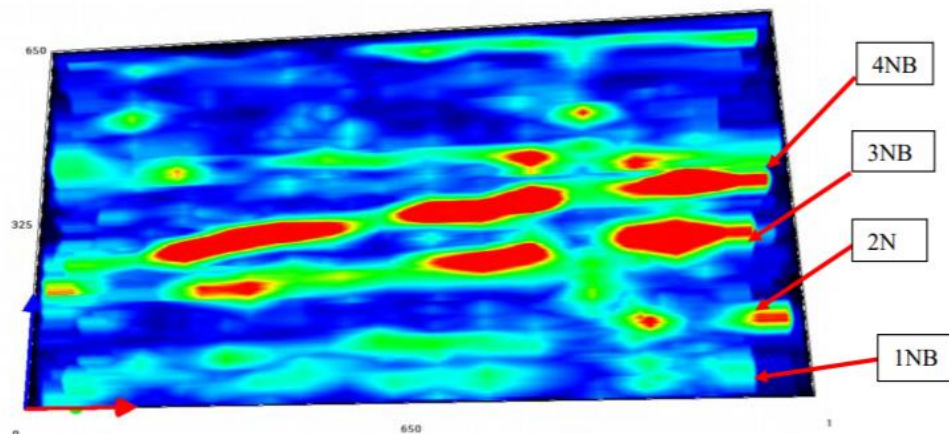


Figure 67 UPE scan from point 5.5 [76]

To summarize, the case study emphasizes the importance of following the general principles of maintenance, repair, and upgrading. Combining CM, GPR, UPE, IE, and VI are adequate approaches to evaluate the condition of the tendon ducts. Every NDT method used in this inspection has served an important task for detecting the condition of the tendon ducts. From the inspection, point 5.4 showed the largest defects in the ducts where 6 out of 8 tendons ducts had missing grouting, and cable 3 in both points 5.1 and 5.2, in the Southern girder, was not fully grouted near the anchors. In several cases, larger voids were detected, signifying the need for maintenance and repair. Further, wire breakage was discovered in cable 3SC, and lack of grouting combined makes it difficult to locate the breakage. Load cracks at the bottom of the girders were observed, which may have affected the un-grouted tendon ducts at the bottom of the girders and resulted in corrosion.

### 3.4.3 Field test of Dalselva bridge

Information presented in the field test is from the research paper *“Inspection and Assessment of Corrosion in Pretensioned Concrete Bridge Girders Exposed to Coastal Climate,”* elaborated by Osmolska et al. [11]. The bridge inspection was conducted in 2018, where the condition of NIB girders was evaluated by combining HCP, CR, and VI. Structural cracks, delaminations, and wet concrete areas were briefly documented. According to Osmolska et al. [11], Girder 2 was selected for a detailed investigation, where combining CR, HCP, and VI were emphasized. A four-point Wenner Probe was used to evaluate the CR in girder 2. Along the whole span length of the girder’s bottom surface, HCP measurements were included to detect locations with a high probability of corrosion in girder 2. Figure 68 shows different views of girder 2 [11].

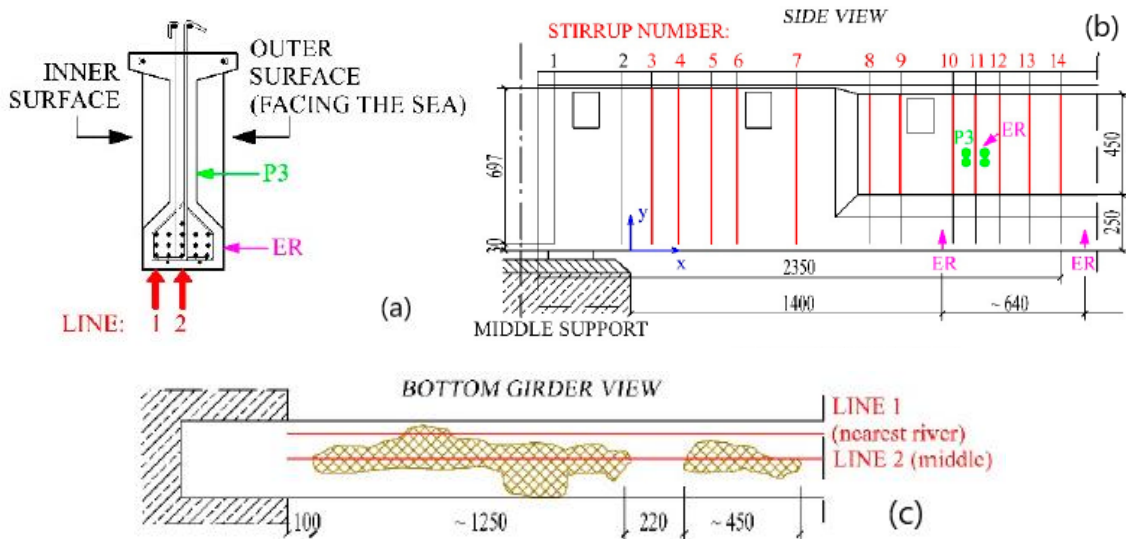


Figure 68 (a) Bottom flange of girder 2; (b) Side view of girder 2; (c) Bottom view of girder 2 [11]

Osmolska et al. [11] confirm that the electrical connection between the reinforcement and Profometer Corrosion was established from the second point. HCP measurements were performed against a copper-copper sulfate electrode (CSE) with a one-wheel electrode type. A fine grid was included for the HCP values to increase the probability of corrosion detection, measuring every 50 mm along the lengths. Based on VI and cover thickness results in the following inspection, corrosion was visible in the pre-tensioned NIB girders of the Dalselv bridge. Girders 2, 11, and 12 near the middle support area were affected by the most severe corrosion damage. Cracks with evidently corroding strands in girders 1 and 2 were visible in the top flange closest to the middle support. Removal of concrete cover revealed major corrosion damages in the bottom flange of girder 2 [11].

According to Osmolska et al. [11], an important finding from this field test in the Dalselva bridge was the correlation between HCP and ER measurements for the right part of girder 2, specified in Figure 69. The potential decreases when the ER values are below approximately 580-950  $\Omega\text{m}$ . The mentioned values are close to the ER thresholds from a range between 500 and 1000  $\Omega\text{m}$ , referring to a negligible and low corrosion probability [160]. According to Pailles [161], ER values should be between 350 and 530  $\Omega\text{m}$ . No clear relationship was visible between HCP and ER for the left half of girder 2. The conclusion from Figure 69 is that HCP measurements were more consistent for corrosion assessment than ER measurements. A recommendation is to include VI to verify ER results [11].

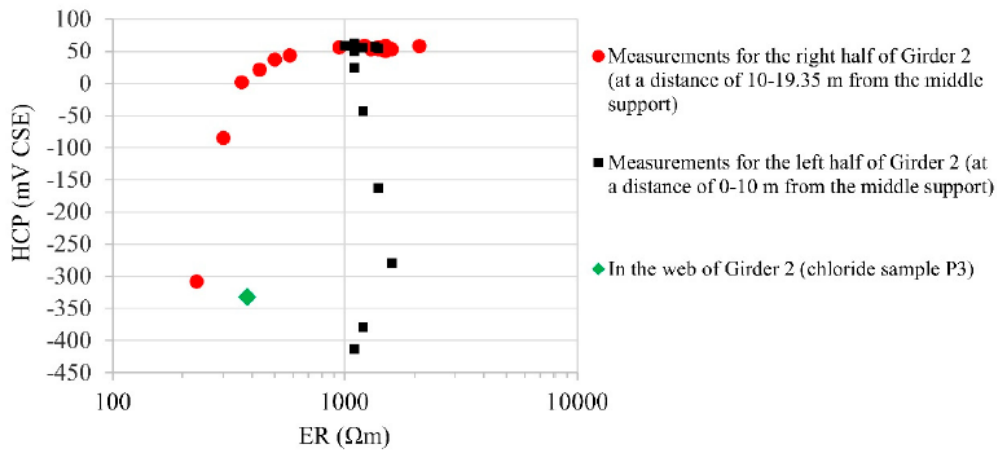


Figure 69 The relationship between HCP and ER measurements [11]

This research paper [11] emphasizes that HCP measurements should be performed on a small grid size of 50 mm. A local inspection of the reinforcement in the cover zone is vital for confirming the corrosion condition. Interpretation of the strands is relevant for describing the bond strength, critical prestressing transfer, and development length. A large amount of concrete cover is removed to evaluate strands in their anchorage zone, where strand slippage is dominating with reduced bond strength. Therefore, removing the concrete cover is recommended for confirming corrosion conditions on the strands but requires precision and knowledge [11].

Conclusions that are valid for this field test on the Dalselva bridge contribute to major findings of pre-tensioned bridge girders. Reinforcement corrosion can easily be perceived before corrosion damage is visible, where the zones influenced by high corrosion probability expand beyond visible corrosion damage. However, the conditions of the strands are only indicated by removing the concrete cover. In addition, HCP measurements are not pinpointing corrosion probability between strands and electrically connected reinforcement in the girder's bottom flange, for example, mounting bars and stirrups. Based on the obtained results, HCP measurements were described as more reliable than ER. Although corrosion was noticed on the strands, it comprises a small area. High ER in the span corresponds to negligible corrosion probability. Corrosion assessment should consider a combination of NDT methods such as HCP, ER, and VI.

## 4. Non-destructive tests

An important part of the report was to conduct experimental tests under a controlled environment, emphasizing different specimens carried out at a research and development facility in Hamar. The authors carried out the specimen tests in the laboratory. The main purpose was to investigate the ability of UPE equipment by providing accurate data and information of air voids, cracks, delamination, and defects in ducts. Following investigation is a significant part of detecting the possibility of deterioration and damage of strands in tendon ducts. For the experiments, the main objective for the authors was to uncover the condition of the strands in the tendons and detect defects in post-tensioned elements. This objective is important for evaluating the serviceability and safety of existing concrete structures, which is an important part of the SHM of existing construction.

A limitation related to the laboratory experiments conducted by the authors was that the construction and defects in the test specimen are known, making it less demanding to interpret the data presented from the UPE equipment. However, an advantage of this approach is the verification of the data provided by the UPE equipment. The authors can, through these experiments, prove that the information provided by following UPE equipment is reliable. Another advantage of this approach is that investigating different concrete specimens will reveal the best practice of the addressed NDT methods and possible shortcomings. Although, only one specific type of UPE equipment was available in Hamar. Therefore, a one-sided data interpretation of UPE technology is present to detect deterioration in concrete structures. Overall, this assessment will be a useful guide for the utilization of the different NDT methods.

### 4.1 Test specimen

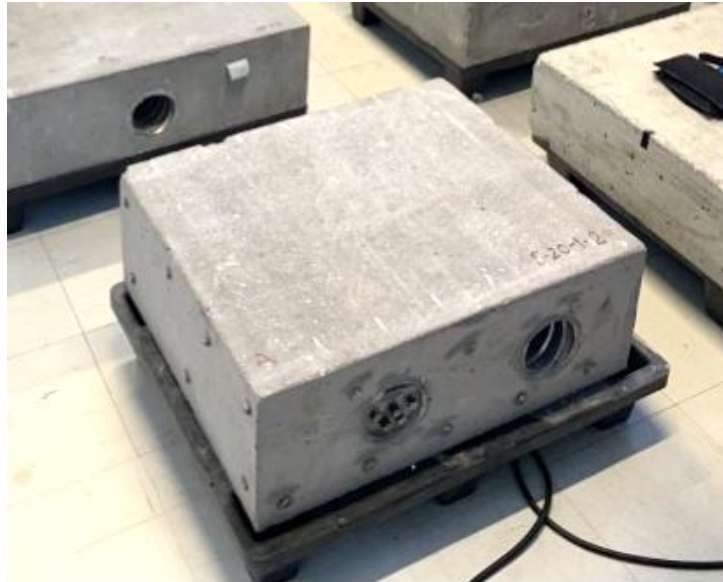
Several concrete specimens in Elop's research and development facility were available in Hamar, where some of these specimens had intentional internal defects and deteriorations. For the thesis project, only three test specimens were investigated. Table 31 addresses these specimens and other relevant information. As noticed, the specimen has different values of  $D_{max}$ .

Table 31 Test specimen specifications

Test specimen	Strength class	Maximum aggregate size ( $D_{max}$ )	Length (mm)	Width (mm)	Height (mm)
S-20-1-2	B45	24	700	550	260
S19-2-2	B45	16	805	600	220
S62	B30	4	800	600	200

The first specimen the authors tested was S-20-1-2: *Tendon duct with full and airgap in the grouting*, seen from Figure 70. This specimen consists of two ducts and a rebar mesh. One of the ducts was empty, while the other tendon duct was fully grouted one half of the duct and grouted 3/4 on the other half. A drawing of this test specimen with the different components

and details is illustrated in Figure 71. The purpose of this test specimen is to demonstrate possible defects that can occur on a tendon duct, in case of not properly executed grouting or presence of corrosion. In either case, the presence of air will be observed because air reflects 100% with ultrasonic scanning. Therefore, the empty and the grouted duct are supposed to be observed clearly in the results.



*Figure 70 Test specimen S-20-1-2*

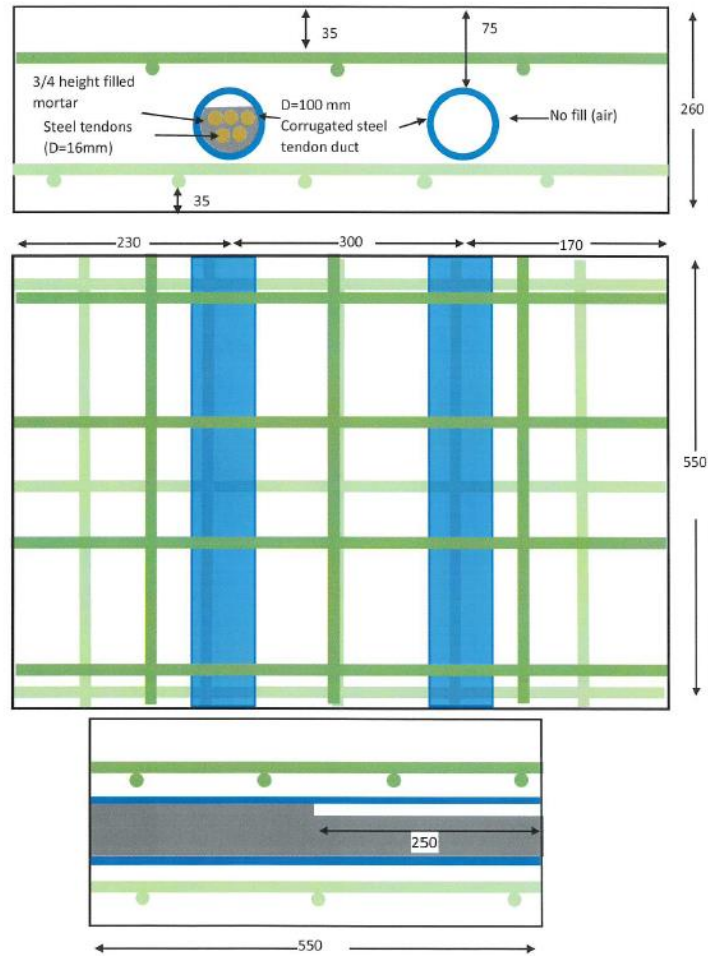


Figure 71 Drawing of S-20-1-2

The second specimen tested by the authors was S19-2-2: *An empty tendon duct*. This specimen consisted of one empty and ungrouted tendon duct in the center of the test specimen, as illustrated in Figure 72 and Figure 73, and has the same purpose as the empty duct in S-20-1-2.



Figure 72 Test specimen S19-2-2

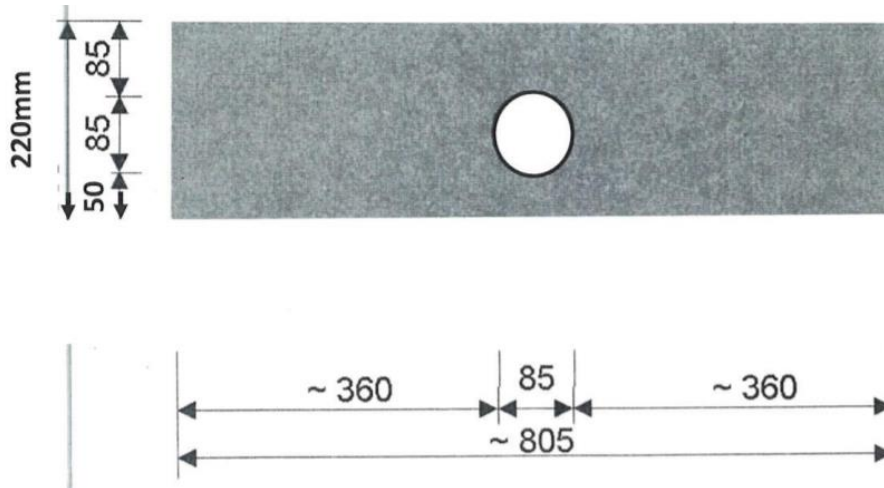


Figure 73 Drawing of S19-2-2

The third specimen the authors tested was S62: *Delamination*. This specimen has no reinforcement or tendon ducts and was casted with a cavity on the bottom of the slab to resemble delamination, as seen in Figure 74.



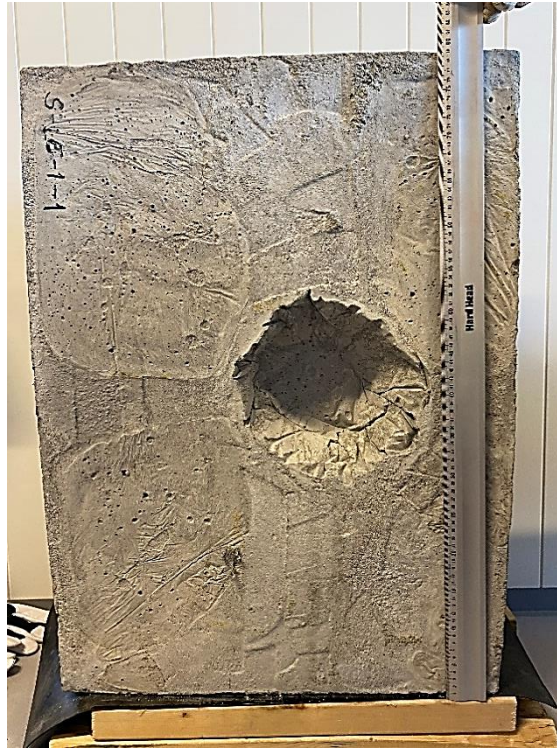


Figure 74 Delamination of S62 slab

#### 4.2 Test procedure

The UPE scanner applied by the authors has the following three scanning modes: high speed, high resolution, and surface scans. These scanning modes provide improvement of data quality, flexibility, and efficiency. The high-speed mode offers a speed limit of up to 50 cm/s, which is applicable for an efficient scan of a larger area. Improved scanning accuracy is possible from the high-resolution mode to detect defects. After a scan, a mathematical analysis is performed to analyze the data and to filter noise levels. The authors considered visualization features on the UPE equipment for optimal interpretations of the concrete specimens.

The author's testing procedure was simple and straightforward. During the whole testing, the scanning mode high resolution was utilized to achieve the best possible measurements. Chalks were included to indicate 10 cm between each scan on the specimen. Based on that, the UPE equipment should completely cover the surface of the test specimen, and edges on all the test specimens remained unmarked. This consideration gives better flow between the scans and movement of the UPE equipment, directing towards valuable and significant results. Laser from the UPE scanner was used as a guiding tool for following the chalk path from one end to another, as seen in Figure 75. The yellow lines in Figure 76 – Figure 78 illustrate the scanning procedure on the surface of *S-20-1-2 B* and *S19-2-2*. From 2D visualization, the scanning for test specimen *S-20-1-2 B* along the ducts started 13 cm from the left corner of the specimen. In addition, the scanning across the ducts for similar specimens started 15 cm from the top corner. Scanning for the *S19-2-2* specimen started 16

cm from the left corner, and between the red lines, the empty duct is localized. A similar approach was also followed for the test specimen S62, with 10 cm between every scan.



Figure 75 Scanning S-20-1-2 B with laser pointing on the center chalk marking

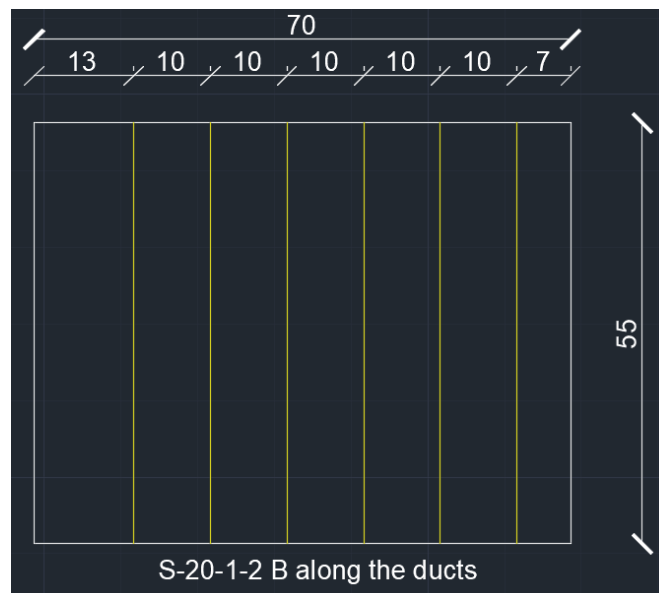


Figure 76 Scanning procedure for S-20-1-2 B along the ducts (dimensions in cm)

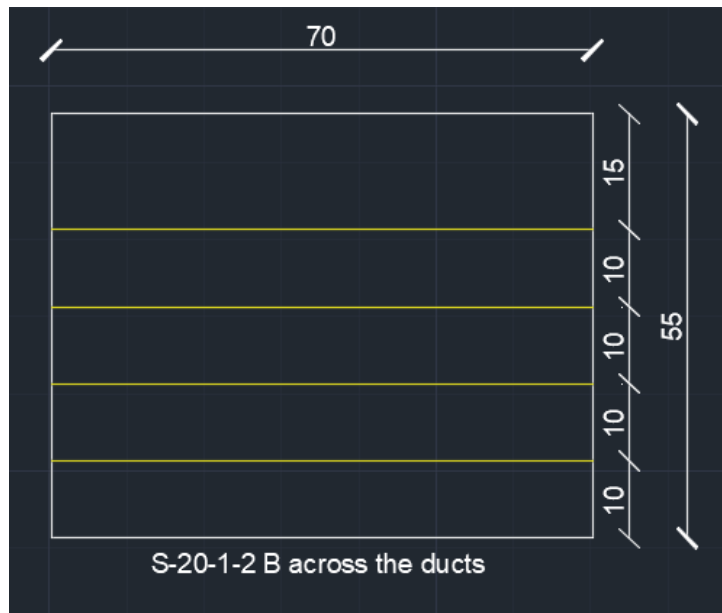


Figure 77 Scanning procedure for S-20-1-2 B across the ducts (dimensions in cm)

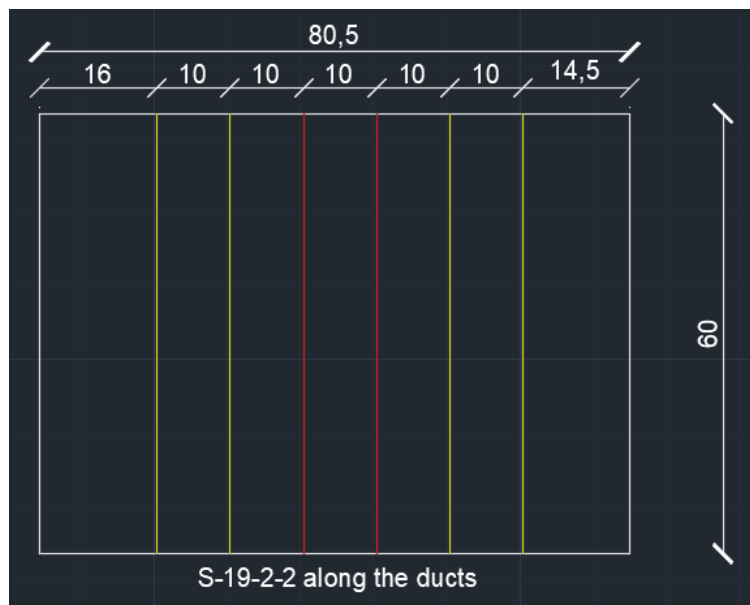


Figure 78 Scanning procedure for S19-2-2 across the ducts (dimensions in cm)

#### 4.3 Mockup test in Hamar

Another approach for investigating possible concrete deteriorations and damages is emphasized in *Report 699* by the Norwegian Public Roads Administration (NPRA) [76]. The relevance of NDT methods for following mockup tests in Hamar is highly connected to the report's main objective. The main scope of this mockup test is to evaluate how efficiently the NDT methods are to detect internal damages of reinforced and prestressed concrete, especially for UPE and IE equipment. Following evaluation counts for the air gap in ducts, internal crack damages, voids, and corrosion on reinforcement. For UPE measurements, scans UPE 2 and UPE 1 were performed on the partially grouted duct along the duct. From this investigation, the data from the UPE 2 scan on the left side of Figure 79 detects a strong sign of void at the right side of the duct. Similar results were visible with scans from UPE 1, but

there were differences in length of the void and color resolution, shown on the right side of Figure 79. A higher resolution of the partially grouted duct was observable on UPE 1 scan [76].

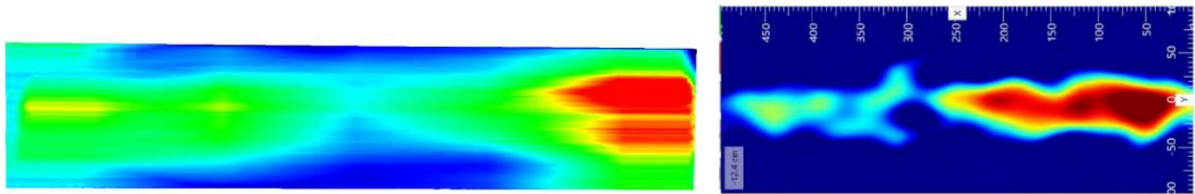


Figure 79 UPE 2 scan vs UPE 1 scan for duct A [76]

A scan along the empty duct with UPE 2 was performed, where huge signs of air gaps were detected, as seen in Figure 80:

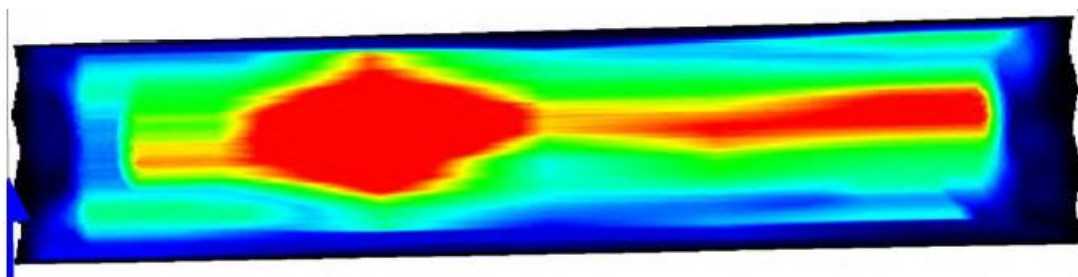


Figure 80 UPE 2 scan of empty duct B [76]

Several UPE 1 scans were performed in the inspection to indicate the differences between each side of concrete specimen, known as B-scans. Figure 81 illustrates the grouted duct and the empty duct, meanwhile Figure 82 shows void in the grouted duct and the empty duct.

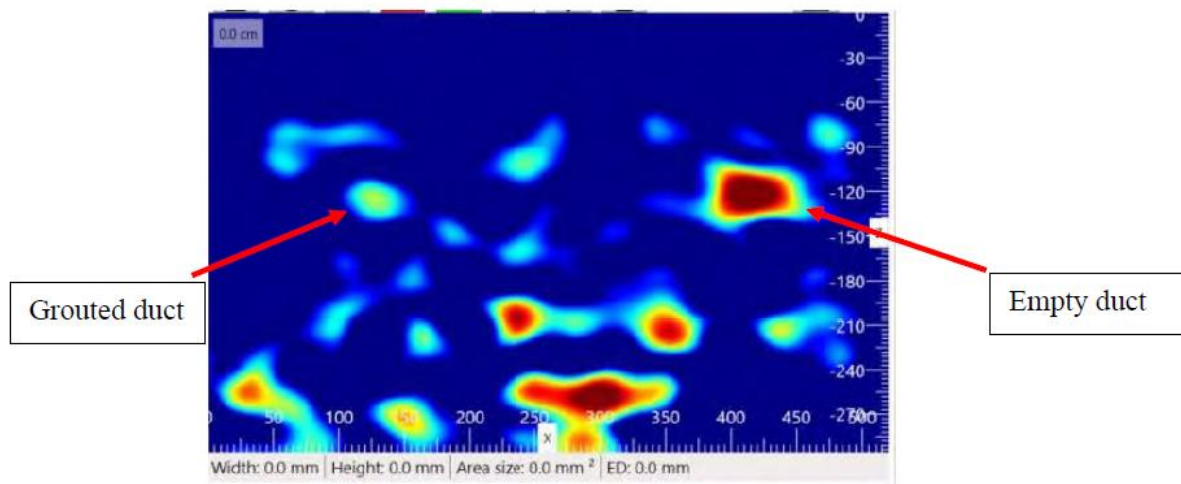


Figure 81 Grouted and empty duct in UPE 1 scan [76]

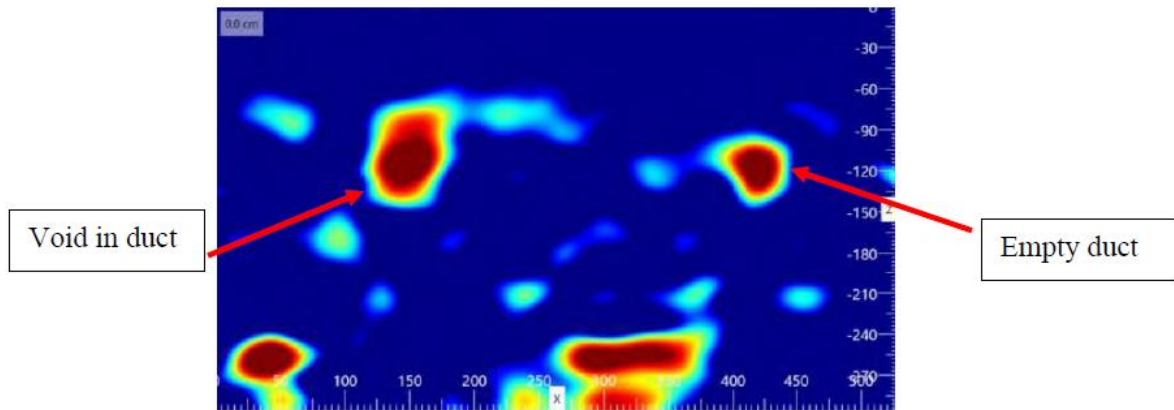


Figure 82 Void in duct and empty duct in UPE 1 scan [76]

4 different testing points were selected along both cable ducts to interpret the differences between results, shown in Figure 83:

Table 32 Testing points along cable ducts

Location of testing points	Duct type
1	Grouted duct
2	Partially grouted duct
3	Empty duct
4	Empty duct

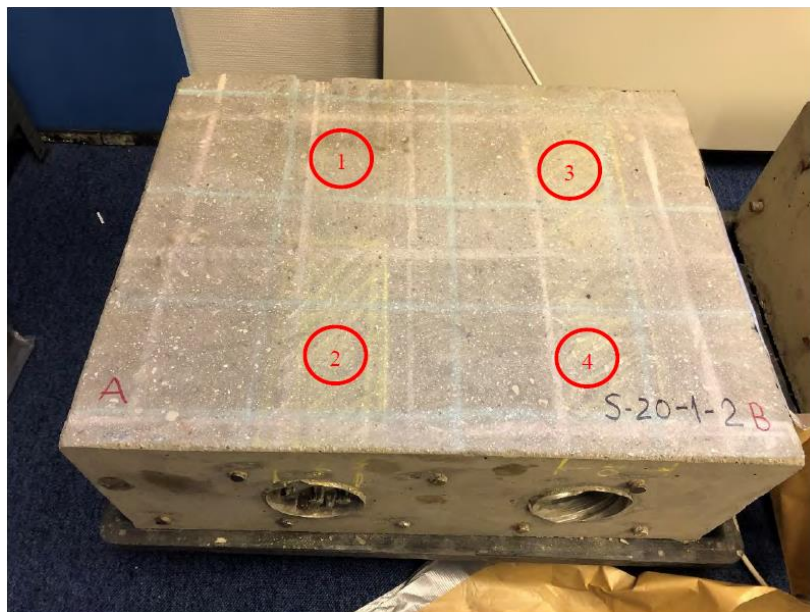


Figure 83 Location of testing points on the concrete specimen [76]



IE measurements were performed for test point 1 (TP1) and test point 2 (TP2). It was clear from TP1 that the thickness peak (blue line on Figure 84) was accomplished. The lines between the thickness peak verify that the reflection goes directly through the injected duct before counter reflecting from the concrete specimen. For TP2, the thickness peak is obtained with a lower thickness frequency, clarifying that the signal will travel a longer distance because of facing obstacles. Since TP2 is partially filled with grout, signal from the depth should be prioritized with suspicion of void.

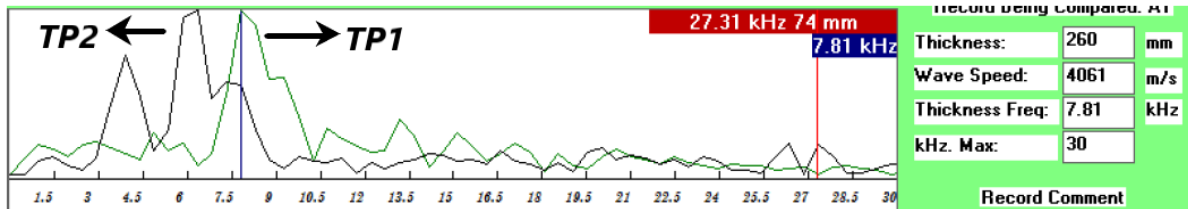


Figure 84 Comparison between test point 1 (TP1) and test point 2 (TP2) [76]

IE results from TP3 and TP4 were identical since both are referring to empty cable ducts, shown in Figure 85 and Figure 86. The most impressive part from these points compared with TP1 and TP2 from Figure 84 is a clearer visualization of peak at the depth of the void.

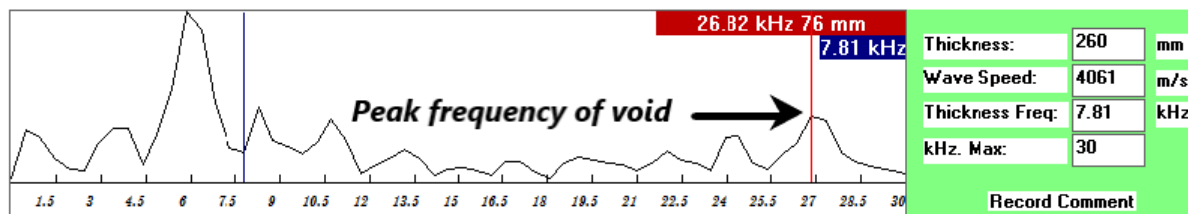


Figure 85 Peak frequency of void at TP3 [76]

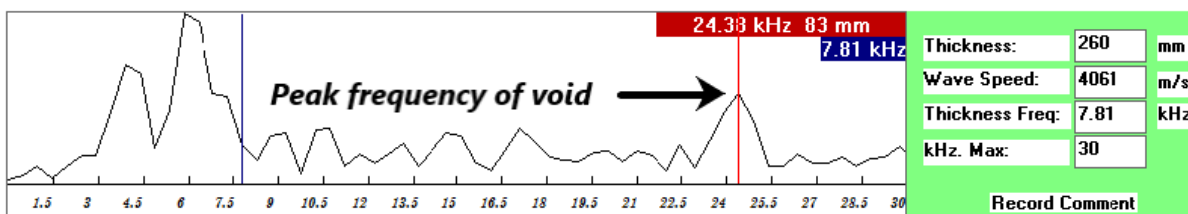


Figure 86 Peak frequency of void at TP4 [76]

To summarize, differences are clearly visualized between injected and empty ducts. Signals from instrument UPE 1 was clearer than signals from instrument UPE 2, but voids were still visible from UPE 2 scan. Adjustments in setting options for instrument UPE 2 would have contributed to improvement in the results. Correct settings are vital to avoid additional costs related to incorrect assessments and frequently visit to the bridge. UPE technology is impressively detecting voids and conducts the scan along the tendon ducts magnificently. In addition, UPE technology is simply covering larger areas of inspected ducts. However, UPE demands training and expertise to interpret the results. Using the rule of thumb is recommended to understand results related to voids, where larger voids give better accuracy in assessment. During the scan performance, it is necessary to have proper contact with the concrete surface, otherwise realistic results are not achieved. At the same time, there are a

lot of ultrasonic equipment available in today's market. The inspector must be acquainted with the equipment and the software, making the scans mostly executable.

The results from IE are promising with success in locating the voids in the concrete specimen. However, calibration of the equipment is possible in various ways. The fastest way to calibrate is to know the thickness of the test specimen. Unknown thickness value makes the IE calibration more cumbersome, where preparatory tests are recommended to detect the correct thickness frequency number. Performance of IE tests are time-consuming over larger areas. Therefore, IE tests are mostly performed with other NDT methods to verify the test results. In addition, IE is an efficient NDT method to confirm the drill depth. Drilling on concrete specimen is regarded as a destructive test, where the drilling must be performed carefully to not damage the tension wires. IE method requires training, expertise, and experience to interpret the results. Preliminary work and additional calculations must be included together with the testing procedure.

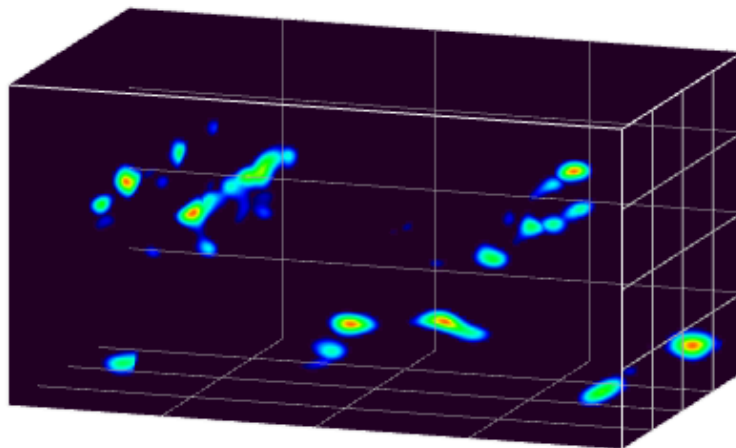


#### 4.4 Results

Tests of the UPE equipment in Hamar resulted in excellent data interpretations. These data were sent to a cloud-based application (web portal), allowing further analysis, where the data is visualized through a heatmap defining the signal amplitude. Results obtained from the different concrete specimens are defined in the sections below:

##### 4.4.1 S-20-1-2 along the tendon duct

Figure 87 shows a 3D scan of the test specimen S-20-1-2 along the ducts. From the UPE scans, one can observe different reflection interpretations. Different properties of materials in the concrete will have different wave velocities, and therefore a variation in reflection is observed. The amount of reflection was minimized to detect structural flaws and air gaps in the grouted and empty duct. It should be noted that the reflection at the bottom of the 3D scan is the backwall. A better data of the measurements was possible from a C-scan, as seen in Figure 88. The scan reveals a higher level of reflection with red colors, insinuating air pockets.



*Figure 87 3D scan of S-20-1-2 along the ducts*

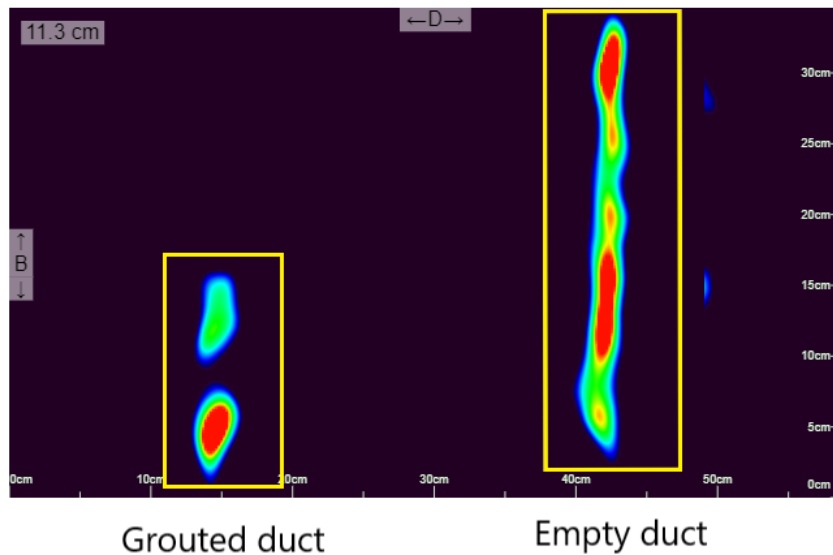


Figure 88 C-scan of S-20-1-2 along the ducts

A closer observation of the C-scan in Figure 88 indicates longitudinal reflection on the right side along with the test specimen, clarifying a continuous opening filled with air due to the strong reflection. A partial reflection is observed on the left side, indicating the presence of an air gap. The measurements indicate that the duct on the right side is filled with air. The duct on the left side is not fully grouted due to the observed air voids. Otherwise, the measurements and collected data sort well with the construction of the test specimen. The D-scans in Figure 89 show the grouted duct (in the yellow rectangle box) and the empty duct located 14.4 cm and 42.3 cm along with that coordinate, respectively. In addition, the surrounding signals are reflections from the ducts.

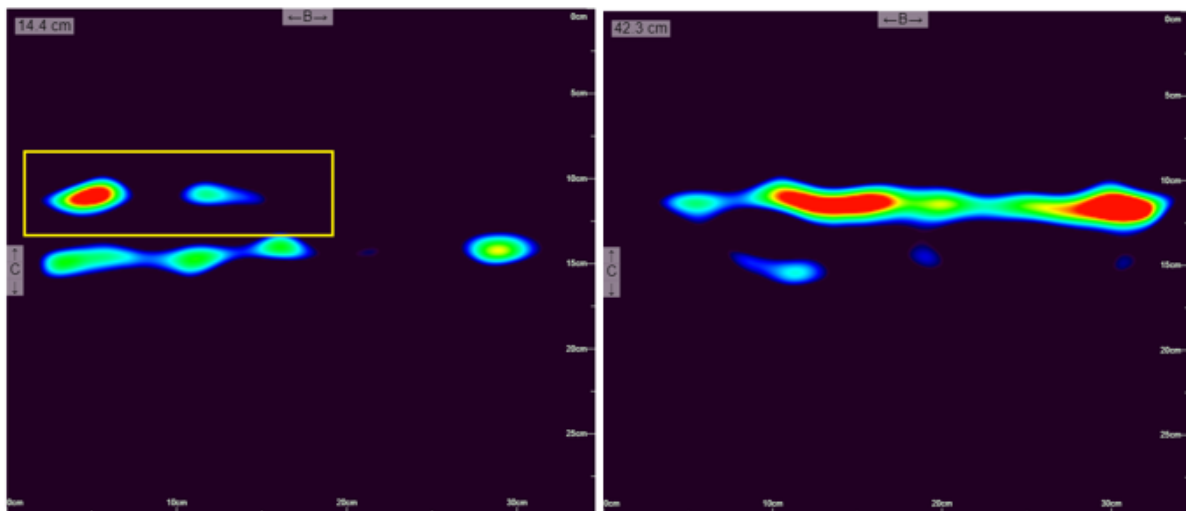


Figure 89 D-scans of the grouted duct and empty duct

#### 4.4.2 S-20-1-2 across the tendon duct

Collected data from S-20-1-2 was very poor and challenging to interpret. As observed, extremely weak signals are reflected after the minimization of the amount of reflection. The only clear detection of structural flaws and air gaps in the duct is observed 13 cm into the concrete, as seen in Figure 90, indicating an air void due to the high signal reflection. According to Figure 91, this is the same location as the grouted duct. However, there is no clear indication of the empty duct in this scan. Figure 91 shows the backwall 25.9 cm into the concrete, which is accurate compared to the thickness of the concrete specimen.

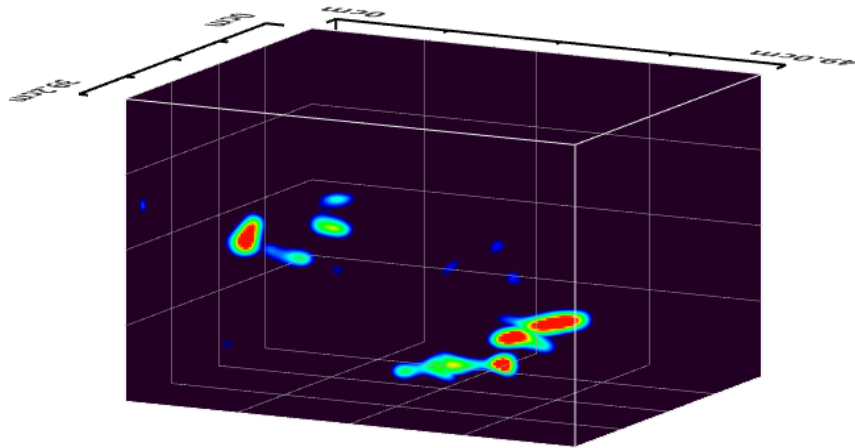


Figure 90 3D scan of S-20-1-2 across the ducts

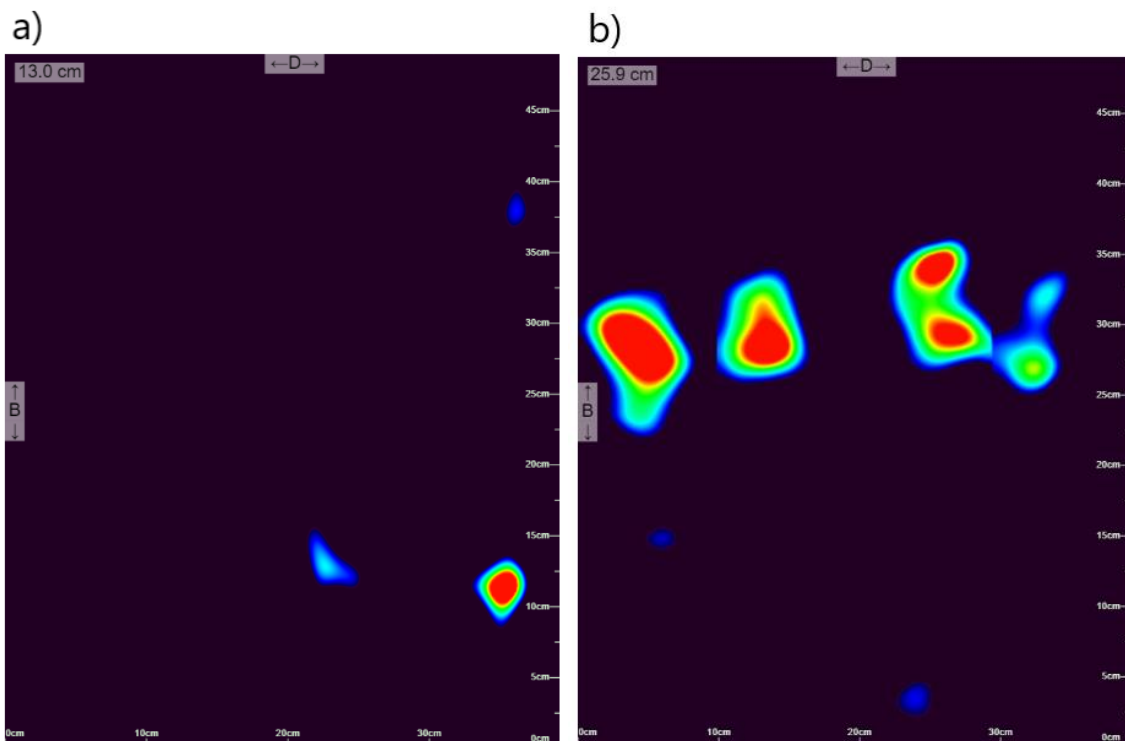


Figure 91 C-scan a) 13 cm into the concrete, b) 25.9 cm into the concrete

#### 4.4.4 Source of errors

In advance, the same data was expected as for the *scan S-20-1-2 along the ducts*. Literature research reveals that the procedure for UPE assessment is conducted along the length of the location of the ducts. The following procedure applies for transverse and longitudinal post-tensioning systems, where the scans are conducted along the duct [162, 163]. Therefore, a possible explanation of the poor results compared to the scan along the duct is clarified. Based on the procedure of the UPE method, the measurements should be done according to a grid with a constant measuring point distance, where a smaller grid provides sufficient data. The grid size used in the testing with the UPE equipment was 8 mm, resulting in inefficient data. The scanning across a duct is not an objective approach, and therefore this is a source of error.

#### 4.4.3 S19-1-2 along the tendon duct

The scanning of the test specimen *S19-1-2* along the tendon duct resulted in very accurate data. Figure 92 shows a C-scan 12.6 cm into the test specimen, indicating strong signals across the entire duct, clearly indicating an air-filled duct.

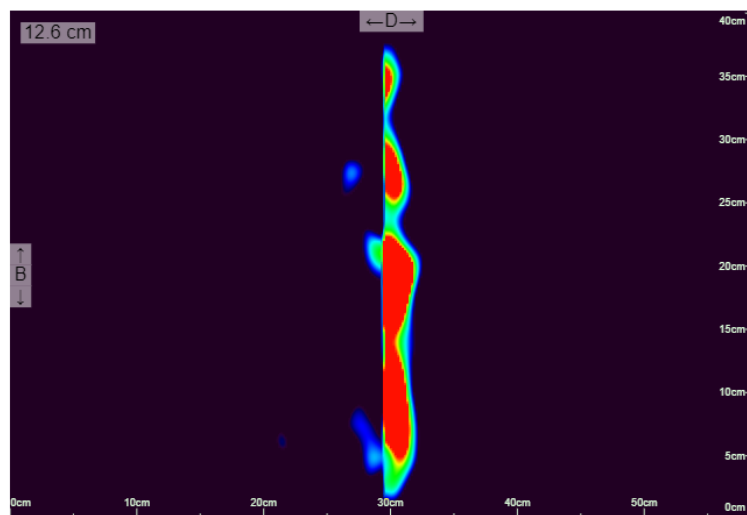


Figure 92 C-scan of S19-1-2 along the duct

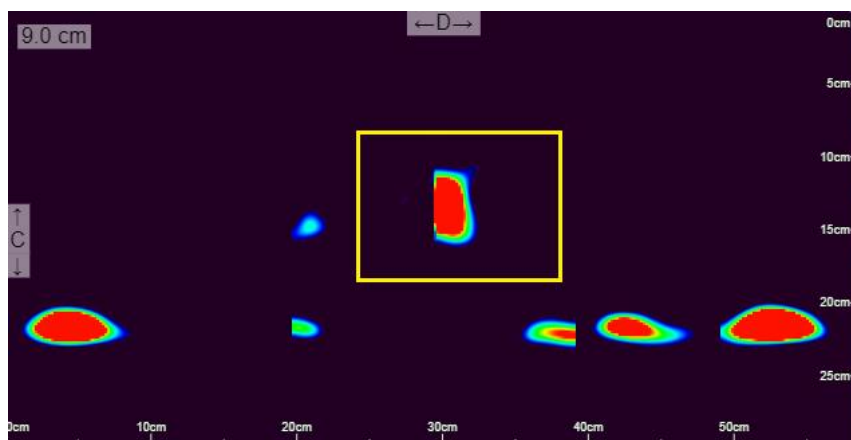


Figure 93 B-scan 9 cm into S19-1-2

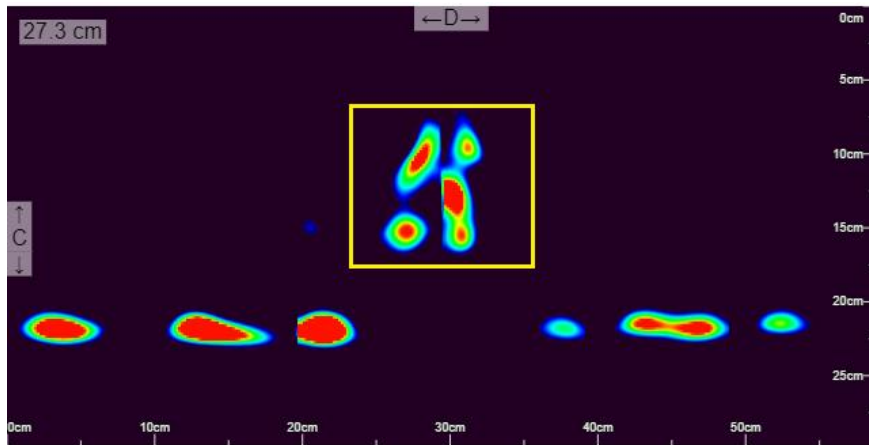


Figure 94 B-scan 27.3 cm into S19-1-2

Further, Figure 93 and 94 visualize two different B-scan of 9 cm and 27.3 cm into the concrete, respectively. The purpose with these two scans is to demonstrate the continuity of the strong signals received and that the signals have almost the same location (in the yellow rectangular box), which are indicating the empty duct. On the other hand, the strong reflection at the bottom of both scans clarifies the reflection of the backwall approximately 20-25 cm into the test specimen. This is an accurate measurement according to the thickness of the test specimen of 22 cm.

The web portal for used UPE equipment offers different features, and one of them is *Realistic Representation*. This feature allows a 3D realistic visualization of the scanned concrete element. From the collected data, a realistic representation of S19-1-2 along the tendon duct is seen in Figure 95, based on the original scan showing the reflection of the air and backwall. This feature also enables the creation of rebars and tubes to get a more realistic visualization of the scanned element. Flaws and air results in cavities in the realistic representation, and in this case the cavities are replaced with a duct as seen in the Figure 95.

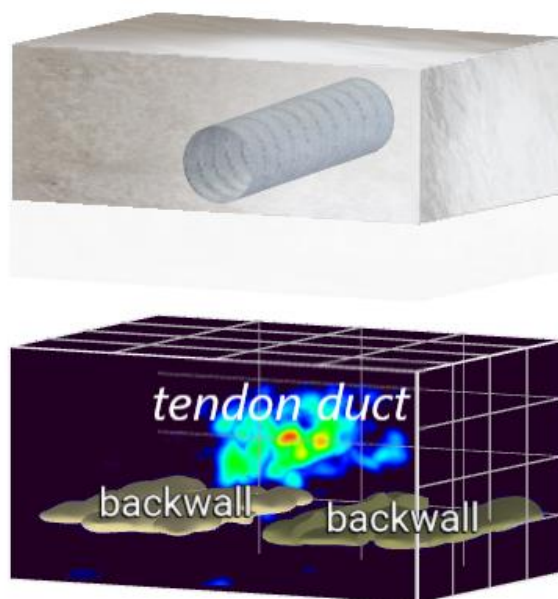


Figure 95 Realistic representation of S19-1-2

#### 4.4.4 S62 delamination

When conducting tests of specimen S62, the delamination in this test specimen was easily detectable. One of the advantages of different scans are the opportunity of observing the flaws and airgaps from different points of view. From a C- and D-scan (Figure 96 and 97), the delamination is clearly observed. Based on these scans, it is possible to clarify that the delamination is bowl shaped.

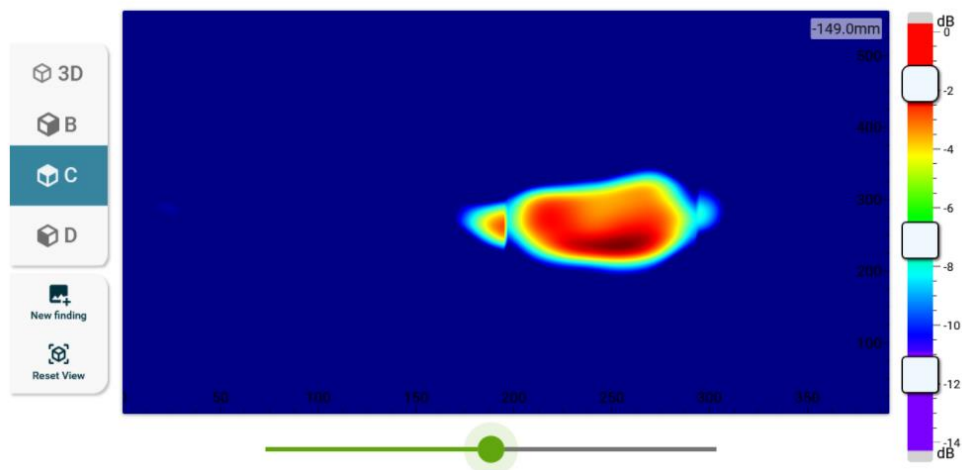


Figure 96 Snapshot of a C-scan of S62 from Elop Insight

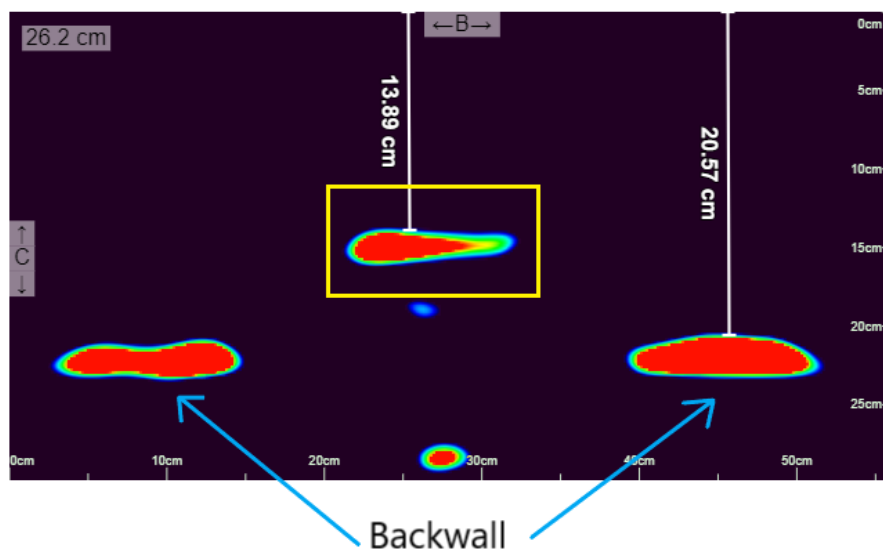


Figure 97 D-scan of S62

From Figure 97, the backwall is observed 20-25 cm into the concrete, which is accurate with the thickness of the test specimen of 20 cm. Figure 98 is a snapshot of a C-scan of the backwall 22.4 cm into the concrete and is obtained direct from the UPE equipment after the scan. Strong signals are observed, but there are no signal in the middle of the scan. A closer look at the D-scan reveal no great reflections beneath the marked area. Through these examinations, the scans detected an uneven backwall with a cavity at the bottom of the test specimen. The realistic 3D model in this analysis gave an excellent image of this delamination as seen in Figure 99, where this cavity is very visible.

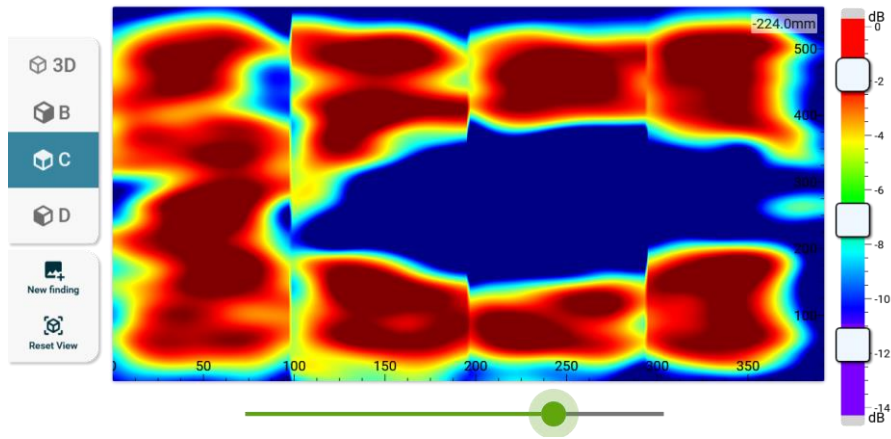


Figure 98 C-scan of S62 backwall



Figure 99 Realistic Representation of S62



## 5. Discussion

In this report, different NDT methods have been investigated and evaluated for reinforced and post-tensioned concrete structures with respect to certain deteriorations. Generally, there are several deterioration mechanisms such as mechanical, physical, structural, chemical, biological, and corrosion. The deterioration mechanisms are mainly affected by the environment and concrete composition, influencing the durability and safety of the concrete structures. Therefore, NDT methods can be implemented for the assessment of concrete structures. The NDT methods are categorized according to different principles and application areas, such as acoustic, electromagnetic, and electrochemical methods, implying various degree of property analysis. The principles ensure to identify deteriorations and map the condition of the concrete structure.

However, the usefulness of NDT methods is limited due to issues of identifying deterioration mechanisms. As seen in this report, the methods can quantify the consequences of deterioration. The present investigations in the literature specify the cause of deterioration or investigate the effects of the deterioration mechanisms. Overall, several NDT methods can detect the effects of the deterioration mechanisms, clearly visible in the measurements. An investigation carried out in this thesis considers the effectiveness and accuracy of provided data from various NDT methods. A score system is presented to evaluate the ability of different NDT methods for detecting certain deteriorations. Other parameters that are necessary for the assessment is also included, specifically location of reinforcement and post-tensioning systems. The score system was defined as following:

- 0 – Not possible to detect deterioration
- 1 – Possible to detect deterioration, but not suitable
- 2 – Suitable, but there are limitations
- 3 – Suitable and preferable

Deterioration parameters investigated in this report were cracks, voids, delaminations, corrosion of reinforcement, and corrosion of strands. It is important to emphasize that deterioration has a wide definition, including different mechanisms. The severity of the damages can variate due to the exposure conditions as addressed. Many of these mechanisms are interrelated because they can accumulate the deteriorations and the extent of the damage. According to the authors, these investigated parameters are some of the central parameters in accordance with concrete deterioration and are often addressed in the literature. To clarify the differences between the NDT methods, a chosen approach is to analyze the assessment scores for the different deterioration parameters, presented in bar diagrams. Figure 100 – Figure 107 consider these parameters in correlation to NDT methods. The following NDT-methods are included in the bar diagrams:

- Visual Inspection (VI)
- Ultrasonic Pulse Velocity (UPV)
- Ultrasonic Pulse Echo (UPE)
- Impact Echo (IE)

- Impulse Response (IR)
- Ground-penetrating radar (GPR)
- Concrete Resistivity (CR)
- Cover Meter (CM)
- Half-Cell Potential (HCP)

However, it should be emphasized that the assessment scores presented are based on the author’s knowledge, the findings in the literature and their own conducted UPE tests. Other researchers may evaluate results differently. Nevertheless, the presented approach gives a good understanding of the usefulness of different NDT methods and how they could be combined.

From the evaluation of cracks, as seen in Figure 100, the UPV method demonstrates better performance in measuring cracks compared to the other NDT methods. For the UPV method, crack measurements were efficient with low error estimation. In addition, the distance between the transducers is a significant factor for the accuracy of cracks estimation. Therefore, the authors agree on that these considerations contribute to valuable crack detections from the UPV method. Furthermore, GPR, UPE, and IE show the capability to detect cracks. Although, the crack geometry influences the GPR data, and a change in crack direction can result in possible misinterpretation due to several reflections. For the IE method, the crack size influences the registered impact energy due to reflection from the cracks, resulting in a lower amplitude. However, the small cracks can be challenging to detect. VI is more suitable for visible cracks, but it can be challenging to evaluate the extent of the damage, e.g., crack depth. Still, a crack width microscope can be included to measure crack widths. IR detects cracks with lower probability and is dependent on damping, which can be challenging to evaluate due to the influence of crack size and extension. CM, HCP, and CR are not recommended NDT methods for the assessment of cracks due to lack of detection.

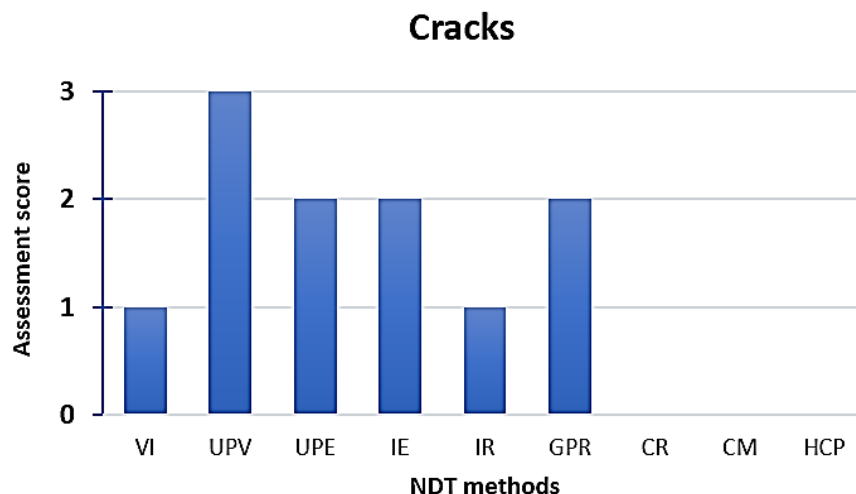


Figure 100 Assessment score of cracks in accordance with NDT methods

The evaluation of voids in RC and PT concrete from Figure 101 indicates that several NDT methods are applicable for detecting voids. GPR, UPE, and IE show clear signs through reflections, and the obtained data are often easily interpreted. On the other hand, IE method

is a more applicable method for detecting voids in PT ducts compared to UPV. IR shows possibilities to detect voids, but the thickness size of the concrete structure is conclusive for the correct interpretation of the following method. Therefore, a challenge can be to detect corner voids.

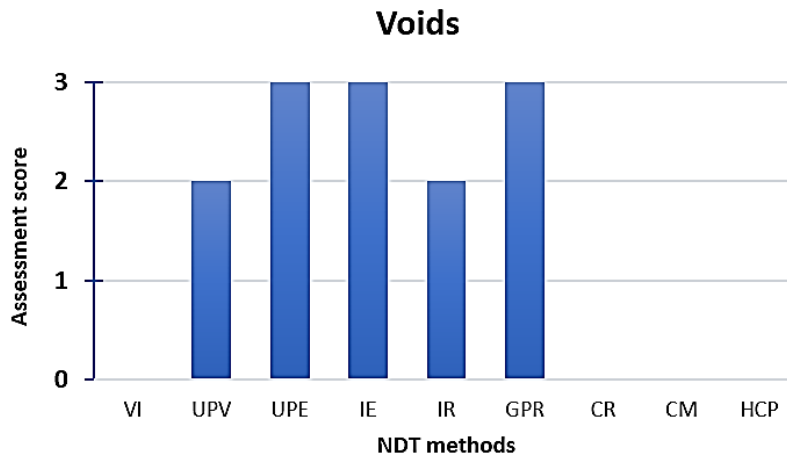


Figure 101 Assessment score of voids in accordance with NDT methods

Several NDT methods demonstrate a decent detection of delamination, such as UPV, UPE, and IE, as seen in Figure 102. Longitudinal waves (P-waves) from UPV show a correlation with the size and location of the delamination. From the UPE tests conducted by the authors, the sample with delamination (S62) showed strong reflections with the ability to locate and estimate the shape of the damage. The authors are convinced that the UPE method is a suitable approach for illustrating delamination. Although, the authors knew about delamination in specimen S62, the UPE equipment managed to represent clear visualizations and therefore the interpretation of the UPE results was a minimal issue. IE detects delaminations depending on size and can be challenging to detect small delaminations. Still this method is less challenging compared to cracks. The reason for the given delamination score in GPR is related to the uncertainties addressed in the report. Similar to cracks, the interpretation of data can be complicated.

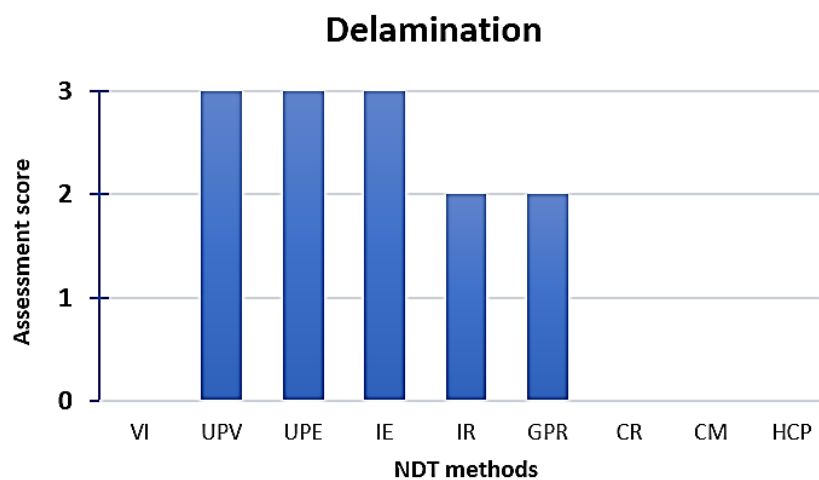


Figure 102 Assessment score of delamination in accordance with NDT methods

Figure XX shows the assessment score for corrosion of reinforcement. Moreover, the NDT methods provides different approaches for the identification and evaluation of corrosion. Although the HCP and CR are some of the most suitable methods for evaluating corrosion of reinforced concrete, these NDT methods are often combined to interpret the corrosion rate quantitatively. However, the proposed approach of assessment scores aims to evaluate each of the NDT methods separately and does not account for a combination of several methods.

For HCP, there is uncertainty about the accuracy of this that can provide misleading interpretations about the possibility of corrosion. Hence, it is important to emphasize that the HCP method only provide information about the probability of corrosion. On the other hand, the CR method measures the concrete resistivity of the concrete surface. The reliability is influenced by the composition of the concrete, reinforcement, and the distance of the probes which may result in an inaccurate indication of possible corrosion rate. These mentioned considerations are the reason for the given assessment score of the methods. The GPR can indicate areas of corrosion by the signal attenuation, thus the method does not provide information about the corrosion rate. A VI can only detect corrosion if rust spots, spalling or completely disintegration of the surface exposes visible corrosion of the reinforcement. The UPV and IE can quantify cracks because of corrosion. However, this is not a clear enough indication unless corrosion is noticeable,

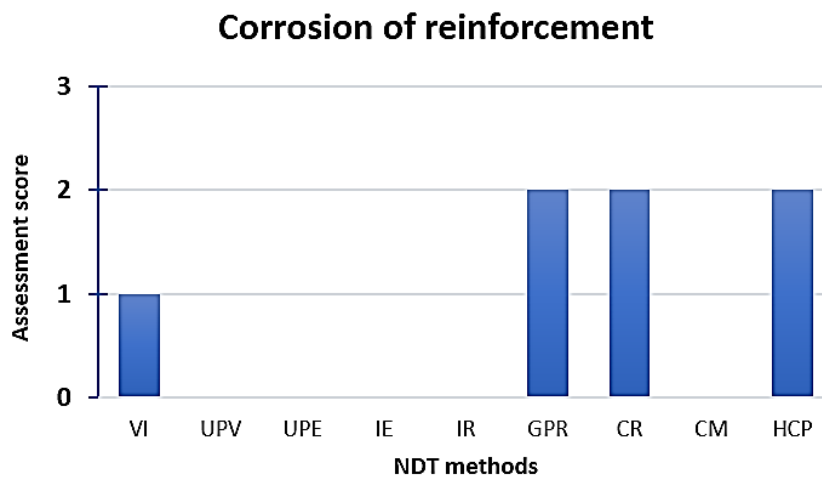


Figure 103 Assessment score of corrosion of reinforcement in accordance with NDT methods

None of the NDT methods has the capability to detect corrosion directly in PT strands. The approach used for identifying corrosion is through assessing presence of voids and the grouting in the ducts. It is important to mention that this does not indicate the extent of damages of the strands. The assessments scores have accounted this fact. The assessment scores (Figure 104) demonstrate a decent ability of the UPE and IE. The investigated field tests in chapter 3.4 are great examples demonstrating some of these NDT methods to detect voids. However, investigation of Farris bridge is doubtful regarding simplified interpretation of the results from UPE.

The authors' own UPE tests provided detailed void detection with reliable data interpretation and quick cloud transformation. The cloud-based application permitted an on-site analysis of the obtained data contributing to a beneficial approach for detecting the voids in the partially

grouted duct of the test specimens. For the UPV method, detection of voids is possible. However, strands in post-tensioning systems influence the velocity, affecting the interpretation of data. For the VI, the only approach is through endoscope and drilling into the duct as seen in the field tests, visualizing corrosion damages of post-tensioning strands. The GPR can be a possible method but is not applicable for steel ducts. Even if the UPE and IE method has been given a score of 2, the accuracy of corrosion in post-tensioning strands is not fully integrated for UPE and IE, demanding more interpretation from obtained results.

### Corrosion of post-tensioning strands

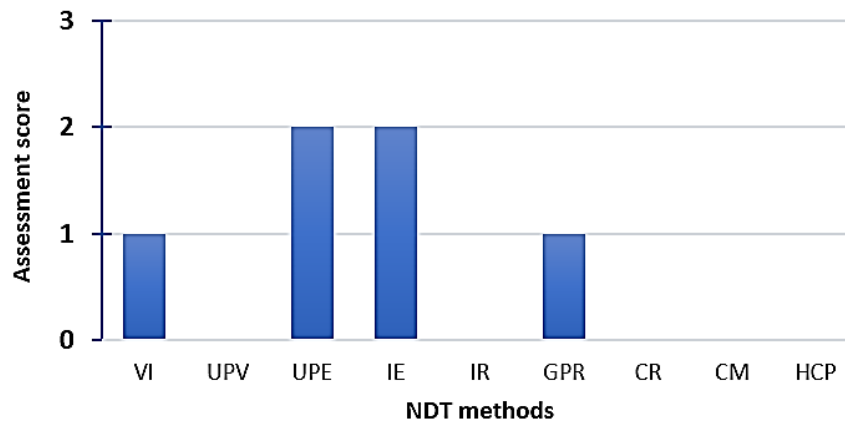


Figure 104 Assessment score of corrosion of PT strands in accordance with NDT methods

The location of reinforcement is CM and GPR, shown in Figure 105. Proximity reinforcements are detected from CM measurements of the concrete cover, which is a positive sign for test accuracy. Nevertheless, an additional layer of reinforcement can decrease the accuracy of the CM method, especially for multiple layers with a larger diameter and close spacing reinforcement. For the GPR method, locating reinforcement is preferable for depth range detection. Reinforcement quantity can minimally influence the location of the bars. UPE shows signs to locate reinforcement, but several limitations regarding frequency range must be considered. Moreover, the authors agree with the assessment scores for location for reinforcement. Farris bridge and Herøysund bridge give precise accuracy of locating reinforcement with CM method. Still, concrete structures with high reinforcement depth creates challenges on locating the steel bars from CM. Nevertheless, combining CM with GPR is a promising solution based on that GPR method can provide deep reinforcement localization. For the assessment scores of UPE, the authors initially gave this method a score of 2. Even though some of the test specimen contained reinforcement, the conducted testes UPE did not showed any ability to locate or visualize reinforcement clearly. Therefor the assessment score for the UPE method were changed to 1.

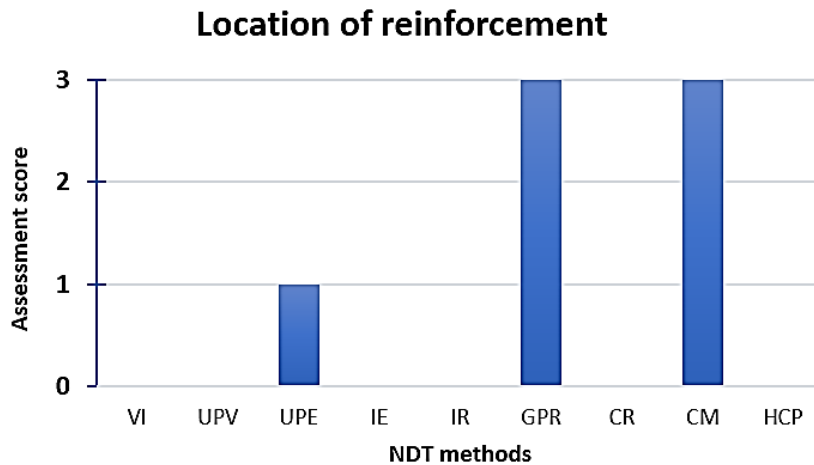


Figure 105 Assessment score of location of reinforcement in accordance with NDT methods

The GPR method is a decent approach for locating internal and external ducts in PT systems, independent of metal and nonmetal ducts (Figure 106). UPE and IE are suitable methods for locating ducts in PT systems with certain limitations. Although, selected grid size is influential for detecting a clear difference between air-filled and grouted ducts. In addition, registered air reflections from ducts are decisive for UPE measurements. Additionally, the reflection of the ducts is dependent on the material of the duct. Locating ducts in PT concrete with the IE method is suitable for empty and grouted ducts, where valuable frequency peak numbers are measured. However, the thickness of the concrete structure has an impact on obtained frequency values, affecting the interpretation of ducts. Therefore, the authors agree with the assessment scores for location of post-tensioning systems. The field tests from Farris bridge and Herøysund bridge contribute to valuable results for localizing ducts. Still, result interpretations from UPE and IE are more demanding compared with GPR, making GPR a more sufficient NDT approach for the ducts.

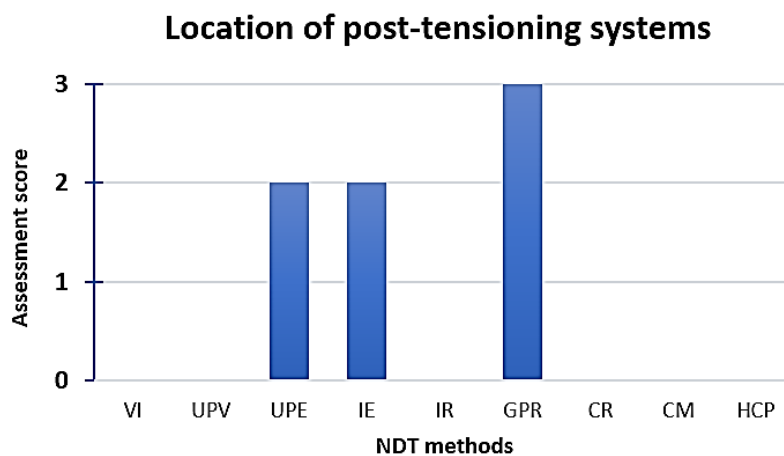


Figure 106 Assessment score of location of post-tensioning systems in accordance with NDT methods

In the report, a wide variety of equipment from different manufacturers is available for the NDT methods. The technical specifications differentiate from accessible NDT equipment in the market, considering features such as accuracy, depth, frequency range, and data presentation, which influence the extent of detection of different parameters. The necessary

equipment features depend on the purpose of the investigation and the extent of requested detection. As observed, the manufacturers have accounted for this consideration by offering several models of equipment. A consequence of this fact is observed in the varying prices of the equipment. However, it is important to emphasize that these differences impact the result and analysis of the result, which may affect the quality of the assessment.

An interesting pattern observed in the bar diagrams is a correlation between the NDT categories and the detection level of the certain parameter in several cases. This fact demonstrates that certain categories have a better ability to detect specific damages and flaws than other categories, proving that underlying principles of the NDT methods have a great impact on the degree of detection. In some cases, the NDT methods provide different information about a parameter, and a comparison of the methods can detect various information about that specific parameter. Therefore, a combination of NDT methods can improve the perception of a problem, and the methods can be implemented in the application area it best performs. Additionally, the NDT methods can be combined with the purpose of verification to improve the accuracy of the obtained data

In the report, this have been proven to be a significant approach for the investigation of post-tensioning systems, as seen in the field tests of Farris and Herøysund bridge. CM and GPR located reinforcement and tendon ducts, while UPE and IE were used to investigate the grouting of the ducts. Further, from the field test of Dalselva bridge, the combination of VI, HCP and CR demonstrated an increased probability of corrosion. Considering the correlation between these NDT methods, the authors will not exclude an assessment score of 3 for these NDT methods. Based on the investigation in this report and the given assessment score of the NDT methods, the authors suggest that the best application of the methods in combination is presented in Table 33. One must not ignore that a VI is a very helpful method and in used as a supplementary method.

Table 33 Final evaluation

Parameters	NDT combinations	
	Primary	Secondary
Cracks	<ul style="list-style-type: none"> <li>• UPV</li> </ul>	<ul style="list-style-type: none"> <li>• UPE</li> <li>• IE</li> </ul>
Voids	<ul style="list-style-type: none"> <li>• UPE</li> <li>• IE</li> <li>• GPR</li> </ul>	<ul style="list-style-type: none"> <li>• UPV</li> <li>• IR</li> </ul>
Delaminations	<ul style="list-style-type: none"> <li>• UPV</li> <li>• UPE</li> <li>• IE</li> </ul>	<ul style="list-style-type: none"> <li>• IR</li> <li>• GPR</li> </ul>
Corrosion of reinforcement	<ul style="list-style-type: none"> <li>• GPR</li> <li>• CR</li> <li>• HCP</li> </ul>	<ul style="list-style-type: none"> <li>• VI</li> </ul>
Corrosion of strands	<ul style="list-style-type: none"> <li>• UPE</li> <li>• IE</li> </ul>	<ul style="list-style-type: none"> <li>• VI</li> <li>• GPR</li> </ul>



Location of reinforcement and	<ul style="list-style-type: none"><li>• GPR</li><li>• CM</li></ul>	<ul style="list-style-type: none"><li>• UPE</li></ul>
Location of post-tensioning systems	<ul style="list-style-type: none"><li>• GPR</li></ul>	<ul style="list-style-type: none"><li>• UPE</li><li>• IE</li></ul>

## 6. Conclusion and future recommendations

Different NDT methods have been investigated for reinforced and post-tensioned concrete structures. The durability of these structures is mainly affected by concrete composition and deterioration. For that reason, assessment of existing structures is a fundamental approach to ensure long-term performance. This aspect entails that structural condition is monitored by collecting essential data during the service life of the concrete structure, which provides an insight into the structural behavior. Therefore, NDT methods can be integrated with SHM to estimate the remaining service life of concrete structures.

Moreover, the NDT methods provide different approaches for identifying and evaluating deterioration, damages, and flaws. There are both advantages and limitations to apply NDT methods, and the principles of the NDT categories are conclusive for the capability to detect different problems. However, available equipment for NDT methods influences the reliability and interpretation of obtained data. Technical specifications and algorithms for NDT methods can differentiate depending on accuracy, depth, and frequency range. Variations in these parameters can result in the imprecision of promising data, influencing the degree of detection for concrete deteriorations. For a specific concrete deterioration, different NDT equipment emphasizing identical principles can provide differences in obtained results.

By considering the report's methodology, the assessment scores indicate that NDT methods are applied in various areas of applications. The application areas emphasize different analysis methods for the extent of damage, where this approach clarifies promising ability to detect deterioration, damages, and flaws. A more impressive approach is to combine the NDT methods to accomplish an enhanced perception of durability. The combination of NDT methods contributes to a broader insight into identifying the deterioration to a higher degree than a single NDT method. Hence, combining multiple NDT methods increases accuracy and reliability to detect concrete deterioration by considering their best area performance.

The conducted UPE tests were beneficial in the sense of giving the authors the opportunity to evaluate some of the investigated parameters for the UPE method based on the obtained data and comparing these to the findings in the literature study. This approach allowed the authors to approve or change the assessment scores.

To summarize, an important consideration the authors want to emphasize is that even if the NDT methods are available to detect various deteriorations, there is no clear indication of a correlation between the cause of deterioration mechanism and the collected data. Although, the NDT methods can quantify damage extent due to a specific deterioration mechanism. As addressed in the report, the data from the methods do not identify the cause of the deterioration. This can create delays on observing concrete damages at the correct time. However, one should not neglect the efficiency of this methodology, providing sufficient information about the concrete structures. Based on the investigation and discussion from literature study and lab test, the authors completely agree on that NDT methods are efficient for the evaluation of damages and flaws in reinforced and post-tensioned concrete. In addition, the authors conclude with that combining NDT methods improve the evaluation of reinforced and post-tensioned concrete massively.

Future recommendations that the authors suggest from this report is represented as followed:

- A more reliable comparison between the different NDT methods is recommended. Existing NDT equipment available in the market should highlight extensive investigation in field and lab in a higher degree. Normally, product details for different NDT methods describe the accuracy range, but an improved development here is possible.
- Well established NDT methods for detecting deterioration mechanisms need further improvement. NDT methods manage to contribute with major findings, but deterioration mechanisms such as ASR and freeze-thaw can be improved.
- Measurements for detecting corrosion damages with NDT methods need more development, improving the accuracy and reliability of corrosion detection.

## 7. References

- [1] M. Alexander, A. Bentur, and S. Mindess, "*Durability of concrete: design and construction*". CRC Press, 2017.
- [2] I. Assakkaf, H. Kamal, and M. Safar, "Assessment of Reinforced Concrete Structural Components for an Aging Complex Building Using Reliability and Risk Methodologies," presented at the ICOSSAR-13, Columbia University, New York, 2013.
- [3] D. Breyse, "*Non-destructive assessment of concrete structures: reliability and limits of single and combined techniques: state-of-the-art report of the RILEM technical committee 207- INR*". Springer Science & Business Media, 2012.
- [4] D. Breyse, "Nondestructive evaluation of concrete strength: An historical review and a new perspective by combining NDT methods," *Construction and Building Materials*, vol. 33, pp. 139-163, 2012.
- [5] W. Mosley, J. Bungey, and R. Hulse, "Properties of reinforced concrete," in *Reinforced Concrete Design*: Springer, 1999, pp. 1-13.
- [6] *Eurocode 2: Design of concrete structures - Part 1-1: General rules and rules for buildings*, NS-EN 1992-1-1, Standard Norge, 2018.
- [7] Statens Vegvesen, "Håndbok N400: Bruprosjektering - Prosjektering av bruer, ferjekaier og andre bærende konstruksjoner," Statens Vegvesen Vegdirektoratet, Oslo, 2015.
- [8] D.J. Hannant, S.B. Venkata Siva, and P. S. R. Sreekanth, "5.15 Cement-Based Composites," in *Comprehensive Composite Materials II*, C. H. Z. Peter W.R. Beaumont Ed.: Elsevier, 2018, pp. 379-420.
- [9] C. C. L. de Bruyn, "Corrosion problems with prestressed concrete," in *Proceedings of the fifth congress of the Fédération internationale de la précontrainte, Paris 1966, 1967*: Cement and Concrete Association for the FIP, p. 83.
- [10] R. Szilard, "Corrosion and corrosion protection of tendons in prestressed concrete bridges," in *Journal Proceedings*, 1969, vol. 66, no. 1, pp. 42-59.
- [11] M. J. Osmolska, K. Hornbostel, T. Kanstad, M. A. Hendriks, and G. Markeset, "Inspection and assessment of corrosion in pretensioned concrete bridge girders exposed to coastal climate," *Infrastructures*, vol. 5, no. 9, p. 76, 2020, doi: <https://www.mdpi.com/2412-3811/5/9/76>.
- [12] *Eurocode: Basis of structural design*, NS-EN 1990:2002, Standard Norge, 2016.
- [13] L. Bertolini, B. Elsener, P. Pedferri, E. Redaelli, and R. B. Polder, "*Corrosion of Steel in Concrete : Prevention, Diagnosis, Repair*", 2. ed. Weinheim, GERMANY: John Wiley & Sons, Incorporated, 2014.
- [14] C. Gehlen, S. Von Greve-Dierfeld, and K. Ostermink, "4 - Modelling of ageing and corrosion processes in reinforced concrete structures," in *Non-Destructive Evaluation of Reinforced Concrete Structures*, vol. 1, C. Maierhofer, H.-W. Reinhardt, and G. Dobmann Eds.: Woodhead Publishing, 2010, pp. 57-81.
- [15] K. A. Snyder, L. P. Sung, and G. S. Cheok, "Nondestructive testing (NDT) and sensor technology for service life modeling of new and existing concrete structures," 2013.
- [16] P. I. Modi and C. N. Patel, "*Repair and Rehabilitation of Concrete Structures*". Delhi: PHI Learning Pvt. Ltd., 2015.
- [17] *Guide for conducting a visual inspection of concrete in service*, ACI 201.1R-08, ACI Committee 201, Farmington Hills, 2008.
- [18] Portal on Deterioration of RC Structures. "Abrasion of concrete." <https://18de154.wordpress.com/2018/12/07/abrasion-of-concrete/> (accessed May 21, 2021).
- [19] The Engineering Community. "Types and Causes of Concrete Deterioration." <https://www.theengineeringcommunity.org/types-and-causes-of-concrete-deterioration/> (accessed May 21, 2021).

- [20] C. Baes , H. Szilagy, C. Mircea, P. Criel, and N. Belie, "Concrete structures under impact loading : General aspects," 2016.
- [21] C. Zhang, G. Gholipour, and A. A. Mousavi, "Nonlinear dynamic behavior of simply-supported RC beams subjected to combined impact-blast loading," *Engineering Structures*, vol. 181, pp. 124-142, 2019/02/15/ 2019, doi: <https://doi.org/10.1016/j.engstruct.2018.12.014>.
- [22] M. Priyanka and N. Munirudrappa, "Blast loading and its effects on structures," *PG dissertation, Dayananda Sagar College of Engineering, KS Layout, Bengaluru*, 2013.
- [23] SINTEF Byggforsk. "Frostnedbrytning av betong og andre porøse byggematerialer." [https://www.byggforsk.no/dokument/2624/frostnedbrytning\\_av\\_betong\\_og\\_andre\\_poroese\\_byggematerialer](https://www.byggforsk.no/dokument/2624/frostnedbrytning_av_betong_og_andre_poroese_byggematerialer) (accessed January 25, 2021).
- [24] V. Penttala, "Causes and mechanisms of deterioration in reinforced concrete," in *Failure, distress and repair of concrete structures*: Elsevier, 2009, pp. 3-31.
- [25] Z. A. Etman and T. I. Ahmed, "Effect of freezing-thawing on concrete behavior," 2018, doi: [https://www.researchgate.net/publication/324201881\\_Effect\\_of\\_freezing-thawing\\_on\\_concrete\\_behavior](https://www.researchgate.net/publication/324201881_Effect_of_freezing-thawing_on_concrete_behavior).
- [26] H. Shang and T.-H. Yi, "Freeze-Thaw Durability of Air-Entrained Concrete," *TheScientificWorldJournal*, vol. 2013, p. 650791, 03/21 2013, doi: 10.1155/2013/650791.
- [27] C. Karakurt and Y. Bayazit, "Freeze-thaw resistance of normal and high strength concretes produced with fly ash and silica fume," *Advances in Materials Science and Engineering*, vol. 2015, 2015.
- [28] M. Gutzwiller and F. Musleh, "Freezing and Thawing Effects on Prestressed Concrete," *Transactions of the American Society of Civil Engineers*, vol. 128, no. 2, pp. 152-167, 1963.
- [29] M. Ghoreishi, A. Bagchi, and M. Sultan, "Estimating the response of structural systems to fire exposure: State-of-the-art review," *Conference Proceedings - Fire and Materials 2009, 11th International Conference and Exhibition*, 01/01 2009.
- [30] I. Fletcher, S. Welch, J. Torero, R. Carvel, and A. Usmani, "Behaviour of concrete structures in fire," *Thermal Science - THERM SCI*, vol. 11, pp. 37-52, 01/01 2007, doi: 10.2298/TSCI0702037F.
- [31] R. Rogerson. "Fire Damaged Concrete." <https://www.sandberg.co.uk/site/inspection/fire-damaged-concrete/> (accessed May 25, 2021).
- [32] M. Tufail, K. Shahzada, B. Gencturk, and J. Wei, "Effect of elevated temperature on mechanical properties of limestone, quartzite and granite concrete," *International Journal of Concrete Structures and Materials*, vol. 11, no. 1, pp. 17-28, 2017, doi: 10.1007/s40069-016-0175-2.
- [33] Portland Cement Association, "Types and causes of concrete deterioration," *Portland Cement Association: Skokie, IL, USA*, 2002, doi: [https://www.cement.org/docs/default-source/fc\\_concrete\\_technology/durability/is536-types-and-causes-of-concrete-deterioration.pdf?sfvrsn=4https://www.cmwgeosciences.com/geotechnical-services/ground-settlement](https://www.cement.org/docs/default-source/fc_concrete_technology/durability/is536-types-and-causes-of-concrete-deterioration.pdf?sfvrsn=4https://www.cmwgeosciences.com/geotechnical-services/ground-settlement).
- [34] R. F. Warner, "Overload behaviour of concrete structures: design considerations," *Australian Journal of Structural Engineering*, vol. 5, no. 2, pp. 139-144, 2004, doi: <https://doi.org/10.1080/13287982.2004.11464933>.
- [35] D. W. Hoepfner, "Cyclic Loading and Cyclic Stress," in *Encyclopedia of Tribology*, Q. J. Wang and Y.-W. Chung Eds. Boston, MA: Springer US, 2013, pp. 691-698.
- [36] A. K. Saha, M. N. N. Khan, P. K. Sarker, F. A. Shaikh, and A. Pramanik, "The ASR mechanism of reactive aggregates in concrete and its mitigation by fly ash: A critical review," *Construction and Building Materials*, vol. 171, pp. 743-758, 2018, doi: <https://www.sciencedirect.com/science/article/pii/S0950061818306640>.
- [37] N. B. Winter. "Alkali-silica reaction in concrete." <https://www.understanding-cement.com/alkali-silica.html> (accessed February 23, 2021).

- [38] R. Figueira *et al.*, "Alkali-silica reaction in concrete: Mechanisms, mitigation and test methods," *Construction and Building Materials*, vol. 222, pp. 903-931, 2019, doi: <https://www.sciencedirect.com/science/article/pii/S0950061819318811>.
- [39] I. Fernandes and M. A. Broekmans, "Alkali-silica reactions: an overview. Part I," *Metallography, Microstructure, and Analysis*, vol. 2, no. 4, pp. 257-267, 2013, doi: [https://www.researchgate.net/publication/257806232\\_Alkali-Silica\\_Reactions\\_An\\_Overview\\_Part\\_I](https://www.researchgate.net/publication/257806232_Alkali-Silica_Reactions_An_Overview_Part_I).
- [40] Federal Highway Administration Research and Technology, "Chapter 2 Alkali-Silica Reaction," America, 2016.
- [41] G. Giaccio, R. Zerbino, J. Ponce, and O. R. Batic, "Mechanical behavior of concretes damaged by alkali-silica reaction," *Cement and Concrete Research*, vol. 38, no. 7, pp. 993-1004, 2008, doi: <https://www.sciencedirect.com/science/article/pii/S0008884608000537>.
- [42] Statens Vegvesen, "Alkalireaksjoner – Prøving av materiale fra Nautesund bru: Etatsprogrammet Varige konstruksjoner 2012-2015," Statens Vegvesen, Norway, December 2015. [Online]. Available: <https://vegvesen.brage.unit.no/vegvesen-xmloi/handle/11250/2623527>
- [43] T. Nijland and J. Larbi, "Microscopic examination of deteriorated concrete," in *Non-destructive Evaluation of Reinforced Concrete Structures*: Elsevier, 2010, pp. 137-179.
- [44] R. Siddique and P. Cachim, *Waste and Supplementary Cementitious Materials in Concrete: Characterisation, Properties and Applications*. Woodhead Publishing, 2018.
- [45] *Concrete - Specification, performance, production and conformity*, NS-EN 206:2013, Standard Norge, 2013.
- [46] M. Hayek, M. Salgues, J.-C. Souche, E. Cunge, C. Giraudel, and O. Paireau, "Influence of the Intrinsic Characteristics of Cementitious Materials on Biofouling in the Marine Environment," *Sustainability*, vol. 13, no. 5, p. 2625, 2021.
- [47] J. Monteny *et al.*, "Chemical, microbiological, and in situ test methods for biogenic sulfuric acid corrosion of concrete," *Cement and Concrete Research*, vol. 30, no. 4, pp. 623-634, 2000.
- [48] J. Monteny, N. De Belie, E. Vincke, W. Verstraete, and L. Taerwe, "Chemical and microbiological tests to simulate sulfuric acid corrosion of polymer-modified concrete," *Cement and Concrete Research*, vol. 31, no. 9, pp. 1359-1365, 2001.
- [49] S. Okabe, M. Odagiri, T. Ito, and H. Satoh, "Succession of sulfur-oxidizing bacteria in the microbial community on corroding concrete in sewer systems," *Applied and environmental microbiology*, vol. 73, no. 3, pp. 971-980, 2007.
- [50] A. R. Erbehtas, O. B. Isgor, and W. J. Weiss, "Comparison of Chemical and Biogenic Acid Attack on Concrete," *ACI Mater. J*, vol. 117, pp. 255-264, 2020.
- [51] SINTEF Byggeforsk. "Armeringskorrosjon." <https://www.byggeforsk.no/dokument/298/armeringskorrosjon#i3> (accessed February 3, 2021).
- [52] M. Elsalamawy, A. R. Mohamed, and E. M. Kamal, "The role of relative humidity and cement type on carbonation resistance of Concrete," *Alexandria Engineering Journal*, vol. 58, no. 4, pp. 1257-1264, 2019, doi: <https://www.sciencedirect.com/science/article/pii/S1110016819301115>.
- [53] H. Cui, W. Tang, W. Liu, Z. Dong, and F. Xing, "Experimental study on effects of CO2 concentrations on concrete carbonation and diffusion mechanisms," *Construction and Building Materials*, vol. 93, pp. 522-527, 2015, doi: <https://www.sciencedirect.com/science/article/pii/S0950061815006844>.
- [54] P. Liu, Y. Chen, Z. Yu, and R. Zhang, "Effect of Temperature on Concrete Carbonation Performance," *Advances in Materials Science and Engineering*, vol. 2019, 2019, doi: [https://www.researchgate.net/publication/332886326\\_Effect\\_of\\_Temperature\\_on\\_Concrete\\_Carbonation\\_Performance](https://www.researchgate.net/publication/332886326_Effect_of_Temperature_on_Concrete_Carbonation_Performance).

- [55] J. Balayssac, C. H. Détriché, and J. Grandet, "Effects of curing upon carbonation of concrete," *Construction and Building Materials*, vol. 9, no. 2, pp. 91-95, 1995, doi: [https://doi.org/10.1016/0950-0618\(95\)00001-V](https://doi.org/10.1016/0950-0618(95)00001-V).
- [56] L. Czarnecki, P. Woyciechowski, and G. Adamczewski, "Risk of concrete carbonation with mineral industrial by-products," *KSCE Journal of Civil Engineering*, vol. 22, no. 2, pp. 755-764, 2018, doi: <https://link.springer.com/article/10.1007/s12205-017-1623-5>.
- [57] A. A. Almusallam, "Effect of degree of corrosion on the properties of reinforcing steel bars," *Construction and Building Materials*, vol. 15, no. 8, pp. 361-368, 2001/12/01/ 2001, doi: [https://doi.org/10.1016/S0950-0618\(01\)00009-5](https://doi.org/10.1016/S0950-0618(01)00009-5).
- [58] K. Lau and I. Lasa, "3 - Corrosion of prestress and post-tension reinforced-concrete bridges," in *Corrosion of Steel in Concrete Structures*, A. Poursaeed Ed. Oxford: Woodhead Publishing, 2016, pp. 37-57.
- [59] A. S. Sason, "Evaluation of degree of rusting on prestressed concrete strand," *PCI Journal*, vol. 37, no. 3, pp. 25-30, 1992.
- [60] R. A. Reis, "Corrosion Evaluation and Tensile Results of Selected Post-Tensioning Strands at the SFOBB Skyway Seismic Replacement Project," *California Department of Transportation: Sacramento, CA, USA*, 2006.
- [61] R. A. Reis, "Corrosion Evaluation of Rejected Tendon E3E-C04S SFOBB Skyway Seismic Replacement Project (Post-Tensioning Strand-Phase II Report)," *California Department of Transportation: Sacramento, CA, USA*, 2007.
- [62] R. A. Reis, "Corrosion Evaluation and Tensile Results of Selected Post-Tensioning Strands at the SFOBB Skyway Seismic Replacement Project Phase III Report," *California Department of Transportation: Sacramento, CA, USA*, 2007.
- [63] *Bases for design of structures—Assessment of existing structures*, ISO 13822:2010, ISO - International Organization for Standardization, 2010.
- [64] *Maintenance and repair of concrete structures - Part 2: Assessment of existing concrete structures*, ISO 16311-2:2014, ISO - International Organization for Standardization, 2014.
- [65] *Guide for Evaluation of Concrete Structures Prior to Rehabilitation*, ACI 364.1 R-94, ACI Committee 364, Farmington Hills, 1999.
- [66] B. Täljsten, "The Elop Insight technique for non-destructive testing of concrete structures," 2020, doi: <https://elop.no/whitepapers/non-destructive-testing-of-concrete-structures/>.
- [67] Statens Vegvesen, "Håndbok V441 Bruinspeksjon," Statens Vegvesen Vegdirektoratet, Oslo, 2019.
- [68] R. Wan-Wendner, "Aging concrete structures: a review of mechanics and concepts," *Die Bodenkultur: Journal of Land Management, Food and Environment*, vol. 69, no. 3, pp. 175-199, 2018, doi: <https://content.sciendo.com/view/journals/boku/69/3/article-p175.xml>.
- [69] B. Glišić, D. Inaudi, and S. Vurpillot, "Structural monitoring of concrete structures," in *Como, Italy, Third World Conference on Structural Control*, 2002, vol. 12, no. 10, doi: <https://roctest.com/wp-content/uploads/2017/03/c68.pdf>.
- [70] A. Parrot and L. Warshaw, "Industry 4.0 and the digital twin: Manufacturing meets its match," *Retrieved January*, vol. 23, p. 2019, 2017.
- [71] I. Kapustina, O. Kalinina, A. Ovchinnikova, and S. Barykin, "The logistics network digital twin in view of concept of the non-destructive quality control methods," in *E3S Web of Conferences*, 2020, vol. 157: EDP Sciences, p. 05001.
- [72] S. H. Khajavi, N. H. Motlagh, A. Jaribion, L. C. Werner, and J. Holmström, "Digital twin: vision, benefits, boundaries, and creation for buildings," *IEEE Access*, vol. 7, pp. 147406-147419, 2019.
- [73] A. N. Nasaruddin, T. Ito, and T. B. Tuan, "Digital twin approach to building information management," in *The Proceedings of Manufacturing Systems Division Conference 2018*, 2018: The Japan Society of Mechanical Engineers, p. 304.



- [74] INTERNATIONAL ATOMIC ENERGY AGENCY, "Guidebook on non-destructive testing of concrete structures," *Training Course Series*, 2002.
- [75] TWI Ltd. "Radiography testing - NDT inspection." <https://www.twi-global.com/what-we-do/services-and-support/asset-management/non-destructive-testing/ndt-techniques/radiography-testing> (accessed May 5, 2021).
- [76] A. Karlsson, P. Jilderda, and B. Täljsten, "Utredning av metoder for inspeksjon av etterspent armering i betongbruer," Statens Vegvesen, Norway, 699, January 14 2021. [Online]. Available: <https://vegvesen.brage.unit.no/vegvesen-xmlui/handle/11250/2728767>
- [77] *Report on Nondestructive Test Methods for Evaluation of Concrete in Structures*, ACI 228.2R-13, ACI Committee 228, Farming Hills, 2013.
- [78] S. Kashif Ur Rehman, Z. Ibrahim, S. A. Memon, and M. Jameel, "Nondestructive test methods for concrete bridges: A review," *Construction and building materials*, vol. 107, pp. 58-86, 2016, doi: <https://www.sciencedirect.com/science/article/abs/pii/S0950061815306905?via%3Dihub>.
- [79] O. Abudayyeh, M. Al Bataineh, and I. Abdel-Qader, "An imaging data model for concrete bridge inspection," *Advances in Engineering Software*, vol. 35, no. 8-9, pp. 473-480, 2004, doi: <https://www.sciencedirect.com/science/article/pii/S0965997804001073>.
- [80] Gilson Company. "Crack Width Microscope." <https://www.globalgilson.com/concrete-crack-measuring-microscope> (accessed May 7, 2021).
- [81] A. Humpe, "Bridge Inspection with an Off-the-Shelf 360° Camera Drone," *Drones*, vol. 4, no. 4, p. 67, 2020, doi: <https://www.mdpi.com/2504-446X/4/4/67>.
- [82] Commercial drone professional. "VIDEO: Tech giant Intel ramps up bridge inspection drone programme." <https://www.commercialdroneprofessional.com/video-tech-giant-intel-ramps-up-bridge-inspection-drone-programme/> (accessed June 1, 2021).
- [83] *Testing concrete – Part 4: Determination of ultrasonic pulse velocity*, BS EN 12504-4, British Standard, 2004.
- [84] German Instruments. "PUNDIT Lab." <http://germann.org/products-by-application/ultrasonic-pulse-velocity/pundit> (accessed January 28, 2021).
- [85] V. M. Malhotra and N. J. Carino, *Handbook on nondestructive testing of concrete*. CRC press, 2003.
- [86] J. Malek and M. Kaouther, "Destructive and non-destructive testing of concrete structures," *Jordan journal of civil engineering*, vol. 159, no. 3269, pp. 1-10, 2014, doi: [https://www.researchgate.net/profile/Malek-Jedidi/publication/279547128\\_Destructive\\_and\\_Non-destructive\\_Testing\\_of\\_Concrete\\_Structures/links/5596be6b08ae21086d21fa97/Destructive-and-Non-destructive-Testing-of-Concrete-Structures.pdf](https://www.researchgate.net/profile/Malek-Jedidi/publication/279547128_Destructive_and_Non-destructive_Testing_of_Concrete_Structures/links/5596be6b08ae21086d21fa97/Destructive-and-Non-destructive-Testing-of-Concrete-Structures.pdf).
- [87] C. Marshman. "An Overview of Ultrasonic Pulse Velocity (UPV) Testing for Concrete." <https://www.magnumndt.com/an-overview-of-ultrasonic-pulse-velocity-upv-testing-for-concrete-blog> (accessed June 3, 2021).
- [88] A. Lorenzi, F. T. Tisbirek, and L. Silva, "Ultrasonic pulse velocity analysis in concrete specimens," in *IV Conferencia Panamericana de END, Buenos Aires*, 2007, doi: <https://www.ndt.net/article/panndt2007/papers/83.pdf>.
- [89] I. Lawson *et al.*, "Non-destructive evaluation of concrete using ultrasonic pulse velocity," *Research Journal of Applied Sciences, Engineering and Technology*, vol. 3, no. 6, pp. 499-504, 2011, doi: [https://www.researchgate.net/profile/Isaac-Lawson/publication/265144573\\_Non-Destructive\\_Evaluation\\_of\\_Concrete\\_using\\_Ultrasonic\\_Pulse\\_Velocity/links/5764067808ae\\_b4b997fd6504/Non-Destructive-Evaluation-of-Concrete-using-Ultrasonic-Pulse-Velocity.pdf](https://www.researchgate.net/profile/Isaac-Lawson/publication/265144573_Non-Destructive_Evaluation_of_Concrete_using_Ultrasonic_Pulse_Velocity/links/5764067808ae_b4b997fd6504/Non-Destructive-Evaluation-of-Concrete-using-Ultrasonic-Pulse-Velocity.pdf).
- [90] R. C. Pinto, A. Medeiros, I. J. Padaratz, and P. B. Andrade, "Use of ultrasound to estimate depth of surface opening cracks in concrete structures," *E-Journal of Nondestructive Testing and Ultrasonics*, vol. 8, pp. 1-11, 2010.

- [91] M. Andi and G. Yohanes, "Experimental study of crack depth measurement of concrete with ultrasonic pulse velocity (UPV)," in *IOP Conference Series: Materials Science and Engineering*, 2019, vol. 673, no. 1: IOP Publishing, p. 012047.
- [92] S. A. Kumar and M. Santhanam, "Detection of concrete damage using ultrasonic pulse velocity method," in *National Seminar on Non-Destructive Evaluation*, 2006.
- [93] S. Garg and S. Misra, "Efficiency of NDT techniques to detect voids in grouted post-tensioned concrete ducts," *Nondestructive Testing and Evaluation*, pp. 1-22, 2020.
- [94] M. Sargolzhahi, S. A. Kodjo, P. Rivard, and J. Rhazi, "Effectiveness of nondestructive testing for the evaluation of alkali-silica reaction in concrete," *Construction and Building Materials*, vol. 24, no. 8, pp. 1398-1403, 2010/08/01/ 2010, doi: <https://doi.org/10.1016/j.conbuildmat.2010.01.018>.
- [95] S. H. Diab, A. M. Soliman, and M. R. Nokken, "Changes in mechanical properties and durability indices of concrete undergoing ASR expansion," *Construction and Building Materials*, vol. 251, p. 118951, 2020/08/10/ 2020, doi: <https://doi.org/10.1016/j.conbuildmat.2020.118951>.
- [96] D. Adamatti, A. Lorenzi, J. Chies, and L. Silva Filho, "Analysis of reinforced concrete structures through the ultrasonic pulse velocity: Technological parameters involved," *Revista IBRACON de Estruturas e Materiais*, vol. 10, no. 2, pp. 358-385, 2017.
- [97] K. Komlos, S. Popovics, T. Nürnbergrová, B. Babal, and J. S. Popovics, "Ultrasonic pulse velocity test of concrete properties as specified in various standards," *Cement and Concrete Composites*, vol. 18, no. 5, pp. 357-364, 1996.
- [98] Proceq. "Pundit ultrasonic pulse and echo technologies." <https://www.screeningeagle.com/en/product-family/pundit> (accessed 2021, April 22).
- [99] Olson Instruments. "Freedom Data PC Platform for Nondestructive Testing." <https://olsoninstruments.com/data-platforms/freedom-data-pc-platform-for-nondestructive-testing/> (accessed May 25, 2021).
- [100] Olson Instruments. "NDE 360 Platform." <https://olsoninstruments.com/data-platforms/nde-360-platform/> (accessed May 25, 2021).
- [101] Proceq. "Pundit ultrasonic pulse velocity and pulse echo tomography." [https://www.proceq.com/products/list/Category/pundit-ultrasonic-pulse-velocity-and-pulse-echo-testing/?fbclid=IwAR16nsTpTsfY6bszZxOQ\\_2V8JNA4NfH811JCJ\\_IIfrcBPI05H4Th3rMbHQ](https://www.proceq.com/products/list/Category/pundit-ultrasonic-pulse-velocity-and-pulse-echo-testing/?fbclid=IwAR16nsTpTsfY6bszZxOQ_2V8JNA4NfH811JCJ_IIfrcBPI05H4Th3rMbHQ) (accessed April 25, 2021).
- [102] Test Equipments Center. "Products meeting the search criteria." <http://testequipmentscenter.com/index.php?route=product/search&search=Proceq%20pundit%20PL-200> (accessed April 21, 2021).
- [103] Gilson Company. "Ultrasonic Pulse Velocity Testers." <https://www.globalgilson.com/proceq-pundit-upv-test-instruments> (accessed May 23, 2021).
- [104] F. Gemander. "Ultrasonic Pulse-Echo Method." <https://wiki.tum.de/display/zfp/Ultrasonic+Pulse-Echo+Method#UltrasonicPulseEchoMethod-Literature> (accessed February 8, 2021).
- [105] PCTE. "MIRA - Ultrasonic Concrete Tomography." <https://www.pcte.com.au/images/pdf/MIRA-ultrasonic-pulse-echo-imaging/MIRA-Ultrasonic-Concrete-Tomography-Data-Sheet.pdf> (accessed May 16, 2021).
- [106] R. Beutel *et al.*, "Comparative performance tests and validation of NDT methods for concrete testing," *Journal of Nondestructive Evaluation*, vol. 27, no. 1-3, pp. 59-65, 2008.
- [107] M. Krause *et al.*, "Ultrasonic imaging of post-tensioned concrete elements: New techniques for reliable localization of grouting defects," 2009.
- [108] S. Wagle and K. Chapagain, "Seeing beneath the surface," 2020, doi: <https://elop.no/whitepapers/seeing-beneath-the-surface/>.

- [109] K. Schabowicz, "Ultrasonic tomography-The latest nondestructive technique for testing concrete members-Description, test methodology, application example," *Archives of Civil and Mechanical Engineering*, vol. 14, pp. 295-303, 2014.
- [110] Elop. "Technical Specifications." <https://elop.no/technical-specifications/> (accessed May 16, 2021).
- [111] Humboldt. "Pundit 250 Array, Rapid Ultrasonic Pulse Echoing Imaging." <https://www.humboldtmg.com/rapid-ultrasonic-pulse-echoing-imaging-pundit-250-array.html> (accessed April 21, 2021).
- [112] N. J. Carino, "The impact-echo method: an overview," *Structures 2001: A Structural Engineering Odyssey*, pp. 1-18, 2001.
- [113] *Standard Test Method for Measuring the P-Wave Speed and the Thickness of Concrete Plates Using the Impact-Echo Method*, ASTM C1383:04, ASTM International, 2004.
- [114] C. Cheng and M. Sansalone, "The impact-echo response of concrete plates containing delaminations: numerical, experimental and field studies," *Materials and Structures*, vol. 26, no. 5, pp. 274-285, 1993.
- [115] B. J. Jaeger, M. J. Sansalone, and R. W. Poston, "Detecting voids in grouted tendon ducts of post-tensioned concrete structures using the impact-echo method," *Structural Journal*, vol. 93, no. 4, pp. 462-473, 1996.
- [116] C. Grosse, H. Reinhardt, M. Krüger, and R. Beutel, "Application of impact-echo techniques for crack detection and crack parameter estimation in concrete," *Biochim. Biophys. Acta*, vol. 47, pp. 417-422, 2005.
- [117] German Instruments. "MIRADOR." <http://germann.org/products-by-application/flaw-detection/mirador> (accessed June 5, 2021).
- [118] FPrimeC Solutions, "Impact-Echo." [Online]. Available: [https://www.fprimec.com/wp-content/uploads/2021/03/2021\\_03\\_fprimc\\_impactecho\\_specsheet\\_Rev-1.0.pdf](https://www.fprimec.com/wp-content/uploads/2021/03/2021_03_fprimc_impactecho_specsheet_Rev-1.0.pdf).
- [119] *Standard Practice for Evaluating the Condition of Concrete Plates Using the Impulse-Response Method*, ASTM C1740:10, ASTM International, 2010.
- [120] A. G. Davis, "The nondestructive impulse response test in North America: 1985–2001," *NDT & E International*, vol. 36, no. 4, pp. 185-193, 2003.
- [121] S. Nazarian, S. Reddy, and M. Baker, "Determination of Voids Under Rigid Pavements Using Impulse Response Method," 1994.
- [122] S. Sajid and L. Chouinard, "Impulse response test for condition assessment of concrete: A review," *Construction and Building Materials*, vol. 211, pp. 317-328, 2019.
- [123] Olson Instruments. "Slab Impulse Response." <https://olsoninstruments.com/test-systems-for-platforms/slab-impulse-response/> (accessed May 25, 2021).
- [124] F. Solutions. "The Most Advanced Pile Integrity Tester." <https://www.fprimec.com/ipile/> (accessed June 4, 2021).
- [125] *Standard guide for using the surface ground penetrating radar method for subsurface investigation*, ASTM D6432:19, ASTM International, 2019.
- [126] Sensors & Software. "Concrete Scanning with GPR Guidebook." <https://www.sensoft.ca/wp-content/uploads/2015/11/Concrete-Scanning-with-GPR-book.pdf> (accessed February 13, 2021).
- [127] U. B. Halabe, "18 - Non-destructive evaluation (NDE) of composites: techniques for civil structures," in *Non-Destructive Evaluation (NDE) of Polymer Matrix Composites*, V. M. Karbhari Ed.: Woodhead Publishing, 2013, pp. 483-517e.
- [128] Federal Highway Administration. "Ground Penetrating Radar (GPR)." [https://fhwaapps.fhwa.dot.gov/ndep/DisplayTechnology.aspx?tech\\_id=25](https://fhwaapps.fhwa.dot.gov/ndep/DisplayTechnology.aspx?tech_id=25) (accessed April 23, 2021).
- [129] Sensors & Software. "Concrete Scanning & Assessment." <https://www.sensoft.ca/georadar/concrete-scanning-assessment/> (accessed April 23, 2021).

- [130] Sensors & Software. "Bridge Deck Condition Assessment." <https://www.sensoft.ca/case-studies/bridge-deck-condition-assessment/> (accessed April 23, 2021).
- [131] J. Rhazi, O. Dous, and S. Kaveh, "Detection of fractures in concrete by GPR technique," *University of Sherbrooke, Canada*, 2002.
- [132] R. Forest and V. Utsi, "Non destructive crack depth measurements with ground penetrating radar," in *Proceedings of the Tenth International Conference on Grounds Penetrating Radar, 2004. GPR 2004.*, 2004: IEEE, pp. 799-802.
- [133] S. Li, C. Wang, P. Sun, G. Wu, and D. Wang, "A localization method for concealed cracks in the road base based on ground penetrating radar," *Advances in Mechanical Engineering*, vol. 8, no. 12, p. 1687814016683154, 2016.
- [134] A. Sultan and G. Washer, "Reliability Analysis of Ground-Penetrating Radar for the Detection of Subsurface Delamination," *Journal of Bridge Engineering*, vol. 23, 02/01 2018, doi: 10.1061/(ASCE)BE.1943-5592.0001182.
- [135] Proceq. "Proceq GPR Live - Ground Penetrating Radar." <https://www.proceq.com/compare/proceq-gpr-live/> (accessed April 22, 2021).
- [136] Sensors & Software. "Ground Penetrating Radar (GPR) Solutions." <https://www.sensoft.ca/> (accessed May 5, 2021).
- [137] HILTI. "PS 1000-B X-Scan concrete scanner." [https://www.hilti.com/c/CLS\\_MEA\\_TOOL\\_INSERT\\_7127/CLS\\_CONCRETE\\_SCANNERS\\_7127/r83732](https://www.hilti.com/c/CLS_MEA_TOOL_INSERT_7127/CLS_CONCRETE_SCANNERS_7127/r83732) (accessed May 23, 2021).
- [138] Humboldt. "Proceq Ultraportable GP8800." <https://www.humboldtmg.com/proceq-ultraportable-gp8800.html> (accessed April 22, 2021).
- [139] Advanced Tool & Equipment. "Sensors & Software Conquest® 100 Concrete Scanner (Standard)." <https://advancedtoolcorp.com/product/sensors-software-conquest-100-concrete-scanner/> (accessed May 23, 2021).
- [140] Zenith Survey. "NOGGIN 1000 Antenna." <https://www.zenithsurvey.co.uk/product/noggin-1000-antenna/> (accessed May 23, 2021).
- [141] Proceq. "Corrosion potential, concrete resistivity and permeability testers." (accessed April 22, 2021).
- [142] Elcometer. "Elcometer 331 Covermeters & Half-Cell Meters." <https://www.elcometer.com/en/coating-inspection/concrete-inspection/covermeters-half-cell-meters/elcometer-331-covermeters-half-cell-meters.html> (accessed May 24, 2021).
- [143] Gilson Company. "Corrosion Measurement Equipment." <https://www.globalgilson.com/corrosion-measurement-equipment> (accessed April 22, 2021).
- [144] *Testing Concrete: Part 204-Recommendations on the use of electromagnetic covermeters*, BS 1881-204:1988, British Standard, 1988.
- [145] D. Algernon, D. R. Hiltunen, C. C. Ferraro, and C. Ishee, "Rebar detection with cover meter and ultrasonic pulse echo combined with automated scanning system," *Transportation research record*, vol. 2251, no. 1, pp. 123-131, 2011.
- [146] S. Hübllová, P. Cikrle, O. Karel, and D. Kocáb, "Experimental measurement of the diameter and cover depth of steel reinforcement using an electromagnetic concrete cover meter," in *IOP Conference Series: Materials Science and Engineering*, 2019, vol. 549, no. 1: IOP Publishing, p. 012011.
- [147] P. Cikrle, S. Hübllová, D. Kocáb, and O. Karel, "Non-destructive diagnostics of steel-reinforced concrete structures: detecting and locating reinforcement," in *IOP Conference Series: Materials Science and Engineering*, 2019, vol. 549, no. 1: IOP Publishing, p. 012010.
- [148] Proceq. "Profometer and Profoscope rebar locators and concrete cover meters." <https://www.proceq.com/compare/rebar-detection-and-cover-measurement/> (accessed May 18, 2021).

- [149] HILTI. "PS 200/250 Ferrosan system." [https://www.hilti.co.uk/c/CLS\\_MEA\\_TOOL\\_INSERT\\_7127/CLS\\_CONCRETE\\_SCANNERS\\_7127/r6436646](https://www.hilti.co.uk/c/CLS_MEA_TOOL_INSERT_7127/CLS_CONCRETE_SCANNERS_7127/r6436646) (accessed May 24, 2021).
- [150] Gilson Company. "Profometer® 6 Cover Meters." <https://www.globalgilson.com/profometer-6-cover-meters> (accessed May 20, 2021).
- [151] Gilson Company. "Profoscope Rebar Locators/Cover Meters." <https://www.globalgilson.com/profoscope-rebar-locators-cover-meters> (accessed May 20, 2021).
- [152] Amazon. "Hilti 2044474 Ferrosan kit PS 200 S measuring systems." <https://www.amazon.com/Hilti-2044474-Ferrosan-measuring-systems/dp/B01MXHFL95> (accessed May 24, 2021).
- [153] Gilson Company. "Elcometer 331 Cover Meters." <https://www.globalgilson.com/elcometer-cover-meters> (accessed May 24, 2021).
- [154] Zenith Survey. "Elcometer 331 basic cover meter." <https://www.zenithsurvey.co.uk/product/elcometer-331-basic-cover-meter/> (accessed May 24, 2021).
- [155] P. Gu and J. J. Beaudoin, *Obtaining effective half-cell potential measurements in reinforced concrete structures*. Citeseer, 1998.
- [156] *Standard test method for corrosion potentials of uncoated reinforcing steel in concrete*, ASTM C876:15, ASTM International, 2015.
- [157] T. Frølund, O. Klinghoffer, and H. Sørensen, *Pro's and con's of half-cell potentials and corrosion rate measurements*. 2003.
- [158] Proceq, "Corrosion analysis with the Profometer," ed. Switzerland, 2016, pp. <https://www.youtube.com/watch?v=-QIWdiiUAoc>.
- [159] Humboldt. "CorMap Rebar Corrosion Mapping System." <https://www.humboldtmfg.com/cormap-rebar-corrosion-mapping-system.html> (accessed May 24, 2021).
- [160] R. B. Polder, "Test methods for on site measurement of resistivity of concrete—a RILEM TC-154 technical recommendation," *Construction and building materials*, vol. 15, no. 2-3, pp. 125-131, 2001.
- [161] B. M. Pailles, "Damage identification, progression, and condition rating of bridge decks using multi-modal non-destructive testing," Rutgers University-Graduate School-New Brunswick, 2014.
- [162] B. Pavlakovic, M. Lowe, and P. Cawley, "The inspection of tendons in post-tensioned concrete using guided ultrasonic waves," *Insight*, vol. 41, no. 7, pp. 446-448, 1999.
- [163] E. Jensen, N. Grace, and S. Kumi, "Evaluating prestressing strands and post-tensioning cables in concrete structures using nondestructive methods," Lawrence Technological University, 2015.

## Appendix 1

### Visual inspection form

<b>1. GENERAL</b>	Report number			
	Purpose of inspection			
	Inspector's name(s)			
<b>1A. DESCRIPTION OF THE STRUCTURE</b>	Name			
	Location			
	Type			
	Size			
	Owner			
	Project engineer			
	Contractor			
	Date(s) of construction			
	Photographs	General view		
		Detailed close-up of condition of area		
Sketch map orientation indicating sunny and shady areas and well and poorly drained regions				
<b>1B. MATERIALS USED</b>	Concrete	Normal weight aggregate type		
		Aggregate size		
		Admixture type		
		Mixture properties		
		Compressive strength		
		Modulus of elasticity		
<b>2. NATURE OF ENVIRONMENTAL AND LOADING CONDITIONS</b>	Exposure	Environment		
		Weather		
		Freeze-thaw		
		Wetting and drying		
		Drying under dry atmosphere		
		Chemical corrosion and environmental agents		
		Abrasion, erosion, cavitation, impact		

		Electric conductivity		
		Deicing chemicals (chloride ions)		
		Heat exposure		
	Drainage	Flashing		
		Joint sealants		
		Weepholes		
		Counter		
		Elevation of drains		
	Loading conditions	Dead		
		Live		
		Impact		
		Vibration		
		Traffic		
		Seismic		
	Soils	Expansive soil		
Settlement soil				
Pumping				
<b>3. DISTRESS INDICATORS</b>	Cracking			
	Staining			
	Surface deposits and exudations			
	Leaking			
<b>4. PRESENT CONDITION OF STRUCURE</b>	Apparent alignment of structure	Settlement		
		Deflection		
		Expansion		
		Contraction		
	Surface condition of concrete	Condition level: good, satisfying, poor		
		Formed and finished surface	Smoothness	
			Surface air voids	
			Sand streaks	
			Honeycomb	
	Soft areas			



			Cold joints	
			Straining	
		Cracking	Location and frequency	
			Crack map	
			Width and pattern	
			Leaching	
			Ongoing	
		Scaling	Area, depth	
			Type	
		Spalls and pop outs	Size and depth	
			Type	
		Stain/efflorescence		
		Corrosion in exposed reinforcement		
		Curling and warping		
		Erosion	Abrasion	
			Cavitation	
		Previous patching or other repair		
		Surface protection	Type and thickness	
			Bond to concrete	
			Condition	
Penetrating sealers	Type			
	Effectiveness			
	Discoloration			